Mechanical and magnetic properties of Biocompatible ferrogels

Programa de Doctorado en Física y Ciencias del Espacio

Mariem Mekni Ep Abrougui

UNIVERSIDAD DE GRANADA

TESIS DOCTORAL 2020

Directores

Juan de Dios García López-Durán
Modesto Torcuato López López

Departamento de Física Aplicada

UNIVERSIDAD DE GRANADA

Aknowledgements

M.Mekni Abrougui

Financial support

Summary

Chapter 1

Introduction

1.1   Background

Due to their high availability, relatively low cost and environmental friendliness, clay nanocomposites have developed and attracted worldwide attention. With the rapid growth of nanotechnology, clay minerals are increasingly being used as natural nanomaterials. One of the reasons why clay nanomaterials are increasingly is the possibility of using them to generate biomaterials that mimic and are potentially capable of substituting native tissues due to their ability to retain (by adsorption and absorption) biomolecules to achieve the required biocompatibility (Malda et al., 2013).

The functionalization of clay is required to obtain materials with combined hydrophilic-hydrophobic behavior, capable of absorbing polar and non-polar substances, such as drugs or biocompatible polymers. By modifying the structure, chemical composition and arrangement of clay particles, it is possible to synthesize high-performance nanocomposites that can form physical, reversible and dense cross-linked structures that are effective in dissipating energy and stabilizing the internal network of complex systems such as hydrogels. In addition, the inclusion of clay nanocomposites in polymer hydrogels represents a versatile way to modulate the mechanical resistance of the whole gel (Chang et al., 2010) (Evans et al., 2018) . These properties play a decisive role for biomedical applications. For example, in targeted drug delivery, in which the hydrogel and the carried drug must reach a specific location without any alteration, or in tissue engineering given that the generated artificial tissues must have mechanical properties similar to those of native ones. Over the years, several research groups demonstrated that introducing clay particles is an efficient and easy route to improve the controlled drug delivery of hydrogels (Li &

Chapter 1. Introduction

Mooney, 2016). Therefore, clays, including montmorillonite (Kokabi et al., 2007) and sepiolite (Mahdavinia & Asgari, 2013) have been used to prepare hydrogel nanocomposites with improved properties, especially for biomedical applications (Kokabi et al., 2007) (Gaharwar et al., 2014).

On the other hand, among the polymers employed to generate the gel network, polysaccharides in general and alginate ones in particular, seem to be excellent candidates because of its natural origin and biocompatibility. In addition, alginate molecules can be crosslinked by addition of calcium ions producing gels in which the polymer chains are bounded by weak electrostatic interactions, instead by strong covalent links (Hua et al., 2010). Therefore, hydrogels-based alginate can behave as viscoelastic materials with very low values of the corresponding mechanical moduli being simultaneously capable of reaching a very high degree of hydration by absorption of water.

When the hydrogels contain inclusions of magnetic nanoparticles or magnetic nanocomposites, they have the remarkable characteristic of being "field-responsive" materials, which in this particular case means that their mechanical properties can be controlled by the action of external (non-contact) magnetic fields (Li et al., 2013) (Lopez-Lopez et al., 2017).

In our research group, we have previously reported magnetic hydrogels (or ferrogels) consisting of hydrogels based on natural biopolymers (fibrin) and spherical bulk or core-shell magnetic nanoparticles (Lopez-Lopez et al., 2015) (Rodriguez-Acro et al., 2016). Using these ferrogels we got a significant increase in the values of the main quantities characterizing the mechanical properties (rigidity modulus, viscoelastic moduli) of the ferrogels by application of even weak magnetic fields (Lopez-Lopez et al., 2017).

The main novelty of the present thesis lies in the incorporation of magnetite-clay composite particles with different sizes and shapes in the formulation of the ferrogels. The main contribution expected from this work is that the incorporation of such composite particles provides of additional colloidal stability and homogeneity to

the resulting ferrogels and, at the same time, that their smart (field-responsive) characteristics can be maintained and controlled.

1.2   Hydrogels

Hydrogels are hydrophilic gels that have the ability to retain a large amount of water without dissolving the polymers. They are formed by a three-dimensional network of flexible chains dispersed in an aqueous medium. The network is formed by linking, through chemical or physical bonds, of a great variety of polymers such as polysaccharides or proteins. In addition, in recent years a new generation of hydrogels made of peptides containing between 2 and 12 amino acids have been reported (Adams, 2011) (Beniash et al., 2005) (Conejero-Muriel et al., 2015). In these gels, the peptides self-associate through physical interactions, forming a three-dimensional network of nanofibers (diameter of the order of 10 nm) that can retain more than 99 % by weight of water.

The hydrophilic nature of the chains that make up the network is due to the presence of hydrophilic chemical groups such as hydroxyl (-OH), carboxyl (-COOH) or amide (-CONRR'), although hydrogels containing a significant amount of hydrophobic groups can also be prepared by combining hydrophilic and hydrophobic compounds (polymers or molecules).

As there is currently a great diversity of hydrogels, their classification can be based on different criteria such as the origin of the polymers that made them up, the way in which the gel is prepared or the physico-chemical behavior of the resulting material. Below we will describe the most common classifications, according to different criteria.

1. According to the origin of the polymers. According to this criterion, they can be classified into natural, synthetic and hybrid (Hoffman, 2012). (i) Natural hydrogels consist of polymers that have been extracted from natural sources such as algae, bacterial culture or biological fluids. They are widely used in biomedical applications because they are usually biocompatible and biodegradable (Zhu, 2011) although they have the disadvantage of low

resistance to mechanical stress. Agarose, hyaluronic acid, alginate or fibrin are examples of natural hydrogels. (ii) Synthetic hydrogels consist of large molecules obtained by polymerization in the laboratory. This allows easy modification as there are a large number of available monomers. One of their major drawbacks may be the absence of biocompatibility. Polyacrylamide, polyethylene glycol and synthetic peptides are typical examples of synthetic polymers. (iii) Hybrid hydrogels are made up of two different types of molecules, one of natural origin and the other of synthetic origin; the advantage of these hydrogels is that they allow the advantages of natural (biocompatibility) and synthetic (versatility) hydrogels to be combined in a single material.

2. Depending on the nature of the crosslinking process. They are classified as chemical or physical hydrogels. (i) Physical hydrogels are those in which the flexible network, consisting of polymer chains or small molecules, as is the case of supramolecular gels, is interwoven through physical interactions between the individual entities. They can be obtained by crystallization, ionic interaction, hydrogen bonding or aggregation induced by heating. (ii) Chemical hydrogels, which consists of a flexible network formed by covalent bonds between different chains. There are different ways to prepare chemical hydrogels, the most important being cross-linking by reaction of complementary chemical groups, enzymatic reaction, high-energy radiation and by polymerization by free radicals (Varaprasad et al., 2017) (Akhtar et al., 2016).

3. Depending on the chemical composition and structure. They can be classified into homopolymers, copolymers, semi-penetrated network and penetrated network (Ullah et al., 2015). (i) Homopolymer hydrogels are formed by polymer networks derived from a single type of hydrophilic monomer. (ii) Copolymer hydrogels are formed by polymer chains consisting of a combination of two types of monomers, which intertwine to form a single polymer network, where at least one of the monomers is

hydrophilic in nature. (iii) Semi-penetrated hydrogels are formed by the penetration of a linear polymer into an interlocking polymer network, with no chemical bonding between the polymer network and the linear polymer, but by physical interactions (Zhang et al., 2009). Finally, (iv) penetrated hydrogels consist of a covalently interlocking polymer network with another polymer network also interlocked by covalent bonds (Muniz & Geuskens, 2001).

i)   According to their sensitivity to a stimulus. They can be classified depending if they react to a physical stimulus or to a chemical or biochemical stimulus. (i) Hydrogels that respond to a physical stimulus may change their physical properties, such as their volume, or undergo a sol-gel phase transition in a reversible manner. This may occur when there is for example a change in temperature (e.g. chytopluronic hydrogel) (Park et al., 2009a), or by exposure to light (e.g. hybrid alginate-polyacrylamide gel with ferric ions) (Giammanco et al., 2015), or when a magnetic field is applied (e.g. fibrin-agarose hydrogel with magnetic nanoparticles) (Rodriguez-Arco et al., 2016). (ii) On the other hand, hydrogels that respond to a chemical or biochemical stimulus are those capable of reversibly changing their physical properties when a change in pH occurs in the surrounding environment, for example in poly-(4-vinylpyridine) gels (Arizaga et al., 2010), or that respond to a specific molecular recognition (e.g. glucose responsive hydrogels) (Chu et al., 2004).

1.2.1   Properties of hydrogels

Once the hydrogels have been prepared, it will be necessary to determine their properties, such as the degree of swelling and the rheological properties, in order to modify them, if necessary, depending on the particular application desired. In this sense, hydrogels are very versatile because, for example, by changing the method of preparation, gels with different physical properties can be obtained.

__Chapter 1. Introduction__

As we have previously mentioned, hydrogels are capable of retaining a large amount of water without dissolving. Their ability to hydrate depends on several factors. One of these is the hydrophilic/hydrophobic balance of the chemical compounds that form them. In this case, hydration is favored by the presence of hydrophilic groups, which can be altered by changes in the pH of the medium or the presence of ions. Another relevant factor is the degree of cross-linking and porosity of the hydrogel. Thus, an excessively crosslinked hydrogel will have less porosity since the more compact packing of the fibers that form the network leaves less space to retain water. Therefore, to achieve an adequate swelling capacity, it is very important to control the cross-linking degree of the polymer network chains.

Given that hydrogels are mainly made of water, another factor important to consider is that small changes in their hydration degree can lead to considerable alterations in their mechanical properties. This represents a problem when handling the samples, since a slight pressure applied on the hydrogel implies an immediate loss of water. This is a problem common to all so-called "soft and wet materials" and is very frequent in the case of hydrogels.

On the other hand, hydrogels usually behave mechanically as viscoelastic materials. Therefore, the relationship between the applied mechanical stress and the subsequent deformation does not meet the linear constitutive equations corresponding to a Newtonian fluid or a Hookenian solid.

Let's remember briefly that a Newtonian fluid is a material that under the action of a shear stress deforms instantly and indefinitely and, when the stress ceases, does not recover its initial form, that is, there are no recovering elastic forces. The general constitutive equation of Newtonian fluids establishes a linear relationship between the stress tensor and the strain rate (or shear rate) tensor (the Stokes equation). However, in conventional viscometers and rheometers, the fluid is usually subjected to a simple shear stress, so the Stokes equation degenerates into the well-known Newtonian scalar equation:

$$\sigma = \eta\dot{\gamma} \qquad\qquad (1)$$

Where σ is the shear stress, γ the shear strain, $\dot{\gamma}$ the shear rate (or transverse velocity gradient) and η the viscosity.

On the other hand, we can define an elastic solid as a material that by action of a stress suffers an instantaneous and finite deformation so that, when the applied stress ceases, the initial shape is recovered by the action of internal recovering forces. Elastic solids follow the Hooke's general law, which establishes a linear relationship between the stress tensor and the deformation (or strain) tensor. Analogous to what is done in fluids, elastic solids are usually experimentally characterized by acting on them through simple shear stress or simple normal stress. The general Hooke equation is then given by a linear scalar equation:

$$\sigma = k\gamma \qquad\qquad (2)$$

In which γ is the transverse or longitudinal deformation (shear or normal stress, respectively) and k is a constant equal to the rigidity or shear modulus (G) or the Young's modulus (E), depending on whether the stress is a shear or a normal stress, respectively.

The hydrogels studied in this work behave as soft viscoelastic solids. This means that under the action of a stationary mechanical stress, the strain interval for which Hooke's law is fulfilled is very small and then the region of plastic (or viscoelastic, or viscoplastic) behavior is reached. In this region there is no linear stress-strain relationship and finally, at high shear, the material is broken. Therefore, to obtain the corresponding elastic modulus, it is necessary to perform a strain (or stress) sweep with a very small strain rate to have experimental access to the initial elastic region and to be able to make a reliable estimate of the corresponding elastic modulus (see an example in Figure 1.1).
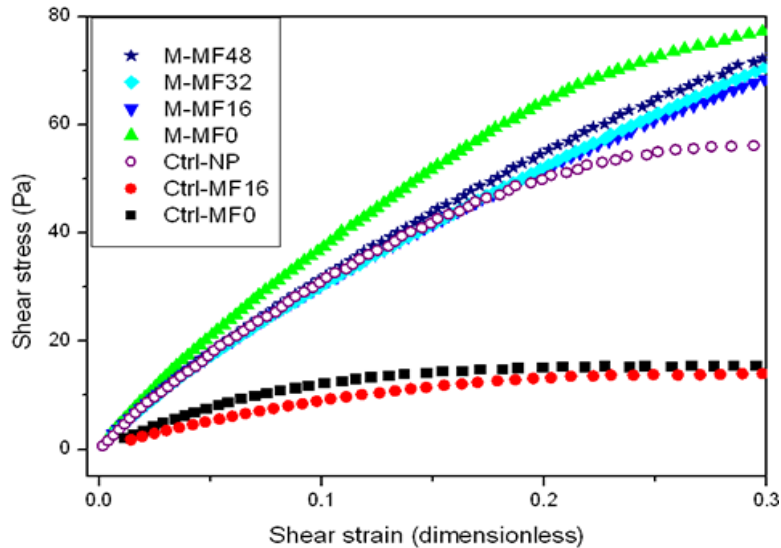
Figure 1.1. Typical result of an experiment to estimate the rigidity modulus of a soft viscoelastic solid. In this case, with fibrin-agarose hydrogels, with and without magnetic nanoparticles embedded inside the gel network, in the absence (MF0) and presence (MF16, MF32, MF48) of applied magnetic fields (intensity H = 16 kA/m, 32 kA/m, 32 kA/m, respectively) during the gelation process. Taken from (Lopez-Lopez et al., 2015). For more details see the original source.

For characterizing a viscoelastic material, it is very common to subject it to the action of a sinusoidal oscillating stress, in order to obtain a more complete information on its mechanical behavior, since in this way both the elastic and the viscous response of the material can be quantified. For this, as we said, a sinusoidal stress (shear or normal) is applied and the corresponding deformation of the material is measured. The fact that a viscous response (in addition to elastic) is produced in the material to a certain degree, makes the corresponding sinusoidal deformation out of phase with respect to the applied stress. Moreover, the deformation will be sinusoidal only if the amplitude of the applied oscillating stress is not excessively large. In this case, the material is said to have linear viscoelastic behavior. In fact, one way to delimit the region of linear behavior is to represent the stress versus strain and, if the typical Lissajous curves are obtained, it can be said that there is a linear response. Otherwise, the behavior is non-linear viscoelastic.

To characterize the behavior of soft materials, it is most common to obtain the corresponding modules within the linear viscoelastic region (LVR). To do this, first the stress amplitude range for which this behavior occurs has to be determined by carrying

out a stress amplitude sweep at constant frequency. Once the LVR is determined the corresponding mechanical spectrum is obtained, by variation of the frequency of the applied stress (at a given constant stress amplitude). In these conditions, the constitutive equation under linear viscoelastic conditions can be written as:

$$\sigma^*(t, \omega) = G^*(t, \omega)\gamma^*(t, \omega) \qquad (3)$$

Where the oscillatory applied stress and the corresponding strain (as a function of time, t, and angular frequency, ω) are represented in complex notation. The quantity G* is the complex rigidity modulus, which only depends on ω (but not on the amplitude of the applied oscillating stress) within the LVR. If the stress is a normal stress, then we have the complex Young's modulus, E*. The complex rigidity modulus (and similarly for the Young's modulus) can be written as:

$$G^*(\omega) = G'(\omega) + iG''(\omega) \qquad (4)$$

Here G' is the elastic or storage modulus and G" is the viscous or loss modulus. The former is proportional to the mean elastic power that, per unit of volume, the material stores/returns on average in each cycle, while G", similarly, is proportional to the power dissipated by viscous friction. Therefore, the two mentioned moduli (G' and G") quantify the degree of elastic and viscous response of a material. The graphic representation of both moduli as a function of the frequency of applied stress is their mechanical spectrum that characterizes the behavior of a material with very high precision. Any minimal change in its composition or internal structure (at nano- or microscopic scale) leads to very significant changes in the corresponding spectrum: see for example Figure 1.2, which corresponds to a pioneering work in which the viscoelastic properties of a native tissue (human oral mucosa) were measured. The changes in the tissue among people of different ages (and gender, not shown in these plots) produce significant changes in the corresponding viscoelastic spectra. This figure illustrates, by the way, how the mechanical properties of native biological tissues present a great variability between different individuals.
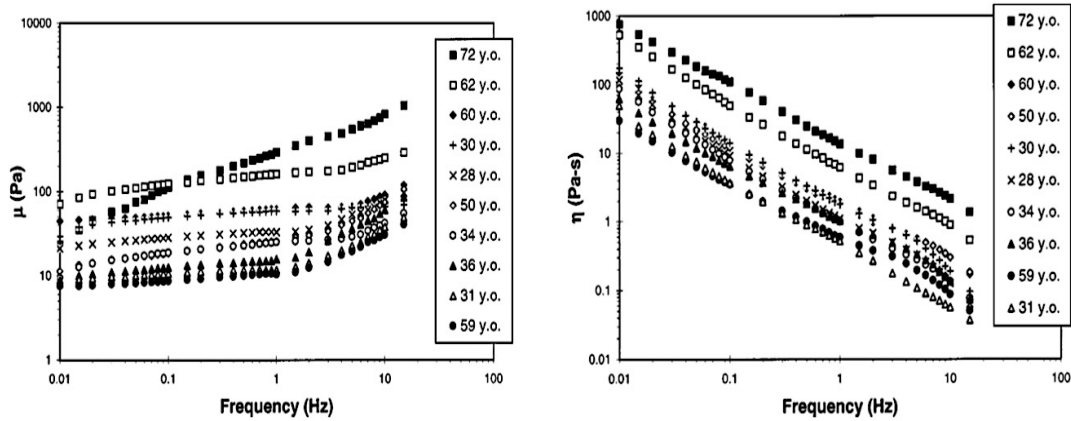
Figure 1.2. Left: elastic modulus of native human oral mucosa tissue as a function of frequency. Right: the viscous modulus of the same tissue as a function of frequency. Both figures are for native tissues of males of different ages. Taken from (Chan & Titze, 1999). With permission from AIP Publishing LLC. The equivalence between the notation in this article (see Y-axis of the graphs) and that in this thesis is: $\mu = G'$ and $\eta = G''/\omega$.

The importance of the study of the rheological properties of hydrogels lies in their applicability. Thus, in biomedicine, hydrogels are often used as extracellular matrices to generate artificial biological tissues. If they are to be used as substitutes for damaged native tissues, it seems obvious that both the native tissue and the artificial one must possess similar rheological properties.

1.2.2   Applications of hydrogels

The diversity in terms of preparation methods, chemical composition and mechanical properties of hydrogels makes them very versatile materials and, therefore, they have a wide range of technological applications.

One of the best-known commercial applications is the use of hydrogels to make contact lenses. In 1960, a hydrogel based on poly-2-hydroxyethyl methacrylate (PHEMA) was first developed as a biocompatible synthetic material suitable for contact lenses (Nature Publishing Group," 1960). The research about hydrogels was carried out until better materials and techniques were obtained for the production of contact lenses to correct vision problems. Later, contact lenses were used for cosmetic purposes, for example, to change the color of the iris by incorporating small reflective

particles embedded in a transparent colored matrix (Carl & Brook, 1985). Later, new contact lenses were developed to improve their physical and chemical properties.

Another important commercial use of hydrogels is their use for the production of hygiene products, which is also well known. Super absorbent polymers and super porous hydrogels (based on highly hydrophilic acrylamide) have been used for more than thirty years to make diapers with excellent water retention capacity. They were then used for other products such as sanitary pads or training pants, generating hydrogels capable of retaining large amounts of fluid and neutralizing bad odor, incorporating enzymes and other additives (Caló & Khutoryanskiy, 2015). This led to the widespread use of disposable products (e.g. diapers) and exponential growth in the amount of waste generated (Sannino et al., 2009). Currently, research in this field is focused on obtaining materials with high water retention capacity that are biodegradable, such as sodium carboxymethyl cellulose and hydroxyethyl cellulose (Caló & Khutoryanskiy, 2015).

Finally, we will mention the most active research field of hydrogels, which is that of biomedical applications, mainly in controlled drug release and tissue engineering. In the first case, the absorbent properties and high porosity of hydrogels make them particularly suitable for retaining drugs and subsequently releasing them locally where their therapeutic effect is required. The advantage of using hydrogels for this purpose is that they enable a controlled release of the drug, at the target tissue of administration, to be maintained over a long period of time (Hoare & Kohane, 2008). Release can occur by various mechanisms such as controlled diffusion, controlled swelling, chemical reaction or by changes in the biological environment.
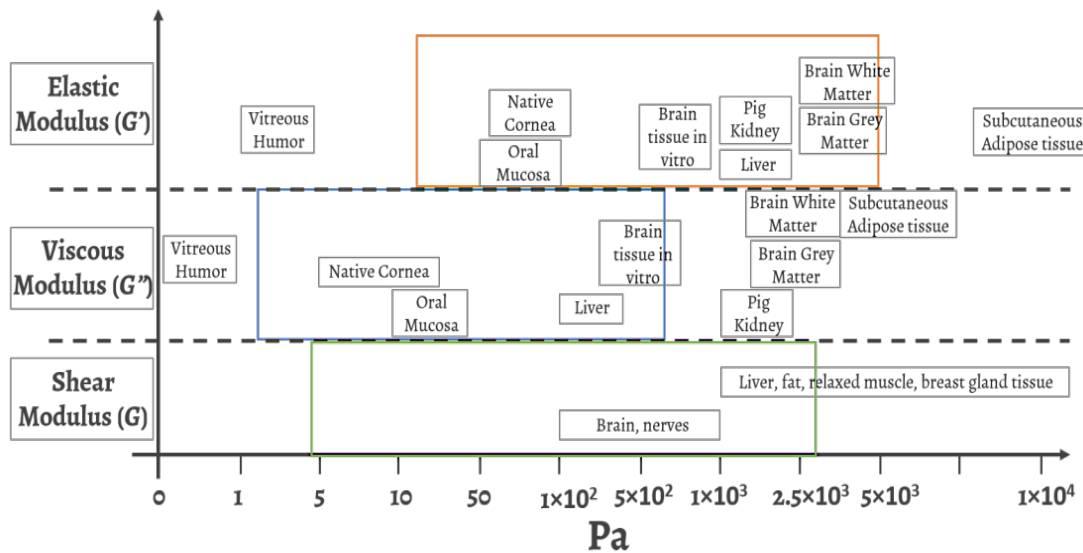
Figure 1.3. Viscoelastic moduli (G', G")and rigidity (or shear) modulus (G) of different biological tissues, taken from (Scionti et al., 2014) with permission from John Wiley and Sons publishers. In addition to the data in this scheme, according to (Stammen et al., 2001), for human articular cartilage G' = 0.23 MPa, while other authors give values between 1 and 2 MPa with a high standard deviation; on the other hand, a value of G = 1.05 ± 0.84 MPa (at low shear strain, 1%) has been reported by (Magnussen et al., 2005).

On the other hand, in tissue engineering the requirement to obtain artificial tissues capable of mimicking the behavior of native tissues is becoming increasingly evident. For this purpose, hydrogels seem to be particularly suitable due to their mechanical properties and biocompatibility. Artificial tissues capable of mimicking the behavior and structure of native biological tissues have already been prepared, successfully generating skin or cornea substitutes using polymeric matrices (M. Alaminos et al., 2006). Generally, natural polymers such as alginate, fibrin or hyaluronic acid are used for this application because they implicitly possess the desired biocompatibility. However, much progress remains to be made in this field, as the biological tissues and organs to be treated in regenerative medicine are very diverse. More particularly, they have very different mechanical properties (with a high variability) as shown in the scheme and caption of Figure 1.3.

In recent years, a very active line of research has been focused on the development of composite hydrogels containing clay nanoparticles. They provide certain advantages associated with the properties of the clay particles or, more precisely, with clay-based composites. Specifically, in this thesis we will study the

effect of the inclusion of particles of magnetic clay-based nanocomposites in polymeric matrices, for obtaining magnetic hydrogels or ferrogels, which has the advantage that the mechanical properties of the resulting materials can be regulated by the remote action of external magnetic fields (Li et al., 2013).

1.2.3   Magnetic hydrogels

Magnetic hydrogels are dispersions of nanoparticles or microparticles of ferromagnetic (iron, metal alloys) or ferrimagnetic (magnetite or other ferrites, and maghemite) particles in a hydrogel. As they contain embedded magnetic particles, the physical properties of these materials, especially their mechanical properties, can be modified by the action of low (magnetic intensity up to H = 10 kA/m) or moderate (H between 10 and 100 kA/m) external magnetic fields.

Magnetic hydrogels belong to a wider group of materials called magnetic colloids. Depending on the continuous phase or the carrier medium containing the particles, this type of magnetizable colloid can be classified into two large groups (see Figure 1.4).

When the carrier is an aqueous or an oil liquid, there are different types of suspensions that, in the absence of a magnetic field, can behave as Newtonian or non-Newtonian liquids, although by application of a magnetic field of enough intensity they can become very rigid viscoelastic solids. They can be classified into three subtypes, as described below.

(i)   *Ferrofluids* (FF) when the magnetic particles are monodomain from the magnetic point of view (size in the order of 10 nm). In this case, if the concentration of particles in the suspension is sufficiently high (around 5 % – 10 % in volume fraction), and the particles are not aggregated, we have a liquid material that is practically a hydrodynamic and magnetic continuum. They behave as Newtonian liquids in the absence of magnetic field, if particle aggregation is effectively hindered. Only the action of strong magnetic fields (H >

100 kA-m^{-1}) can result in slight field-dependent increments in their viscosity: the so-called magnetoviscous effect (Lopez-Lopez et al., 2012) (Odenbach, 2013).

(ii)　　*Magnetorheological fluids* (MRF). They are suspensions of magnetically multi-domain particles (size 10^2 - 10^3 nm). In this case, the action of even weak or moderate fields can induce the formation of chains of particles by magnetic interactions, provoking a transition from a non-Newtonian liquid to a viscoelastic solid with even very high values of the rigidity modulus (magnetorheological effect) (Bossis et al., 2002) (Lo, 2007).

(iii)　　*Composite MRF*. These are suspensions that usually contain two types of particles in suspension, which may be magnetic and non-magnetic (inverse ferrofluids) (Gans et al., 1999), or both magnetic, although with an extremely bimodal size distribution (bimodal FMR) (Vicente, 2005).

The second group of magnetic colloids, in which the carrier medium is a viscoelastic solid, can be called magneto-polymers composites (Zubarev et al., 2018) Among these, two types can be distinguished: magnetic elastomers and magnetic gels.

(iv)　　*Magnetic elastomers*. These consist of magnetic micro-particles embedded in an elastomer which is produced by polymerization from a mixture of monomers and particles. They have a wide range of applications, in particular for the manufacture of vibration damping devices (Vicente, 2005).

(v)　　*Magnetic gels*. They contain magnetic particles, preferably with a size larger than 100 nm, dispersed in a network consisting of polymer chains cross-linked by physical or chemical interactions; see a review of their mechanical properties in (Lopez-Lopez et al., 2016). Among

these, those of greatest technological interest are hydrogels, which contain a very high proportion of water in their composition.
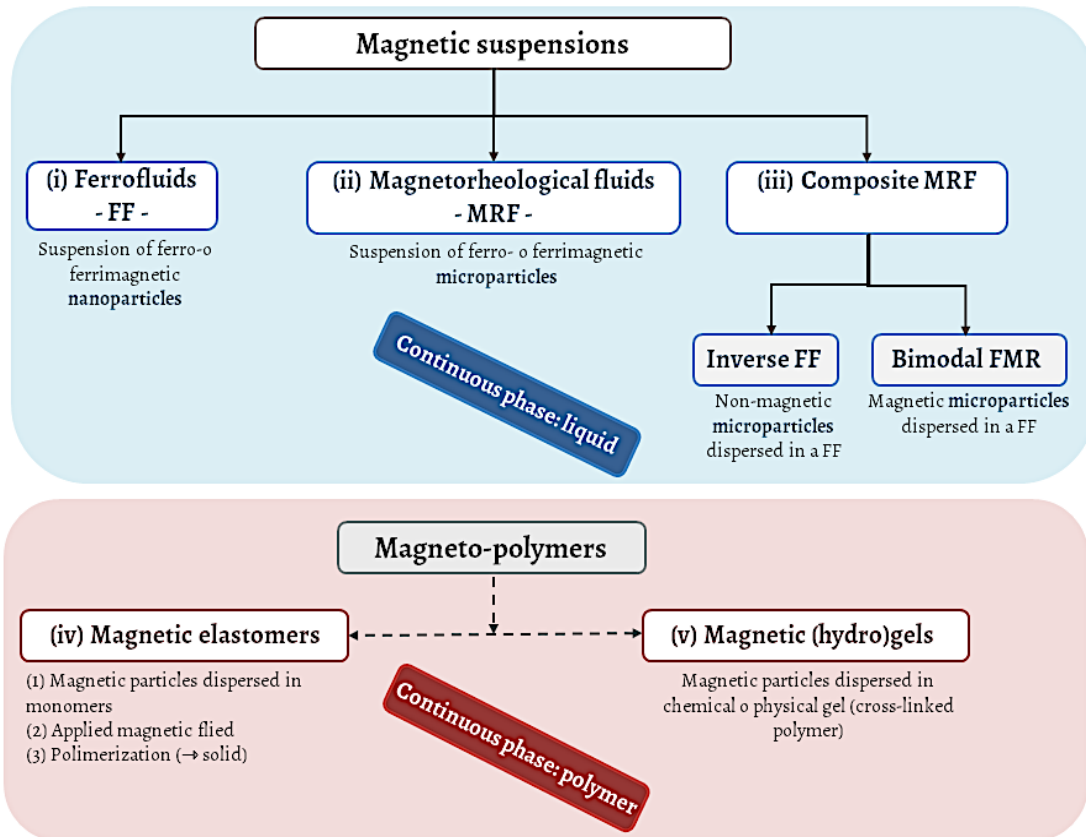
Figure 1.4. Classification of magnetic colloids.

In this work, we will obtain ferrogels by embedding particles of magnetite-clay nanocomposites in polymer matrices consisting of cross-linked alginate chains. The incorporation of magnetic particles provides these materials with new characteristics. For example, the magnetic phase makes possible to detect and control the hydrogel by means of non-invasive methods (Mayer et al., 2000) (Lopez-Lopez et al., 2015).

The main advantages of magnetic hydrogels in the field of biomedicine can be briefly summarized as follows. Firstly, the presence of magnetic particles allows the visualization and monitoring of magnetic hydrogels for in-vivo applications using magnetic resonance (Margel, 2012). Secondly, in vitro studies suggest that the presence of magnetic material in hydrogels stimulates cell adhesion, proliferation and differentiation (Ban, 2014). Thirdly, the use of injected implants formed by magnetic hydrogels would make possible the guidance of functionalized magnetic particles in-

vivo through the action of external magnetic fields (Bock et al., 2010) (Margel, 2012). This represents an interesting strategy for guiding and accumulating growth factors, drugs and cells attached to the injected magnetic particles. Finally, recent works by our research group, in collaboration with the Tissue Engineering group of the Faculty of Medicine of the UGR, have shown that artificial biological tissues can be prepared, based on magnetic hydrogels, which have mechanical properties that can be modulated by magnetic fields (Lopez-Lopez et al., 2015) (Rodriguez-Arco et al., 2016). This is a unique advantage compared to other biomaterials: we would have hydrogel materials that are biocompatible with the human body and that can imitate natural tissues. Therefore, they have a promising potential in this area.

Consequently, the use of clay-based magnetic hydrogels in biomedicine can have considerable advantages, although there are still aspects that need to be tested and improved. The most notable challenge is related with the reinforcement of their mechanical properties by application of moderate magnetic fields. Up to date the field-induced increase reached in the rigidity modulus in magnetic hydrogels is rather low, being of the order of 10% with respect to that in the absence of applied field (Lopez-Lopez et al., 2015). This is one of the main motivations of this work, as well as the verification of their possible biocompatibility when they are used as extracellular matrices for cell growth and proliferation.

1.3 Hypotheses and justification

The foremost aim of this work is to obtain biocompatible hydrogels with mechanical properties that can be controlled by remote action of force fields. For this purpose, magnetic hydrogels with a solid clay phase and sufficiently high magnetic susceptibility will be prepared so that, by the action of external magnetic fields, the viscoelastic moduli of the resulting material can be modified. Therefore, a part of the work will be focused on obtaining magnetic particles with intense magnetic response and that, in addition, are adequately functionalized to be biocompatible. An additional requirement is that they have a low density so that they remain dispersed in the pre-gel mixture without quick settling.

Chapter 1. Introduction

The starting hypotheses of this work are:

1. It is possible to synthetize nanoparticles consisting of magnetite-clay composites with low enough gravitational density and high enough magnetic susceptibility.

2. Homogeneous (without gradients in particle concentration) magnetic hydrogels can be prepared by weak (physical) crosslinking of alginate chains in the presence of magnetite-sepiolite and magnetite-montmorillonite particles dispersed in the pre-gel mixture.

3. The presence of these particles allows obtaining ferrogels with high enough magnetic response.

4. The mechanical properties (viscoelasticity) of the resulting ferrogels can be controlled by magnetic fields from low to moderate intensity (magnetic intensity lower than H = 100 kA/m).

To test these hypotheses, the following specific objectives are defined:

➢ Synthesis of core (sepiolite fibers) – shell (magnetite nanoparticles) of low average mass density and high enough magnetic response.

➢ Synthesis of core (montmorillonite platelets) – shell (magnetite nanoparticles) of low density and high enough magnetic response.

➢ Preparation of aqueous suspensions of both sepiolite-magnetite and montmorillonite-magnetite particles with different solid volume fractions.

➢ Preparation of homogeneous and soft hydrogels with different concentrations of alginate.

➢ Preparation of homogeneous magnetic hydrogels with different volume fraction of clay-magnetite composite particles.

➢ Determination of the magnetic properties (susceptibility, magnetic saturation) of the composite particles obtained.

➢ Visualization at microscopic scale of the network structure of the hydrogels and ferrogels.

➢ Characterization of the mechanical properties of the suspensions and ferrogels, in the absence and in the presence of external magnetic fields, including the following parameters: rigidity modulus, viscosity in steady-state measurement, loss and storage moduli in oscillatory regime.

➢ Evaluation of the *ex vivo* biocompatibility of the nanocomposite particles as well as the magnetic hydrogels. For this purpose, viability and cell proliferation tests will be performed.

1.4   Thesis Organization

The research developed in this work is structured in the following parts:

Chapter 2. In this chapter, the physico-chemical characterization and mechanical properties of magnetic hydrogels containing sepiolite-magnetite particles are studied. First of all, in this chapter the synthesis of sepiolite (fiber-like shaped) clay particles covered by magnetite nanoparticles, carried out by the co-precipitation method, is described. Afterwards, the adsorption of alginate molecules onto the composite particles is checked by means of zeta potential measurements. In addition, the most relevant magnetic properties of the particles are depicted. Then, the preparation of alginate hydrogels and alginate/(clay-magnetite) ferrogels, by crosslinking of alginate molecules with calcium ions, is detailed. Finally, the rheological properties, in the absence and presence of external magnetic field, as well as the microstructural study of the different hydrogels obtained with embedded particles are presented.

Chapter 3. This chapter includes a similar study to that of chapter 2, but in this case for suspensions and magnetic hydrogels containing montmorillonite-magnetite platelets.

Chapter 4. In this one we describe an ex-vivo study, using different techniques, of the biocompatibility of the suspensions and ferrogels containing sepiolite-magnetite particles.

Chapter 5 is devoted to remark the most relevant achievements attained and also the main conclusions drawn from this research work.

Finally, **chapter 6** includes the references cited along whole thesis.

Chapter 1. Introduction

Chapter 2

Rheology of suspensions and ferrogels composed of fiber-like magnetic particles

Summary

Magnetic gels (ferrogels) are heterogeneous systems structured at the nanoscale, which contain magnetic particles dispersed in 3-D networks of polymer chains. For the present chapter, the magnetic particles were synthesized with a core-shell structure, consisting of sepiolite particles covered by magnetite nanoparticles. These composite particles had a fiber-like shape with a high aspect ratio. The obtained sepiolite-magnetite composite particles showed a high enough susceptibility and saturation magnetization. The magnetorheological (MR) properties, and the intensity of the MR effect, of aqueous suspensions of the synthesized particles, were studied. The particles, functionalized by adsorption of alginate molecules, were embedded in alginate hydrogels to get homogeneous soft materials. The particles were linked to the polymer chains as the knots in a network and largely conditioned the mechanical properties of the resulting soft-wet materials. After determining the optimal compositions of the ferrogels, their viscoelastic properties were measured in the absence/presence of external magnetic fields. The results indicated that the MR effect provided by the clay-magnetite particles was considerably more intense than that reported in ferrogels containing spherical magnetic microparticles. Therefore, the embedment of fiber-shaped magnetic particles in hydrogels allows controlling the mechanical properties in a wider range than in conventional ferrogels based on spherical particles.

2.1. Introduction

Magnetic hydrogels (or ferrogels) are magnetisable soft-wet materials that do not exist in nature. They are heterogeneous materials that belong to a more general group of soft materials usually called magnetic colloids. These materials are mainly characterized by their smart nature because by the action of external magnetic fields the macroscopic properties of these systems can be controlled. As we mentioned in the previous Chapter 1, they can be classified, according to the continuous phase in which the magnetic particles are dispersed, in two groups: i) magnetic suspensions (Wiedenmann, 2002), and ii) magneto-polymer composites (Lopez-Lopez et al., 2016). In the case of the former group, the continuous phase is a Newtonian liquid (aqueous solution or oil). There are two kinds of suspensions: ferrofluids (FF) and magnetorheological suspensions (MRS), which essentially differ in the size of the dispersed particles. In FF the particles are less than about 50 nm (magnetically monodomain) while in MRS they are in the micrometric scale (magnetically multidomain). In the second group (magneto-polymer composites), the magnetic particles can be dispersed in a highly elastic and dry polymer network, which is an elastomer, as for example synthetic rubber. In magnetic elastomers the mechanical properties (Young's and shear moduli) can be strongly modulated by applying external magnetic fields (Varga, 2006) (Agirre-olabide et al., 2014). Alternatively, the continuous phase can be a soft viscoelastic gel consisting of polymer chains extended across an oil or aqueous solution (Lopez-Lopez et al., 2016). The present chapter is devoted to these last soft-wet materials, called magnetic hydrogels or ferrogels.

Magnetic hydrogels are one the most versatile magnetic colloids because their macroscopic properties, particularly the mechanical ones, can be modified in very different ways due to the complexity of their internal structure at the nano- and micrometric scale. These systems can be designed modifying different parameters such as the following. i) The composition, concentration, size and shape of the magnetic particles. ii) The length, chemical composition, and the concentration of the polymer chains. iii) The crosslinking degree of the polymer network. iv) The density of bonds (if they exist) among the polymer chains and the solid magnetic particles. v)

Finally, the degree of hydration (swelling by water), which can reach even more than 90% v/v (Bonhome-Espinosa et al., 2017) (Gila-Vilchez et al., 2018).

In addition, magnetic hydrogels can be provided with the required biocompatibility for their use in biomedical applications, such as controlled drug delivery or reparation/regeneration of damaged biological tissues (Culver et al., 2017) (Li et al., 2013). In particular, for biomedical engineering applications, magnetic hydrogels can work as scaffolds to generate artificial tissues. For this purpose, the magnetic particles have to be functionalized, and the polymer usually is a natural one to avoid their rejection by the immune system (Lopez-Lopez et al., 2015).

In the majority of the ferrogels reported in the literature, the particles have a spherical shape, being composed of ferromagnetic metals (mainly iron) or ferrites (especially magnetite). In these cases, a problem arises because the high density of the particles can favour their gravitational settling during the ferrogel preparation and, in consequence, the resulting gel may have a poor homogeneity. This problem can be overcome by using core-shell composites (magnetite-polymer, iron-silica) (Bonhome-Espinosa et al., 2017) (Gila-Vilchez et al., 2018) (Lopez-Lopez et al., 2015) (Zubarev et al., 2019). In this case, usually spherical-shaped particles are employed because of the simplicity of the synthesis procedure.

The magnetic particles used for the work presented in this chapter consisted of sepiolite microparticles covered by magnetite nanoparticles. Sepiolite is a clay mineral with a fiber-like shape and a high aspect ratio (length/thickness ratio). The high porosity of this mineral favoured that their fine pores worked like points for the growth of magnetite nanoparticles and, as a consequence, the formation of composites with a high enough magnetic response. Furthermore, the low average density of the resulting composites resulted in negligible particle settling during the crosslinking of the pre-gel mixture. In the ferrogels reported in this chapter such pre-gel mixture consisted of a suspension of the composite particles in an aqueous solution of sodium alginate. In addition, the sepiolite-magnetite particles were functionalized by adsorption of alginate molecules prior to their mixture with the sodium alginate solution. This functionalization favoured the formation of bonds among the particles and the alginate chains during the gelation process, and as a result we obtained a

ferrogel with a polymer network reinforced by particles that worked as knots linking to the polymer chains.

Besides the preparation of the sepiolite-magnetite-alginate hydrogels, in this chapter the rheological characterization of clay-magnetite aqueous suspensions and also of the corresponding ferrogels was carried out, both in the absence and in the presence of external magnetic fields. The main objective of the work described in this chapter was to quantify the intensity of the magnetorheological effect achieved in these heterogeneous systems.

2.2. Materials and experimental methods

2.2.1. Materials

The sepiolite particles were supplied by Sigma-Aldrich (USA) and had a specific surface area of 300 m^2/g (Valentini et al., 2012). These initial clay particles were homoionized by substituting the exchangeable cations by Na^+ ions as follows: 25 g of sepiolite powder were dispersed in 250 mL of 1 M NaCl solution and stirred during 1 h. After that, the particles were separated by centrifugation (3000 rpm, 5 minutes) and then redispersed in a 1 M NaCl solution. This process was repeated five times. Finally, the particles were repeatedly redispersed in deionized water (Milli-Q Academic, Millipore, and France) and centrifuged, until the conductivity of the supernatant was below 20 $\mu S/cm$. Then, the particles were dried at 90°C and stored. The homoionized sepiolite particles will be called SP particles in what follows.

The chemicals employed in the synthesis of sepiolite-magnetite particles were $FeCl_3 \cdot 6H_2O$, NH_4OH aqueous solution (25% NH_3), and $FeCl_2 \cdot 4H_2O$ (98%). For the preparation of the hydrogels, the chemicals employed were $CaCl_2$ (99%), $CaCO_3$ (99%), D-glucono-δ-lactone (GDL), and sodium alginate [empirical formula $(C_6H_7NaO_6)_n$]. All these chemicals were supplied by Sigma-Aldrich (USA), and used without any further purification.

2.2.2. Synthesis of sepiolite-magnetite particles

The synthesis route of the sepiolite-magnetite particles (SM particles in what follows) used in the present work was adapted from a previous one reported by (Liu et al., 2008) for the preparation of attapulgite-magnetite composites. Attapulgite is also a nano-fibrillar clay mineral. The synthesis of the SM composite particles involved the following steps:

i) First, 1.5 g of SP particles were dispersed in a previously prepared solution containing 4.410 g $FeCl_3 \cdot 6H_2O$ in 200 mL of deionized water.

ii) The resulting suspension in step (i) was kept during 30 min under sonication in an ultrasonic bath. Then, it was deoxygenated by bubbling nitrogen during 15 min. Finally, the flask was closed, and the suspension magnetically stirred for 12 h.

iii) Then, 1.614 g of $FeCl_2 \cdot 4H_2O$ were added to the suspension obtained in step (ii). This new suspension was heated to 90°C. After that, 6 mL of NH_4OH were rapidly added under stirring. A black precipitate appeared immediately. The resulting suspension was stirred under nitrogen atmosphere for 1 h at 90°C.

iv) The mixture obtained in step (iii) was cooled down to room temperature and, finally, washed by repeated cycles of decantation, using a powerful magnet, and redispersion in fresh distilled water until the supernatant conductivity was less than 20 μS/cm.

In parallel, pure magnetite nanoparticles were synthetized following the same procedure just described but, obviously, without adding in step (i) the sepiolite particles in the Fe^{3+} solution.

The magnetite-covered sepiolite particles were functionalized by adsorption of sodium alginate (SMA particles in what follows). For this purpose, 1.0 g of SM particles was dispersed in a solution that contained 0.25 g of sodium alginate in 50 mL of water. This suspension was mechanically stirred at room temperature during 1 h. Then, the suspension was cleaned by successive cycles of decantation/redispersion as described in point (iv) above.

2.2.3. Preparation of the magnetic hydrogels

The magnetic hydrogels, consisting of SMA particles dispersed in an alginate hydrogel, were prepared, by a similar procedure to that described in (Gila-Vilchez et al., 2018). The successive steps were the following:

i) A suspension with a concentration of 10% w/v of SMA particles in deionized water was prepared by mechanical stirring.

ii) Two different solutions of sodium alginate were prepared. The first, containing 0.25 g of alginate in 50 mL of water (0.5% w/v), and the second one with 0.5 g of alginate in 50 mL of water (1% w/v).

iii) Aliquots of 2.5 mL of the suspension prepared in step (i) were mixed with 2.5 mL of each one of the two different alginate solutions prepared in step (ii). These two pre-gel mixtures were carefully shaken by hand until the resulting suspensions were homogeneous.

iv) Then, 22.5 mg of $CaCO_3$ were added to each one of the pre-gel suspensions prepared in the previous step and stirred by a vortex mixer during a few seconds.

v) An amount of 26.7 mg of GDL was added to the two suspensions resulting in step (iv), which were afterwards shaken by hand, and then placed in a Petri dish and left at rest during 4 h.

vi) Finally, 5 mL of a 45 mM $CaCl_2$ solution were added to each sample (with different concentrations of alginate, as indicated in step ii), and then they were left overnight at room temperature in order to obtain the final ferrogels.

Note that the Ca^{2+} ions were the crosslinkers that promoted the formation (gelation) of the alginate hydrogels. The GDL molecules (added in step v) were hydrolysed in water solution to gluconid acid, so imparting the required acidification for the decomposition of calcium carbonate. In this way, the slow release and diffusion of calcium ions into the aqueous medium allowed obtaining homogeneous ferrogels. The calcium solution added in step (vi) provoked the swelling, as well as the final crosslinking (again by diffusion of Ca^{2+}), which resulted in ferrogels with high enough consistence. In what follows, we will refer to the two ferrogels obtained, using the

0.5% w/v or alternatively the 1% w/v alginate solution (step ii), as "Ferrogel-1" and "Ferrogel-2", respectively.

2.2.4. Characterization of the particles and gels

The chemical composition of the sepiolite particles (before homoionization) was determined by X-ray fluorescence (Philips Magix Pro PW-2440 apparatus), in which the main elements present in the sample were determined in the form of oxides.

The zeta potential of the particles was determined from electrophoretic mobility (EM) measurements in a Malvern Zeta-Sizer Nano SZ (Malvern Instruments, UK) at 25°C. For these measurements, different dilute suspensions (less than 1% w/v) of SP, magnetite, SM and SMA particles were prepared in a solution with constant ionic strength (1 mM NaCl) and the pH adjusted in the interval between pH 4 and pH 10. Afterwards, the suspensions were stored for 24 h, and the pH readjusted immediately before the EM measurements. Each value of the zeta-potential reported was the average of at least 9 measurements.

The size and shape of the SP particles and the SM and SMA composites were obtained by observation via high resolution scanning electron microscopy (HR-SEM) using a Zeiss SUPRA40VP (USA) microscope. The microstructure of the ferrogels was observed in a Quanta 650 Field-Emission Environmental Scanning Electron Microscope (FEI, USA). In this case, and to avoid the modification of the original structure of the hydrogel, the samples were previously prepared by the so-called Critical Point Drying (CPD) technique. This technique essentially consists of the substitution of the water in the hydrogel by carbon dioxide; after that, the CO_2 was removed by increasing temperature and pressure up to the critical point.

The magnetic properties of the composite particles (SM, SMA) were measured at room temperature in a vibrating sample magnetometer VSM 4500 (EG&G Princeton Applied Research, USA). First, the samples (dry powders) were magnetized by increasing the external field intensity (H) from 0 to 374 kA/m to obtain the first magnetization curve and, second, the magnetization loop was obtained by variation of H along the cycle 374 – 0 – (-374) – 0 – 374 kA/m. For each H value the corresponding magnetization (M) was obtained.

2.2.5. Rheological measurements

The rheological properties of the SM and SMA suspensions were measured at 25.0 ± 0.1°C in a Haake MARS III rheometer using a titanium double cone-plate geometry with 60 mm diameter and 2° cone apex (DC 60/2° Ti L, Thermo Fisher Scientific, USA). The magnetic field was applied in the vertical direction (perpendicular to the rheometer plate) by an external coil. The external magnetic field intensity in the sample position reached 43 kA/m for the highest electric current in the coil.

The rheological characterization of the ferrogels was carried out at 25.0 ± 0.1°C in a magneto-rheometer Physica MCR 300 (Thermo Fisher Scientific, USA), using a plate-plate geometry with 20 mm in diameter. The plates had a rough surface to avoid wall slip. The magnetic field applied, in the range H = 0 – 282 kA/m, was perpendicular to the plates that confined the samples. The ferrogel samples were carefully drawn from the Petri dish and placed on the bottom plate of the rheometer. Then, the upper plate (rotor) was gently descended until the contact with the sample was reached. A normal force as low as 0.1 N between the rotor plate and the disk-like sample was fixed in order to ensure a good contact of the sample with the measuring system. The gap between the plates was slightly varied according to this condition. During rheological measurement the samples were kept in a vapour saturated atmosphere so that their dehydration was avoided. In addition, a fresh sample was used for each measure to ensure the reproducibility of the initial conditions.

In the case of the SM and SMA suspensions, two different measurement protocols were performed: i) steady-state measurements, and ii) dynamic measurements (oscillometry). In the first one, a shear stress ramp was applied, and the corresponding shear rate was measured in each one of the ramp steps once a stationary value was reached. The corresponding rheograms (shear stress vs. shear rate) that characterize the samples, both in the absence and in the presence of magnetic field, were obtained. The time elapsed between two consecutive steps in the shear ramp was 5 s, which was long enough to attain the stationary level.

In dynamic measurements or oscillometry, the same protocol was employed for both the SM or SMA suspensions and for the ferrogels obtained. The objective was to obtain the values of the viscoelastic moduli (G' elastic or storage modulus, G" loss or

viscous modulus) that characterize the viscoelastic response of the materials. The samples were subjected to a sinusoidal shear strain, maintaining a constant frequency (1 Hz) and increasing the strain amplitude (γ_0) from low values up to values high enough to reach a non-linear viscoelastic response. In the non-linear region, G' and G'' strongly depend on γ_0. On the contrary, the region of low strain, in which G' and G'' are practically independent of γ_0, corresponds to the linear viscoelastic region. These tests were also performed in the absence and in the presence of magnetic fields of increasing intensity. The delay time between two consecutive steps in γ_0 was 5 s for the suspensions and 10 s for the ferrogels.

2.3. Results and discussion

2.3.1. Particles characterization

The bulk chemical composition of the sepiolite particles (before homoionization) is included in Table 2.1. The sepiolite clay is a hydrated magnesium aluminium silicate in which Al(III) ions are substituted in a high extent by Mg(II) and Fe(III) ions in the octahedral layers (Murray, 2000). In particular, in the sepiolite employed in this work, the Mg ions are largely dominants, being Al and Fe in a much smaller concentration.

In order to assess the coverage of the sepiolite particles by magnetite nanoparticles and then by alginate molecules, the zeta potential of the particles was determined in suspensions with variable pH and constant ionic strength (1 mM NaCl). Figure 2.1 shows the results obtained. In the case of magnetite, the zeta potential was positive below the isoelectric point (iep) at pH ≈ 5.5, and negative for larger pH values (up to pH = 10), as a consequence of the adsorption of H^+ and OH^- ions that usually are potential determining ions for metal oxides. The value of the pH(iep) of magnetite nanoparticles in the literature is usually around the value obtained in the present work (Galindo-González et al., 2005) (Viota et al., 2010), although values as high as pH(iep) = 8 have also been reported (Illés & Tombácz, 2006) .

Table 2.1. Chemical composition of the sepiolite powder (before homoionizaton process) obtained by X-ray fluorescence.

Compound	Concentration (weight %)
SiO_2	60.47
Al_2O_3	1.99
Fe_2O_3	0.67
MnO	0.03
MgO	25.29
CaO	0.25
Na_2O	0.17
K_2O	0.51
TiO_2	0.12
P_2O_5	0.04
LOI (lost by ignition)	10.04

The zeta potential of the homoionized sepiolite particles (SP in Figure 2.1) was negative in the entire pH interval studied. This is typically the case of other similar compounds as silica, bentonite, and homoionized montmorillonite (Galindo-González et al., 2005) (Arroyo & Gonz, 2000) (Abrougui et al., 2018). Nevertheless, in sepiolite clays it seems that the interfacial potential is strongly dependent on the origin and treatment of the clay particles. For natural sepiolite (without any physical or chemical treatment) the particles have an isoelectric point at pH ≈ 6 (Kara et al., 2003) (Alkan et al., 2005), although the substitution of the exchange divalent cations by monovalent ones provokes that the positive branch of the zeta-potential, at pH < pH(iep), disappears (Alkan et al., 2005). In fact, for natural palygorskite clays, which have a structure and chemical composition practically identical to sepiolite (Murray, 2000), treated with solutions of alkaline ions or, alternatively, dispersed in acid solution to remove impurities as carbonates, negative values of the zeta potential have been reported at both acid and basic pH intervals (Xu & Wang, 2012) (Zhang et al., 2015). Therefore, when the impurities are removed, or the exchange multivalent cations are replaced by monovalent ones, the electrochemistry of the solid/liquid interface of the sepiolite particles is mainly dominated by the reactions with the silanol (Si-O-H) groups, as in the case of silica particles.
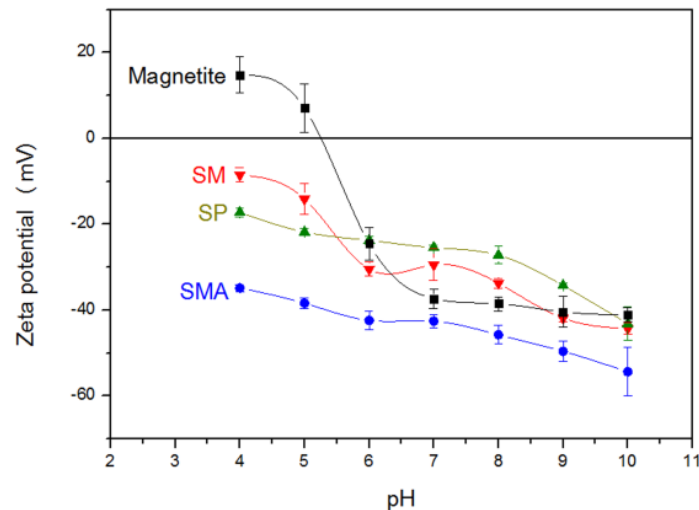
Figure 2.1. Zeta potential as a function of the pH in suspensions of the indicated particles. Magnetite: magnetite nanoparticles. SP: homoionized sodium sepiolite particles. SM: magnetite-covered SP particles. SMA: SM particles with alginate molecules adsorbed. Ionic strength of the solution 1 mM NaCl.

The negative surface charge of the SP particles favoured the adsorption of the Fe(III) and Fe(II) ions, and the subsequent formation of magnetite particles when OH$^-$ ions were added during the synthesis process described in Section 2.2.2. In this reaction, the pores in the SP particles acted as attachment points for the growth of magnetite nanoparticles. The zeta potential of the resulting particles (SM, Figure 2.1) was clearly the result of such coverage. A similar behaviour was reported for magnetite-covered attapulgite (Liu et al., 2008) (attapulgite and palygorskite are synonymous). In a recent work (Ahribesh et al., 2017), devoted to the synthesis of magnetite-covered sepiolite, the pH corresponding to the point of zero charge of the composite particles was found at pH = 6.6, in between of those corresponding to sepiolite (pH = 7.4) and magnetite (pH = 4.8).

Finally, the SM particles were functionalized by adsorption of alginate molecules and, as a consequence, the zeta potential suffered a significant increase in absolute value (SMA, Figure 2.1). In principle, the adsorption of alginate molecules, negatively charged because of the dissociation of the carboxylic group, on the negatively charged particles, should be hindered by electrostatic repulsion. Nevertheless, the great affinity of carboxylate ions for the Fe and Si ions present in the surface of these composite particles provoked their chemisorption by formation of coordinate compounds. This behaviour has been extensively observed in similar systems in which polyelectrolytes

that bear carboxylate groups produce surface compounds with clay minerals or iron oxides (Ramos-Tejada et al.,2003) (Illés & Tombácz, 2006) (Vicente et al., 2012).

The morphology of the SP, the composite particles, and the ferrogels were observed by electron microscopy (see Figure 2.2). The SP particles (Figure 2.2a) showed their typical rod-like or fibrillar shape with a high aspect ratio: the ratio length/diameter was around 1 µm/0.1 µm, although both length dimensions presented a wide size distribution. In the composite particles (SM, Figure 2.2b), spheroidal granules of magnetite nanoparticles appeared attached on the surface of the SP particles. In fact, the EDX (electron dispersive X-ray; see Figure 2.3) microanalysis carried out in the same SEM microscope clearly demonstrated the presence of significant amounts of iron atoms: the peaks of Fe had practically the same intensity than the Si ones. The pictures of the SMA particles (Figure 2.2c) showed that the alginate layer favoured a smoother surface texture than that in the SM particles.

More interestingly, for the goal of the present work, Figure 2.2d shows the microstructure of the magnetic hydrogel (Ferrogel-1). In this picture the more brilliant regions (coloured in false light blue colour) correspond to the heavier atoms (silicon and mainly iron), while the less brilliant regions (brown colour) correspond to the lighter atoms. Thus, we can clearly distinguish the magnetic composites (SMA) from the polymer fibres. The particles did not seem only randomly embedded in the polymer network, but also linked by multiple bonds to the alginate chains. This fact demonstrated the relevant role played by the alginate molecules adsorbed on the particles: both the alginate molecules in the pre-gel solution and those previously adsorbed on the particles should be cross-linked to each other by calcium ions. Therefore, the SMA particles were embedded as knots in a highly entangled network, which will have important effects on the magneto-rheological response of the ferrogels, as we will see in Section 2.3.3.
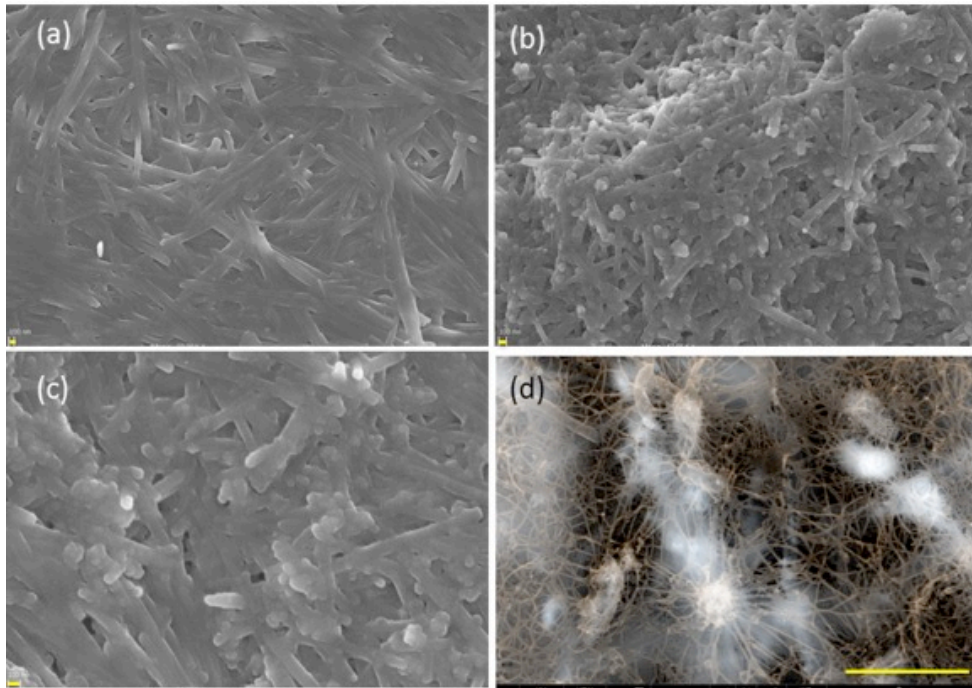
Figure 2.2. Electron microscopy pictures of: a) SEM – sepiolite after homoionization (SP); b) SEM – magnetite-covered sepiolite (SM); c) SEM – SM particles covered by alginate (SMA); d) environmental SEM – ferrogel (SMA particles in alginate hydrogel). Bar lengths in yellow: (a), (b), (c) 100 nm (see short line in lower left corner); d) 3 μm.
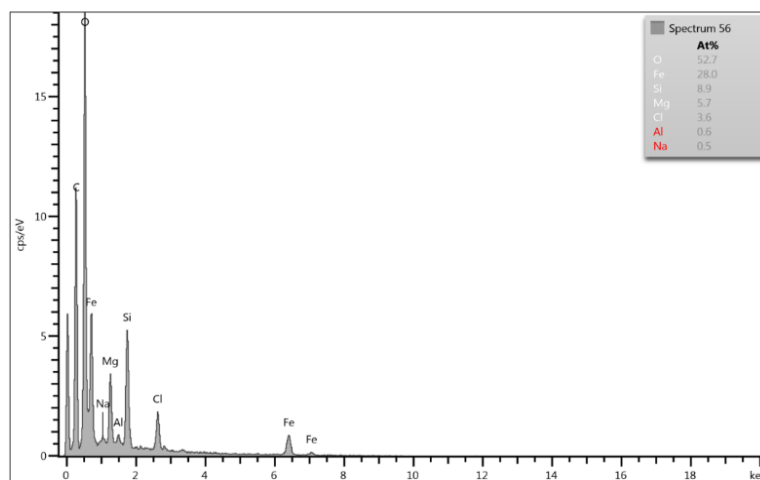
Figure 2.3. Electron dispersive X-ray (EDX) microanalysis of the magnetite-covered sepiolite particles.

As mentioned in the Introduction section of this chapter, one of the advantages of using the SM composite particles is their low average density, as compared with that of pure magnetite, which could make negligible their gravitational settling in the pre-gel solution. Unfortunately, the SM particles settled too fast in water as shown in Figure 2.4. Note that, as demonstrated in a previous work (Galindo-González et al.,

2005), in the total balance of the colloidal forces in clay or clay-magnetite suspensions, usually the long-range van der Waals attraction dominates over the (short range) electrostatic repulsion. Likely, the resultant colloidal force among the particles gave raise to bundle-like aggregates that settled in less than one hour, which was too fast considering the slow kinetics of the gelation process. On the contrary, the SMA suspension remained stable (Figure 2.4) during a high enough time to avoid phase separation during the gelation process.
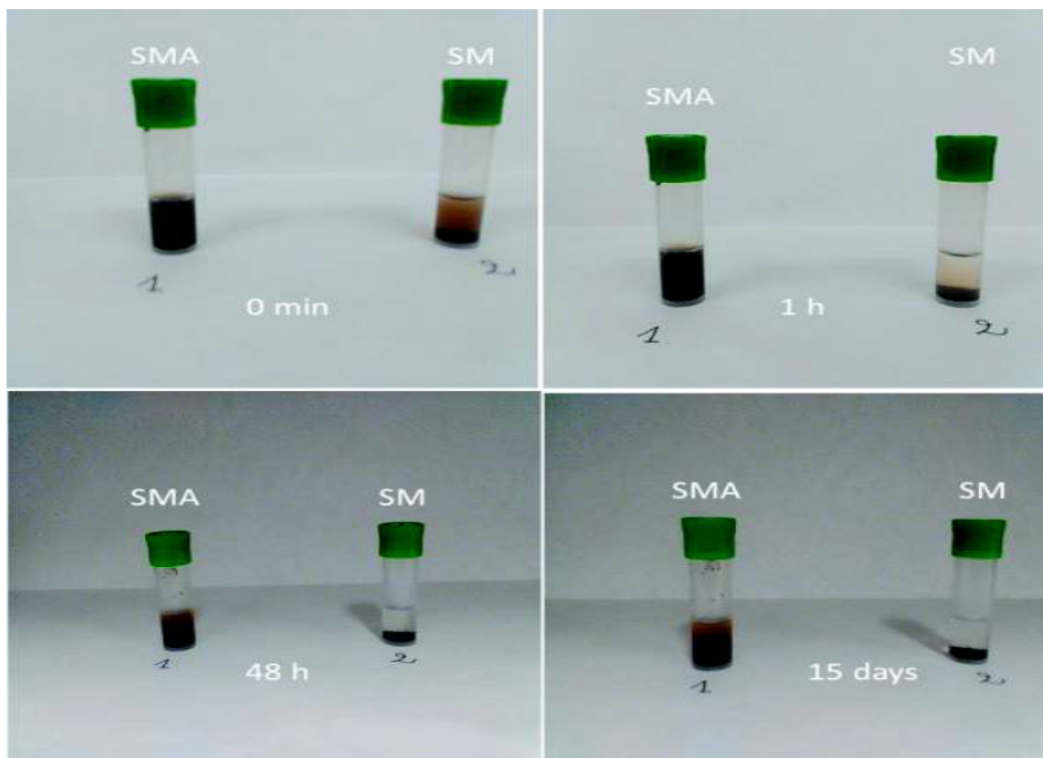
Figure 2.4. Gravitational settling in aqueous suspensions of SM and SMA particles from their preparation (0 min) up to 15 days after particle dispersion.

We have to take into account that the molecular weight of the sodium alginate salt employed ranged between 80,000 and 120,000 g/mol. Thus, the alginate layer provoked a strong electro-steric repulsion among the SMA particles that consequently remained either as individual entities or as aggregates of only a few particles (see Figure 2.2d).

The following step in the particle characterization was to analyse the magnetic properties of the obtained composite particles. Figure 2.5a shows the first magnetization curve of the SM and SMA dry powders, that is the magnetization (M) as a function of the applied magnetic field intensity (H) in the range from 0 kA/m to 374 kA/m. The magnetic susceptibility (χ) and saturation magnetization (M_S) of the SM and SMA particles can be estimated by fitting the data to the Frölich-Kennely equation (Jiles, 1998):

$$M = \frac{\chi M_S H}{M_S + \chi H}$$
(1)

The best fitting parameters were for SM powder: χ = 4.61 $\pm$ 0.08, M_S = 216.3 $\pm$ 1.0 kA/m (coefficient of determination r^2 = 0.992). And for SMA: χ = 6.55 $\pm$ 0.13, M_S = 169.9 $\pm$ 0.6 kA/m (r^2 = 0.988).

In addition, the actual content of magnetic phase in the composite particles can be obtained by considering the mixing law (Rosensweig, 1985):

$$M_{SC} = \phi M_{S,m}$$
(2)

Where $M_{S,C}$ and $M_{S,m}$ are the saturation magnetization of the composite particles (SM or SMA) and bulk magnetite, respectively, and ϕ the volume fraction of magnetic material in the solid particles. Taking into account that $M_{S,m}$ = 446 kA/m, the content of magnetic material in the SM and SMA particles was ϕ(SM) = 48% and ϕ(SMA) = 38%. These results seem reasonable because the presence of the alginate layer in SMA particles diminished the relative volume concentration of magnetite in the composite.

In Figure 2.5b the magnetization loops are included. Both powders behaved as magnetically soft materials because the remnant magnetization (M_R) and the coercitivity (H_C) were negligible. Their values (see the plot inserted in Figure 2.5b), M_R = 1.0 kA/m, H_C = -0.18 kA/m for SM powder; and M_R = 0.3 kA/m, H_C = -0.04 kA/m for SMA powder, were of the same order than the experimental error of the VSM apparatus. This magnetically soft behaviour in the SM composites was also stated in a recent work that described a different synthesis route for obtaining magnetite-covered sepiolite particles (Ahribesh et al., 2017).
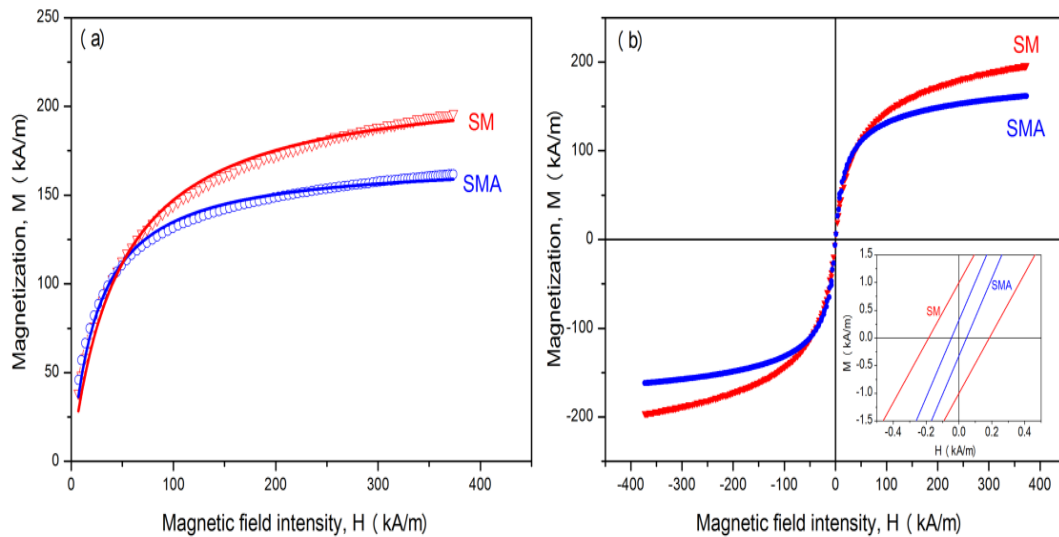
Figure 2.5. Magnetization as a function of the intensity of the applied magnetic field for SM and SMA composite powders. a) First magnetization curve; the lines correspond to the best fits to equation (1). b) Magnetization loop, H varies along the cycle 374 – 0 – (-374) – 0 – 374 kA/m; the insert shows the region of very low field.

2.3.2. Rheology of suspensions

Before analysing the magneto-rheological behaviour of the magnetic hydrogels, it is convenient to study the MR response of the SM and SMA suspensions for determining the particle concentration required for: i) Achieving a high enough MR effect, and ii) obtaining homogeneous ferrogels. This second point must be considered because an excessive particle concentration provokes the formation of lumpy or too fragile (or even fissured) ferrogels, as demonstrated in a previous work with iron/alginate ferrogels (Gila-Vilchez et al., 2018).

The rheograms (shear stress vs. shear rate) of SM and SMA suspensions are included in Figure 2.6. The particle concentration range did not exceed 10% w/v because of the above-mentioned requirement (ii). In both suspensions, the application of even a stress as low as 1 Pa led to shear rates $\dot{\gamma} \approx 100$ s^{-1}. In the SM suspensions (Figure 2.6a) and, especially for the higher concentrations (7% and 10% w/v), there were two regions in the rheograms. For low rates the SM suspensions showed a shear-thinning behaviour: the slope of the rheogram (the viscosity) decreased progressively; while for high rates a shear-thickening response was observed (the viscosity increases). For example, for 7% and 10 % concentrations, the transition occurred at $\dot{\gamma}$ = 90 s^{-1}. This

transition from shear-thinning to shear-thickening has been described by (Wagner & Brady, 2009) considering the balance between hydrodynamic and Brownian forces given by the Péclet number:

$$Pe = \frac{\sigma a^3}{kT} \qquad\qquad (3)$$

Where σ is the shear stress, *a* the particle hydrodynamic radius, *k* the Boltzmann constant, and *T* temperature.
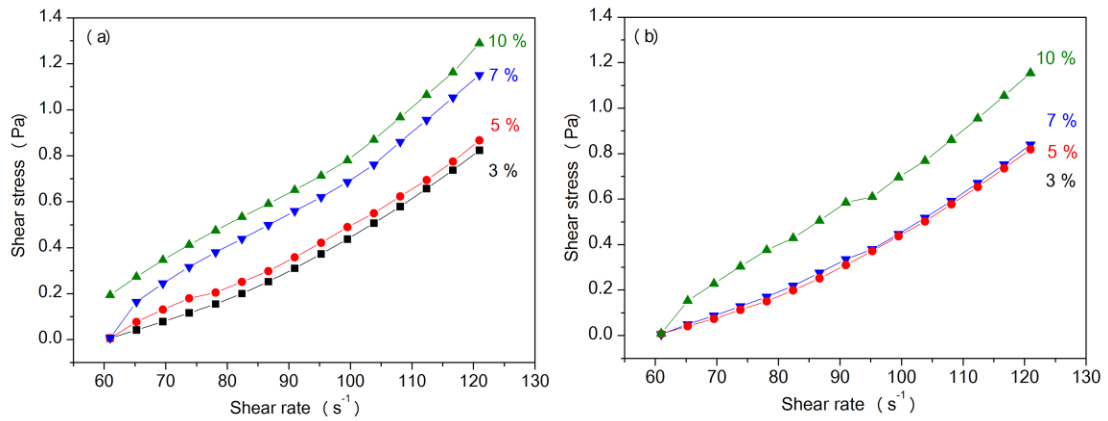
Figure 2.6. Rheograms of suspensions with the indicated particle concentration (% w/v) in the absence of applied magnetic field. a) SM particles. b) SMA particles.

Following the description given in (Wagner & Brady, 2009), there are three possible regions: i) for Pe < 1, the viscosity is constant (Newtonian fluid); ii) for Pe = 1 – 10 the viscosity decreases (shear-thinning behaviour); and iii) for Pe > 10 the viscosity increases (shear-thickening). In the 7% and 10 % w/v SM suspensions, for $\dot{\gamma} \approx 90$ s^{-1} the shear stress is σ ≈ 0.5 Pa, and taking *a* ≈ 1 µm, the Péclet number is Pe = 122, well into the region of hydrodynamic-driven interactions. From a microscopic point of view, in this region the hydrodynamic forces provoke the formation of hydroclusters in which the particles are impeded to flow around each other, which leads to an abrupt increase in viscosity.

The analysis in (Wagner & Brady, 2009) was done for concentrated (ϕ > 10%) suspensions of spherical particles. Although we have suspensions with not so high particle concentration, the particles are far from being spherical and, consequently,

the formation of clusters with difficult internal movement at high shear can appear at much smaller particle concentration than for spheres. Moreover, this is so if one considers that, as demonstrated in previous works (Kuzhir et al., 2010) (Gómez-Ramírez et al., 2010), in fiber-like suspensions the particle-particle solid friction considerably hinders the relative movement of particles inside bundle-like aggregates. On the other hand, as predicted in (Wagner & Brady, 2009), when the particles were functionalized with large molecules (SMA particles), imparting electro-steric repulsion between the particles, the viscosity values reached in the shear-thickening region were considerably reduced. In fact, this decrease is evident if we compare the maximum viscosities reached in the 7% and 10% SM suspensions (9.5 mPa·s and 10.7 mPa·s, respectively) with those for the same concentrations in the SMA suspensions (6.9 mPa·s and 9.6 mPa·s).

The next question arises about the strength of the MR effect in SM and SMA suspensions. For this purpose, the corresponding rheograms (Figure 2.7) were obtained in the range of low-moderate magnetic fields.

For SM suspensions (10% w/v concentration; Figure 2.7a), the general trends of the rheograms obtained with magnetic field applied were similar to those in the absence of field: an initial shear-thinning region (up to $\dot{\gamma} \approx 70$ s^{-1}) followed by a shear thickening region, although the most important feature was the high MR effect. If we quantify the intensity of the MR effect (at a given shear rate) as:

$$MRE - \sigma(\%) = \frac{\sigma(H \neq 0) - \sigma(H = 0)}{\sigma(H = 0)} \times 100 \qquad (4)$$

Then, for example, at $\dot{\gamma} = 100$ s^{-1} and H = 43 kA/m, MRE-σ (%) = 7650% which was quite large taking into account that the particle concentration was 10% w/v, and that the content of magnetite in the solid phase is 48% v/v.
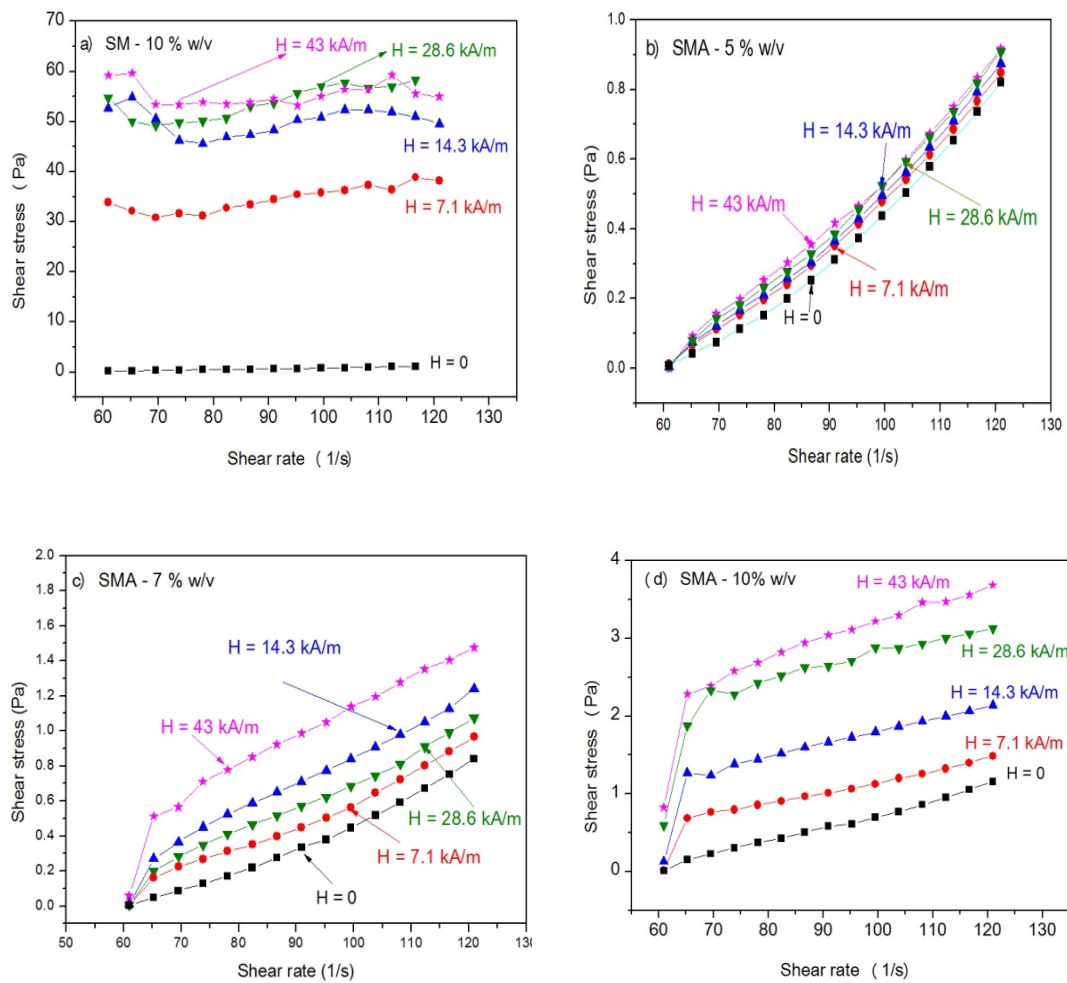
Figure 2.7. Rheograms of the suspensions in the presence of the indicated magnetic fields, containing the following particles: a) SM particles, concentration 10 % w/v. b), c), and d) SMA particles for particle concentrations 5%, 7%, and 10% w/v, respectively. Note that the scales in the Y-axes are different.

In the SMA suspensions the trends of the rheograms under field application (Figures 2.7b-7d) were completely different to those in SM suspensions. The initial (at low shear rate) shear-thinning region was absent for all values of the applied field, and only a slight shear-thickening behaviour remained in the curves for 5% and 7% w/v concentrations. More interestingly, the MR effect was considerably weaker than in the SM suspension (see Table 2.2), reaching a maximum for the SMA suspensions with 10% w/v concentration (Figure 2.7d): at $\dot{\gamma}$ = 100 s^{-1} and H = 43 kA/m, MRE-σ(%) = 360%.

Table 2.2. Intensity of the MR effect for SM and SMA suspensions obtained from data in Figures 7 and 8. The parameter MRE-σ(%) was calculated by means of equation (4), and MRE-G'(%) by equation (5). Δσ = σ (H ≠ 0) − σ (H = 0), and ΔG' = G' (H ≠ 0) − G' (H = 0).

Sample	H (KA/m)	σ (Pa)	Δσ (Pa)	MRE-σ (%)
Suspension of SM particles (10% w/v)	0	0.7	–	–
	43	54.25	53.55	7650
Suspension of SMA particles (5% w/v)	0	0.4	–	–
	43	0.5	0.1	25
Suspension of SMA particles (7% w/v)	0	0.4	–	–
	43	1.1	0.7	175
Suspension of SMA particles (10% w/v)	0	0.7	–	–
	43	3.2	2.5	360
Sample	H (KA/m)	G' (Pa)	ΔG' (Pa)	MRE- G'(%)
Suspension of SMA particles (10% w/v)	0	3.6	–	–
	43	215	211.4	5872

This decrease in the MR effect can be explained considering that the alginate layer in the functionalized SMA particles imposed a steric barrier to the field-induced chaining of the particles. Therefore, as the particles were not in very close contact, the dipole-dipole magnetic interaction was significantly smaller and, consequently, the MR effect was reduced.

The results in Figure 2.7 correspond to the steady state magnetorheology of the suspensions under a very large shear strain. However, for particles embedded into the polymer network, only a slight strain would be needed to induce the breakage of the hydrogel. Therefore, it seemed convenient to determine the magnetorheological behaviour of the SMA suspensions in conditions of small strain. This study can easily be performed by oscillometry, in order to obtain the elastic (or storage) modulus in the absence and presence of magnetic field.

The results obtained for SMA suspensions are plotted in Figure 2.8. In these plots there is a first region in which the elastic modulus (G') weakly depends on the strain amplitude (γ_0) (the so-called linear viscoelastic region, LVR) followed by an abrupt

decrease in G' when the field-induced structures of the systems are disrupted (the non-linear viscoelastic region, N-LVR).
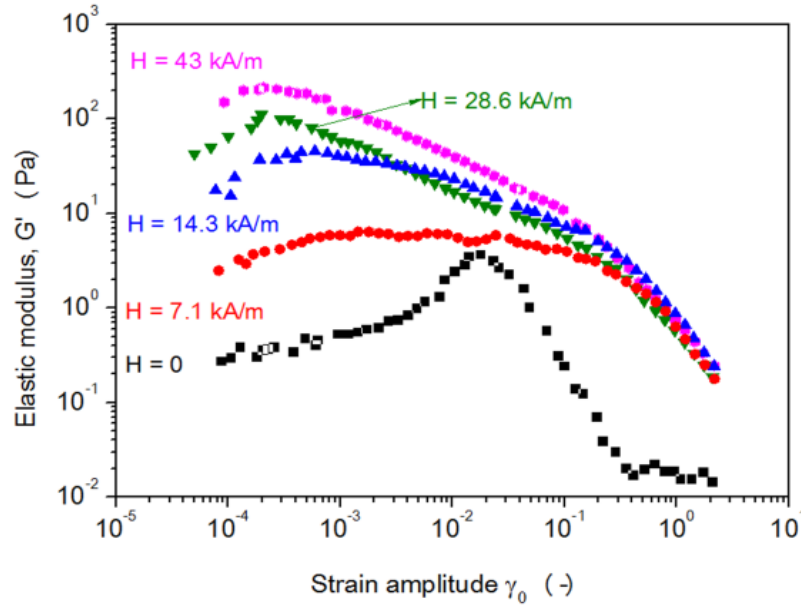
Figure 2.8. Elastic modulus as function of the strain amplitude (at constant frequency of 1 Hz) for SMA suspensions (10% w/v) in the presence of the indicated magnetic fields.

In the LVR, the elastic modulus (G') slowly increased with the strain up to a maximum (the critical strain, γ_c) before going into the N-LVR. The critical strain can be interpreted as the strain reached immediately before the breakage of the microstructure of the suspension. As demonstrated in previous works (Kuzhir et al., 2010) (Gómez-Ramírez et al., 2010), in suspensions of fiber-like magnetic particles, the progressive increase in G' in the LVR is due to the rising in the (field-dependent) static friction between the particles inside the bundle-type columns generated by the field. The values of G' at γ_c can be taken to quantify the intensity of the MR effect, by means of:

$$MRE - G'(\%) = \frac{G'(H \neq 0) - G'(H=0)}{G'(H=0)} \times 100 \qquad (5)$$

Taking G'(H = 43 kA/m) and G'(H = 0) from Figure 2.8, the intensity of the MR effect given by equation (5) for SMA suspensions (10% w/v) is 5872 % (Table 2.2). This value is higher than that obtained in a previous work (Gómez-Ramírez et al., 2009) with suspensions of ferromagnetic Co-Ni nanofibres (56 nm length; 5% v/v concentration) in

which MRE-G'(%), in the field range 0 – 57 kA/m, was around 500%, although certainly the Co-Ni particles were much smaller than the SMA particles. A better comparison could be done with another previous work (Bell et al., 2008) with suspensions of iron fibres (5.4 – 7.6 microns in length; 2 – 6% v/v concentration), in which the MR effect was determined by estimating the dynamic (or Bingham) yield stress of the suspensions under field application. In that work, for a magnetic flux density of around 50 mT, the maximum yield stress reached (for longest particles and the highest concentration employed), was around 1.2 kPa, while in the absence of field the yield stress was approximately 0.1 kPa. Taking these values, the intensity of the MR effect would be around 1100 %, which is an intermediate value between those calculated by equation (4) for the SM suspension (7650%) and SMA (360%) suspensions –see Table 2.2 for suspensions with particle concentration 10% w/v. Nevertheless, note that this comparison, by means of equation (4), corresponds to experimental conditions in which the field-induced structure of the suspensions is completely broken, while the comparison using equation (5) is related to the strain at the initial breakage of the suspensions.

2.3.3. Rheology of magnetic hydrogels

For the preparation of the magnetic hydrogels, 2.5 mL of the 10 % w/v suspension of SMA particles were mixed with 2.5 mL of alginate solution, 5 mL of $CaCl_2$ solution, 22.5 mg of $CaCO_3$ and 26.7 mg of GDL (see Section 2.2.3). Then, the final concentration of SMA particles in the ferrogels was approximately 2.5% w/v. Thus, the expected MR effect in the ferrogels should be lower than those experienced by the SMA suspensions, due to the smaller concentration of the magnetic particles, and also because in the ferrogels the particles were embedded within a viscoelastic medium, instead of dispersed in water as they were in the suspensions. Besides that, the moderate fields (up to H = 43 kA/m) achievable by the coil used in the rheometer Mars III (employed for SM and SMA suspensions) were not capable to provoke a significant strengthening of the ferrogels. For this reason, the characterization of the ferrogels was carried out in a Physica MCR 300 magneto-rheometer, in which the applied field was considerably more intense.

Two different ferrogels were prepared with different alginate concentrations in the pre-gel solution (see step (ii) in Section 2.2.3): 0.25 g/50 mL (0.5 % w/v) in "Ferrogel-1", and 0.5 g/50 mL (1 % w/v) in "Ferrogel-2". Figure 2.9 shows the viscoelastic moduli obtained as the amplitude of the shear strain was increased in a wide enough interval to sweep from the LVR to well into the N-LVR. The moduli were measured for H = 0 and for strong magnetic fields (H > 100 kA/m).

Firstly, it is interesting to comment the behaviour in the absence of magnetic field. The two ferrogels prepared behaved as viscoelastic solids because G' > G" in the LVR, which extends up to the critical strain $\gamma_c \approx 3$ (300 %) where a maximum in G" was reached. At the critical strain, the microstructure of the hydrogels began to break, and after that the hydrogels behaved as viscoelastic liquids (G" > G') with a progressive decrease in stiffness (both G' and G" suffered a quick drop).

Secondly, from the analysis of the results for the different alginate concentrations studied (Ferrogel-1 vs. Ferrogel-2) it can be concluded that Ferrogel-2 (F2) was significantly more rigid in the LVR than Ferrogel-1 (F1). To be precise, the G' values were as follows (see Tables 2.3 and 2.4):

i)   For a strain amplitude γ_0 = 0.03 (3 %), G' (F1) = 20550 Pa and G' (F2) = 27180 Pa, which represents a relative increment of 32.3% in the elastic response.

ii) For γ_0 = 0.1 (10 %), G' (F1) = 28450 Pa and G' (F2) = 35810 Pa, increment 25.8 %. These last values were close to those reached at the maximum in the G'-γ_0 curves, which were: G' (F1) = 30590 Pa and G' (F2) = 38660 Pa, increment 26.3 %.
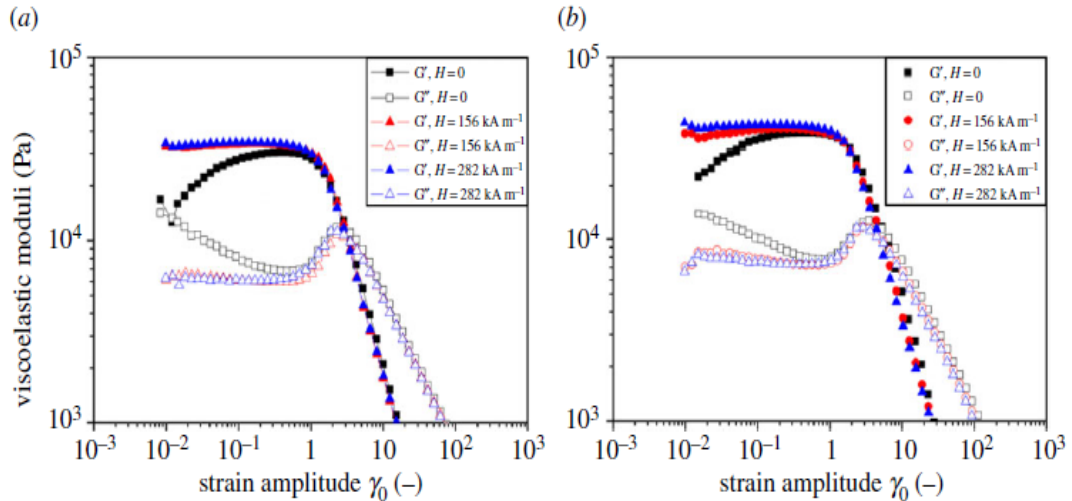
Figure 2.9. Viscoelastic moduli (G' elastic modulus, solid symbols; G'' viscous modulus, open symbols) as a function of the oscillatory strain amplitude for the indicated magnetic field intensities. Frequency 1 Hz. a) "Ferrogel-1"; b) "Ferrogel-2" (see section 2.2.3).

In addition, for both ferrogels, in the absence of applied field, as the strain was increased up to $\gamma_c \approx 300$ %, the elastic response was progressively larger. This behaviour is not usual in elastic solids because in the LVR the G' values are practically constant. Nevertheless, we have to take into account that the microstructure of these gels was a network in which the knots were occupied by magnetic particles linked to the polymer chains. In consequence, at very low strain a part of the net was expected to be relaxed (lower G'). Thereafter, as the network was progressively stretched, more and more branches withstood the mechanical stress. This fact, at the macroscopic scale, should imply a progressive increase in G'. Obviously, when the maximum stretching was reached, the break point was achieved.

Table 2.3. Intensity of the MR effect for "Ferrogel-1" and "Ferrogel-2" (see Section 2c) obtained from data in Figure 2.9. MRE-G' (%) calculated by means of equation (5). $\Delta G' = G'(H \neq 0) - G'(H = 0)$. Data for strain amplitude $\gamma_0 = 0.03$.

Strain amplitude $\gamma_0 = 0.03$ (3%)				
Sample (alginate concentration in pre-gel solution)	H (KA/m)	G' (Pa)	$\Delta G'$ (Pa)	MRE-G' (%)
"Ferrogel-1" (0.5 g/50 mL)	0	20550	–	–
	156	32980	12430	60
	282	33610	13060	64
"Ferrogel-2" (1 g/50 mL)	0	27180	–	–
	156	37480	10300	38
	282	41700	14520	53

Table 2.4. Similar to Table 2.3, but for a strain amplitude $\gamma_0 = 0.1$ (10%)

Strain amplitude $\gamma_0 = 0.1$ (10%)				
Sample (alginate concentration in pre-gel solution)	H (KA/m)	G' (Pa)	$\Delta G'$ (Pa)	MRE-G' (%)
"Ferrogel-1" (0.5 g/50 mL)	0	28450	–	–
	156	33960	5510	19
	282	34600	6150	22
"Ferrogel-2" (1 g/50 mL)	0	35810	–	–
	156	40050	4240	12
	282	42500	6690	19

When an external field was applied, the magnetic particles located in the knots of the network were expected to be brought closer as a consequence of their magnetic attraction and, consequently, the elastic modulus should increase, leading to a significant MR effect in the ferrogels. This effect was evident for low enough strain values, approximately for $\gamma_0 < 1$ (100 %). Nevertheless, as the network was stretched, the magnetic particles were compelled to separate and the dipole-dipole magnetic force decayed; therefore, the MR effect was progressively smaller, as observed in Figure 2.9. Eventually, as the critical strain was approached, the mechanical response of the gels depended only on the network deformation, without any significant role of the magnetic attraction between particles. For this reason, the curves for the different applied magnetic fields overlapped at a relatively large strain (300 %).

The data in Tables 2.3 and 2.4 indicate that the intensity of the MR effect depends on the strain amplitude, the magnetic field intensity, and the alginate concentration in the pre-gel solution, as summarized below.

i) Strain amplitude. The highest values of the MR effect (MRE-G', equation (5)) were reached for the lowest values of strain amplitude. Thus, when the value of γ_0 was increased from 3% (Table 2.3) to 10% (Table 2.4) the MRE-G' values were approximately reduced to a third in the case of Ferrogel-1 (from 60-64 % to 19-22 %) and also in the case of Ferrogel-2 (from 38-53 % to 12-19 %), being practically null for γ_0 > 100%.

ii) Magnetic field. For the maximum applied field (282 kA/m), the maximum MRE values was achieved. This ranged between 64% in the case of Ferrogel 1 at γ_0 = 3%, and 19% for Ferrogel-2 at γ_0 = 10%. The increase of the MRE-G' values as H increased from 156 kA/m to 282 kA/m, was relatively low in practically all cases (only for Ferrogel-2 at γ_0 = 3 % there was a moderate increment from 38% to 53%), indicating that for large enough fields (H > 100 kA/m) the MR effect was close to saturation. This is logical since the slope of the first magnetization curve was considerably reduced for fields larger than 100 kA/m.

iii) Alginate concentration. This was the dominant factor facing the magnetic-induced reinforcement of the magnetic gels because an excessively rigid hydrogel (Ferrogel-2) largely hindered the achievable MR effect. On the contrary, if the hydrogel contained a very low density of cross-linked chains the resulting ferrogels were too soft to be handled.

The maximum intensity of the MR effect, especially in the case of Ferrogel-1 (up to 64%) was not negligible in comparison with those reached in previous works, even employing magnetic particles with a higher saturation magnetization or larger particle concentrations. For example, in (Zubarev et al., 2018), using polymer-covered magnetite spheres (diameter 110 nm) in a fibrin-agarose hydrogel the MR effect was 8%. In another recent work (Gila-Vilchez et al., 2018), with silica-covered iron spheres (diameter 1.4 μm) in alginate hydrogel, the MRE-G' value was around 700%.

A more quantitative comparison can be made if we consider the analytical model on the MR effect proposed by (Ginder et al.,1996) and reported by (Bossis et al., 2002). This model is based on a series of assumptions: i) spherical magnetic particles; ii) the magnetic attraction provokes the linear chaining of the particles; iii) the action of a mechanical shear stress produces the affine deformation of the particle chains; iv) very low strain under mechanical stress; v) intermediate applied field (H), that is well below the field required to reach the saturation magnetization (M_S) of the particles; and vi) particle volume fraction $\phi < 20\% - 30\%$. Following this model:

$$G = 3\mu_0 \phi H M_S \qquad (6)$$

Where μ_0 is the magnetic permeability of vacuum. Therefore, being conscious of the limitations of the Ginder's model and, knowing in particular that the assumptions (i)-(iii) were not accomplished in the ferrogels of the present work, we can define a normalized MRE-G' parameter by means of the following dimensionless expression:

$$\overline{MRE}(\%) = (MRE - G')(\%)\frac{M_{S,0}}{M_S}\frac{H_{max,0}}{H_{max}}\frac{\phi_0}{\phi} \qquad (7)$$

Where MRE-G' is calculated by equation (5); H_{max}, M_S and ϕ are, respectively, the maximum field applied to the ferrogel, the saturation magnetization of the particles, and the particle volume fraction (% v/v) of the ferrogels, for the systems reported in (Gila-Vilchez et al., 2018) (Zubarev et al., 2018). The quantities with subscript "0" correspond to the case of Ferrogel-1 of the present work: $H_{max,0}$ = 282 kA/m, $M_{S,0}$ = 169.9 kA/m, and ϕ_0 = 0.93% v/v –calculated from the particle concentration in Ferrogel-1 (2.5 %w/v), and the average density of the SMA particles (2.7 g/cm^3). By doing so, the $\overline{MRE}(\%)$ values mainly depend on the shape of the particles embedded in the ferrogels, normalizing for the rest of the significant experimental parameters, according to the Ginder's model.

Table 2.5. Comparison between MR effects developed by different magnetic hydrogels (see text).

Ferrogel (reference)	Composition (Particles /Polymer in hydrogel)	M_S (kA/m)	H_{max} (kA/m)	ϕ (% v/v)	MRE-G' (%)	$\overline{MRE}$ (%)
Ferrogel-1 (present work)	Rod-like Fe_3O_4-sepiolite / alginate	169,9 [a]	282 [a]	0.93 [a]	64	64
Ref. (Zubarev et l., 2018)	Spherical polymer-Fe_3O_4 / Fibrin-agarose	161	48.6	3.5 [b]	8 [b]	11.4
Ref. (Gila-Vilchez et al., 2018)	Spherical silica-Fe / alginate	1587	282	4.6 [c]	700 [c]	15.2

[a] $M_{S,0}$, $H_{max,0}$, and ϕ_0 in equation (7)
[b] Taken from Fig. 5 in Ref. (Gila-Vilchez et al., 2018)
[c] Taken from Fig. 10 in Ref. (Zubarev et l., 2018)

From these data, and the $\overline{MRE}$ (%) values summarized in Table 2.5, we can state that:

i) The rod-like particles of Ferrogel-1 provoked a considerably larger normalized MR effect (64 %) than the spherical magnetite particles of the magnetite/fibrin-agarose ferrogel of (Zubarev et al., 2018) (11.4 %). Even more, the effect is more noticeable if we take into account that the fibrin-agarose hydrogels (without particles) were softer (rigidity modulus G = 47 Pa (Zubarev et al., 2018) than the alginate ones (without particles, G' ≈ 10^3 Pa (Gila-Vilchez et al., 2018)).

ii) The composite particles employed in the present work provided a more intense magnetic control of the mechanical properties than the iron microspheres of the alginate ferrogels of (Gila-Vilchez et al., 2018), in which the normalized MR effect was 15.2 %. The difference is even more pronounced if we remember that the volume fraction of the magnetisable material in the clay-magnetite particles was ϕ(SMA) = 38%, while in the silica-covered particles of (Gila-Vilchez et al., 2018) the iron volume fraction was ϕ(Fe) = 93% –we have estimated this

last value by using the mixing law (equation (2)), with M_S(bulk Fe) = 1710 kA/m (Jiles, 1998) and M_S (iron powder in (Gila-Vilchez et al., 2018)) = 1587 kA/m.

In summary, the rod-like SMA composite particles provided a higher MR efficiency to ferrogels, as compared with spherical magnetisable particles.

2.4. Conclusions

Ferrogels are soft-wet materials with an internal microstructure that tends to elongate under the application of a magnetic field along the magnetic field lines and that recovers their previous state when the field is switched off. Such local field-induced structuration, as very recently (Borin et al., 2018) stated, confers to the ferrogels their metastable (far from thermodynamic equilibrium) and non-ergodic character. This character can be achieved if the ferrogels accomplish two conditions: First, they should be homogeneous at the macroscopic scale and, second, they should possess a strong enough response to external magnetic fields. These requirements demand a careful design of the system architecture at the microscale from the magnetic particle composition to the arrangement of the polymer network and, preferably, with a linkage between the particles and the polymer chains too.

Keeping in mind these arguments, we prepared ferrogels containing composite microparticles, consisting of a core of low density (sepiolite clay) covered by a layer of magnetite nanoparticles, dispersed in a polymer network of alginate molecules crosslinked by calcium ions. We chose an electrostatic crosslinking, mediated by the attraction between the positive-charged calcium ions and the negative-charged alginate molecules, instead of a covalent bonding, because the latter usually gives rise to too rigid hydrogels, in which the migration and chaining of the particles along the field lines is avoided. In addition, we functionalized the magnetic particles so that they could be integrated within the polymer network by electrostatic bonding with the polymer chains. Thus, the resulting ferrogels presented an internal structure with the particles embedded in the hydrogel as the knots of the network.

The magnetite layer on the clay particles was thick enough to confer to the composite particles a quite large magnetic response, capable of providing a very high

MR effect in aqueous suspensions, even for a rather low particle concentration of 10% w/v.

The SMA/alginate ferrogels, containing a particle volume fraction as low as 0.93% v/v, developed an MR effect of about 64%, under application of magnetic fields with intensity close to that required for the magnetic saturation of the particles. The MR effect reached significant values for shear strains smaller than 10%. At higher strains, the viscoelastic response of the magnetic gels was predominantly determined by the resilience of the particle-polymer network, and the magnetic forces lost their influence, due to the presumably large gap between the particles, which should make their magnetic attraction negligible.

As a final conclusion, we can state that the rod-like shape of the composite particles played a central role in conditioning the intensity of the MR effect. In fact, we used a parameter for the quantification of the MR effect that only takes into account the particle shape (normalizing by the saturation magnetization, the applied field strength, and the particle volume fraction). Using this parameter, the MR effect experienced by ferrogels based on rod-like particles (64%) became considerably larger than these experienced by ferrogels based on spherical microparticles (11 - 15%).

Chapter 3

Rheology of magnetic colloids containing clusters of particle platelets and polymer nanofibers

Summary

Magnetic hydrogels (ferrogels) are soft materials with a wide range of applications, especially in biomedicine because: (i) they can be provided with the required biocompatibility; (ii) their heterogeneous structure allows their use as scaffolds for tissue engineering; (iii) their mechanical properties can be modified by changing different design parameters and by the action of magnetic fields. These characteristics confer them unique properties for acting as patterns that mimic the architecture of biological systems. In addition, (iv) given their high porosity and high aqueous content, ferrogels can be loaded with drugs and guided toward specific targets for local (non-systemic) pharmaceutical treatments. The ferrogels prepared in this work contain magnetic particles obtained by precipitation of magnetite nanoparticles onto the porous surface of bentonite platelets. Then, the particles were functionalized by adsorption of alginate molecules and dispersed in an aqueous solution of sodium alginate. Finally, the gelation was promoted by crosslinking the alginate molecules with Ca^{2+} ions. The rheological properties of the suspensions of the composite particles and the ferrogels were measured in the absence/presence of external magnetic fields, showing that they exhibited a strong enough magnetorheological effect. The behavior of the ferrogels is explained considering the field-induced strengthening of the heterogeneous (particle-polymer) network generated inside the magnetic gel.

Chapter 3. Rheology of magnetic colloids containing clusters of particle platelets and polymer nanofibers

3.1. Introduction

The development of biocompatible hydrogels has received considerable attention in the last few decades due to a series of biomedical applications, among which it is worth mentioning their use as scaffolds in tissue engineering (Van Vlierberghe et al.,2011) (Ismail et al., 2011), for example bone or cartilage regeneration (Rezwan et al., 2006) (Park et al., 2009b), or alternatively as carriers for local drug delivery in cancer therapy (Norouzi et al., 2016).

Hydrogels can be defined as polymeric networks, capable of absorbing and retaining high amounts of aqueous solutions, without being dissolved in the liquid media. Usually, the polymer chains form three-dimensional structures generated by (chemical or physical) crosslinking among the polymer molecules. However, most hydrogels based on natural polymer suffer from a lack of mechanical strength, which usually limits their applications in a variety of fields. Many efforts have been devoted to improving the stiffness of the hydrogels. Among them, the combination of organic-inorganic compounds through blending of polymers with nanoparticles has received special attention because of its excellent mechanical resilience when compared with conventional hydrogels (Haraguchi & Takehisa, 2002) (Hu & Chen, 2014). In this context, the use of magnetic particles seems a promising approach because of their field-responsive properties (Lopez-Lopez et al., 2016) (Gila-Vilchez et al., 2019). In addition, the use of composite magnetic particles of low average density has been proved as a good way to avoid the heterogeneous distribution of the particles inside the ferrogels (Bonhome-Espinosa et al., 2017). Furthermore, if the composite particles have low density and elongated shape (e. g. sepiolite-magnetite), the magnetic control of the mechanical properties of the resulting ferrogels can be considerably improved (Abrougui et al.,2019).

On the other hand, facing biomedical applications, natural polymers are usually preferred instead of synthetic ones because they satisfy the required biocompatibility of the resulting gels. Among natural polymers, polysaccharides, peptides, and proteins have a demonstrated capability for generating these kind of soft-wet biomaterials

Chapter 3. Rheology of magnetic colloids containing clusters of particle platelets and polymer nanofibers

(Gila-Vilchez et al., 2019) (Contreras-Montoya et al., 2018). In particular, alginate is a natural polysaccharide of particular interest because is soluble in water, relatively inexpensive, non-toxic, and biocompatible. The molecule of sodium alginate bears carboxylate groups and has the ability to form hydrogels by electrostatic interaction with divalent cations (especially Ca^{2+}) at room temperature. This kind of physical crosslinking is the key characteristic for the formation of the alginate hydrogels employed in this work (Kuo & Ma, 2001) (Abrougui et al., 2019).

The aim of the present chapter is to prepare, and study the physical properties, of ferrogels consisting of magnetic particles embedded into a matrix of alginate hydrogel. The magnetic particles were synthetic composites of low density containing a core of clay covered by magnetite nanoparticles. The clay chosen was bentonite because the particles of this mineral have a plate-like shape and, according to our previous experience (Abrougui et al., 2019), the magnetorheological (MR) response of ferrogels based on elongated particles can be significantly stronger than that of ferrogels based on spherical particles. In this chapter, we first describe the synthesis of the clay-magnetite composites. Then, we analyze their more relevant physico-chemical characteristics (including magnetization curves) by different techniques. After that, we describe and discuss the rheological behavior of both the bentonite-magnetite ("BMag" in what follows) aqueous suspensions and the BMag-alginate ferrogels, in the absence/presence of magnetic fields.

3.2. Materials and methods

3.2.1. Materials

The raw bentonite material used in this study was collected from Zaghouan (Northeast of Tunisia). It was subjected to a purification process using the so-called hydrocyclone separation method, previously described in detail in (Abrougui et al., 2018) (Abrougui et al., 2019). This process allowed removing impurities present in the raw material (mainly calcite and quartz), and also the change of the original calcium exchange ions present in the raw clay mineral by sodium ones. The main characteristics of the purified bentonite employed in the present work were (Abrougui et al., 2018) : I) Bulk

chemical composition, obtained by X-ray fluorescence, in weight percentage: 49.28% SiO_2, 20.82% Al_2O_3, 6.98% Fe_2O_3, 3.74% CaO, 2.80% MgO, 1.94% Na_2O, 2.02% K_2O, 0.11% P_2O_5, 1.08% TiO_2, 0.02% MnO; ii) cation exchange capacity 64 meq/100 g; iii) specific surface area 70 m^2/g; iv) the thickness (a) and length (L) of the bentonite platelets were (mean ± standard deviation) a = 0.33 ± 0.06 μm and L = 2.3 ± 0.4 μm, and the corresponding aspect ratio (a/L) = 0.14 ± 0.05.

The chemicals employed (supplied by Sigma-Aldrich, USA) in the synthesis of the composite bentonite-magnetite particles were: $FeCl_3 \cdot 6H_2O$ (98%), NH_4OH aqueous solution (25% NH_3), and $FeCl_2 \cdot 4H_2O$ (98%). For the preparation of the alginate hydrogels the reagents used, without further purification, were: sodium alginate (Across Organics, USA, Sigma Aldrich CAS number 9005-38-3), $CaCl_2$ (anhydrous, minimum 96.0%, Sigma Aldrich, USA), D-(+)-Gluconic acid δ-lactone (GLD) (> 99.0%, Sigma Aldrich, USA, CAS number 90-80-2), and $CaCO_3$ (Sigma Aldrich). All the solutions and suspensions were prepared using Milli-Q quality deionized water (Milli-Q Academic, Millipore, France).

3.2.2. Synthesis of the bentonite-magnetite particles and magnetite nanoparticles

The synthesis of the BMag composites was carried out, adapting a previous protocol reported by (Liu et al., 2008) for attapulgite-magnetite composites, as described by the following steps:

i) Preparation of bentonite suspension in Fe^{3+} aqueous solution: 4.410 g of $FeCl_3 \cdot 6H_2O$ was dissolved in 200 mL of deionized water. Then, 1.5 g of bentonite was dispersed in the Fe^{3+} solution using an ultrasonic bath for 30 minutes until a stable suspension was obtained. After that, the suspension was deoxygenated by bubbling nitrogen for 15 min. The flask was closed, and the suspension was stirred overnight.

ii) In the bentonite-Fe^{3+} suspension obtained in the previous step we added 1.614 g of $FeCl_2 \cdot 4H_2O$. This new suspension, containing Fe^{2+} ions in solution, was heated up to 90 °C. After that, 6 mL of NH_4OH solution was added rapidly under

stirring. Immediately, a black precipitate appeared as a result of the formation of magnetite particles. Then, the suspension was kept under mechanical stirring in nitrogen atmosphere at 90°C for 1 h. The resulting suspension was cooled down to room temperature.

iii) Finally, the BMag particles were washed. For this, the particles were settled using a powerful magnet. Then, the supernatant solution was discarded, and the particles redispersed in fresh water. This procedure was repeated until the conductivity of the supernatant was less than 20 μS/cm.

The samples notation with a brief description is included in Table 3.1.

Table 3.1. Description of the different samples (particles, suspensions, and ferrogels) employed.

Sample	Composition
Bent	Bentonite particles (purified by hydrocyclone process)
Fe_3O_4	Magnetite nanoparticles
BMag	Bare (non-functionalized) magnetite-covered bentonite particles
BMagF1	Particles functionalized by dispersion of 1 g of "BMag" particles in 50 mL of a 0.5% w/v solution of sodium alginate
BMagF2	Similar to "BMagF1" particles, but obtained by dispersion in a 2% w/v solution of sodium alginate
BMag, or BMagF1, or BMagF2 suspensions	Suspensions of the different kinds of particles in aqueous media. Particle concentration 1% w/v (zeta potential measurements) or 10% w/v (rheology)
BMagF1+X%Alg ferrogel	Ferrogel containing 10% w/v of functionalized particles (BMagF1) and X% w/v of sodium alginate in the pregel solution (X = 0.25, 0.5, 1, 2)
BMagF2+X%Alg ferrogel	Similar to ferrogel "BMagF1+X%Alg", but containing BMagF2 particles

The synthesis of the magnetite nanoparticles was identical to that of the BMag particles, except for the following differences: in step i) the Fe^{3+} solution did not

contain bentonite particles; in step iii) the repeated cycles of decantation/redispersion were carried out until the supernatant was at pH ≈ 7.

3.2.3. Preparation of the suspensions and magnetic hydrogels

The suspensions of BMag particles prepared for rheological measurements (see Section 3.2.4 below) was carried out by dispersion in pure water of the BMag particles, at a concentration of 10% w/v.

Previously to the preparation of the ferrogels, the BMag particles were functionalized by adsorption of alginate molecules. To this end, two different suspensions were prepared. In the first one, 1.0 g of BMag particles was dispersed into 50 mL of a solution containing 0.25 g (0.5% w/v) of sodium alginate. In the second one, 1.0 g of BMag particles was dispersed into 50 mL of a solution containing 1 g (2% w/v) of sodium alginate. After allowing 12 h for alginate adsorption on the particle surface, the particles were recuperated and washed following the procedure described in section 3.2.2 of this chapter, point (iii). (See sample notation in Table 3.1).

The BMag particles, functionalized by alginate adsorption (samples BMagF1 and BMagF2), were employed for the preparation of ferrogels. For this purpose, next steps were followed:

i) The magnetic particles were dispersed in four different solutions of sodium alginate. In all these pregel suspensions the particle concentration was 10% w/v and the alginate concentrations were 0.25, 0.5, 1, and 2% w/v. These suspensions were shaken by hand until the suspensions were homogenous.

ii) After that, 22.5 mg of $CaCO_3$ and 26.7 mg of gluconic acid (GLD) were added to each suspension and the resulting mixture was shaken by hand. The role played by GDL was the slow acidification of the aqueous solution, by hydrolysis of this weak organic acid, allowing the gradual liberation of calcium ions from the $CaCO_3$. This controlled reaction favored the homogeneous crosslinking of the alginate molecules, avoiding the formation of thick lumps into the ferrogels.

iii) Finally, 4 hours after the start of the previous step, the gelation process was completed by addition of a solution of $CaCl_2$ (5 mL, 45 mM concentration). The ferrogel was left at rest overnight at room temperature. The addition of this $CaCl_2$ solution provoked the swelling of the ferrogels, and the saturation of the crosslinking (by Ca^{2+} diffusion). Thus, ferrogels with enough tautness for handling were obtained.

3.2.4. Experimental methods

The X-ray diffraction patterns (XRD) of bentonite (Bent) and bentonite covered by magnetite particles (BMag) were obtained in a Philips X'Pert Pro diffractometer (PANalytical, Netherlands) working on K_α monochromatic radiation of copper. In addition, the morphology of Bent and BMag particles was obtained by high resolution scanning electron microscopy (FESEM; Zeiss SUPRA40VP, USA).

The Fourier transform infrared spectra (FTIR) of the particles were recorded in a Perkin Elmer model 597 in the region 4000 - 400 cm^{-1}, using pellets containing 2 mg of the sample studied and 200 mg of KBr.

Zeta potential measurements were carried out in a Malvern Zeta-Sizer Nano SZ (UK) at 25ºC. For these measurements, different suspensions containing 1% w/v particle concentration of Fe_3O_4, Bent, BMag, BMagF1, and BMagF2 (see Table 3.1) in aqueous media (1 mM NaCl ionic strength; pH interval from 3 or 4 up to 10), were prepared. These suspensions were left at rest for 24 h. To avoid the influence of particle sedimentation, the samples were redispersed in an ultrasound bath, and the pH readjusted immediately before the measurements. The values reported correspond to the average ± standard deviation of at least nine measurements of different aliquots.

The magnetization of the dry powder of BMag particles was measured at room temperature in a VSM 4500 magnetometer (EG&G Princeton Applied Research, USA), by applying the following magnetic field intensity (H) sequence: 0 – 374 kA/m (first

magnetization), followed by the cycle (magnetization loop) 374 − 0 − (-374) − 0 − 374 kA/m.

The rheological characterization of the suspensions and ferrogels was carried out in the presence and absence of applied magnetic field in a magnetorheometer (Physica Anton-Paar MCR 300, Germany) with plate-plate geometry (rotor plate diameter 20 mm) at constant temperature of 25.0 ± 0.1 °C. The plates had a rough surface to avoid wall slipping. The applied magnetic field (intensity H = 156 kA/m or 282 kA/m) was perpendicular to the rheometer plates. The samples were placed in the bottom plate and a normal force of 0.1 N was kept on the disk-like samples to ensure a good contact among plates and samples; the gap between the plates was slightly different for different samples, in order to maintain this value of the normal force. A water vapor saturated atmosphere was maintained around the samples to minimize their drying. Furthermore, in order to ensure the same initial conditions, a fresh sample was employed in each measure. In the case of the suspensions of BMag particles, in order to minimize the possible effect of the particle sedimentation, the samples were strongly redispersed before the measurements.

Two different series of rheological experiments were performed: (i) steady-state tests, and (ii) oscillatory tests. For the former, the suspensions were subjected to a shear stress ramp and the corresponding shear rate and viscosity were obtained. The time elapsed in each constant stress step was 5 s. In oscillatory measurements, a sinusoidal shear stress was applied, and the subsequent strain recorded. In all these experiments the frequency was maintained at 1 Hz, and the shear stress amplitude progressively increased until the non-linear viscoelastic region was reached. The time elapsed in each stress step was 5 s. From the values of the stress and strain amplitude and the phase difference between shear and strain, the elastic or storage (G') and viscous or loss (G") moduli were obtained. Both tests (steady-state; oscillatory) were performed under the action of constant magnetic fields (H = 0; 156 kA/m; or 282 kA/m) applied during the total length of the experiment. These field values did not correspond exactly to the internal field in the sample in the rheometer gap, but taking

into account the relatively small particle volume fraction in the suspensions and ferrogels (4.05% v/v; see section 3.3.2 below), and consequently the small demagnetizing fields, both the internal and the external fields were very close.

3.3. Results and discussion

3.3.1. Physico-chemical characterization

The X-ray diffraction patterns of the particles in samples Bent, BMag, and Fe_3O_4 (see Table 3.1 above) are plotted in Figure 3.1. For the Fe_3O_4 sample, the peaks at diffraction angles 2θ = 18.27°, 30.09°, 35.49°, 43.05°, 53.48°, 56.94°, and 62.72° correspond to the planes (111), (220), (311), (400), (442), (511), and (440) in the crystal lattice of pure magnetite. In the pattern of BMag sample the same peaks of pure magnetite remained, and some additional peaks at 2θ = 26.64° and 19.85° (corresponding to the bentonite core) appear. Nevertheless, these peaks become wider and their intensity was reduced as compared with those of pure bentonite, likely due to the (at least partial) coating by magnetite nanoparticles present in the BMag composites. Note that, as this technique does not allow distinguishing between magnetite and maghemite, the presence of maghemite in the BMag particles cannot be excluded.

The FTIR spectra allow confirming the composition of the BMag composites (Figure 3.2). The absorption bands can be attributed as follows. Band around 3625 cm^{-1} to the −OH group; bands at 1007, 788 and 523 cm^{-1} to Si−O stretching vibrations in bentonite (Khabbouchi et al., 2017) (Aliyan et al.,2013), and band at 694 cm^{-1} to Fe−O vibrations. The intensity of the Si−O bands in BMag were weaker than in Bent, indicating that the Fe−O bonds interact with the Si−O groups in the bentonite surface (Mao et al., 2016), very likely due to the attachment among magnetite and Bent particles.

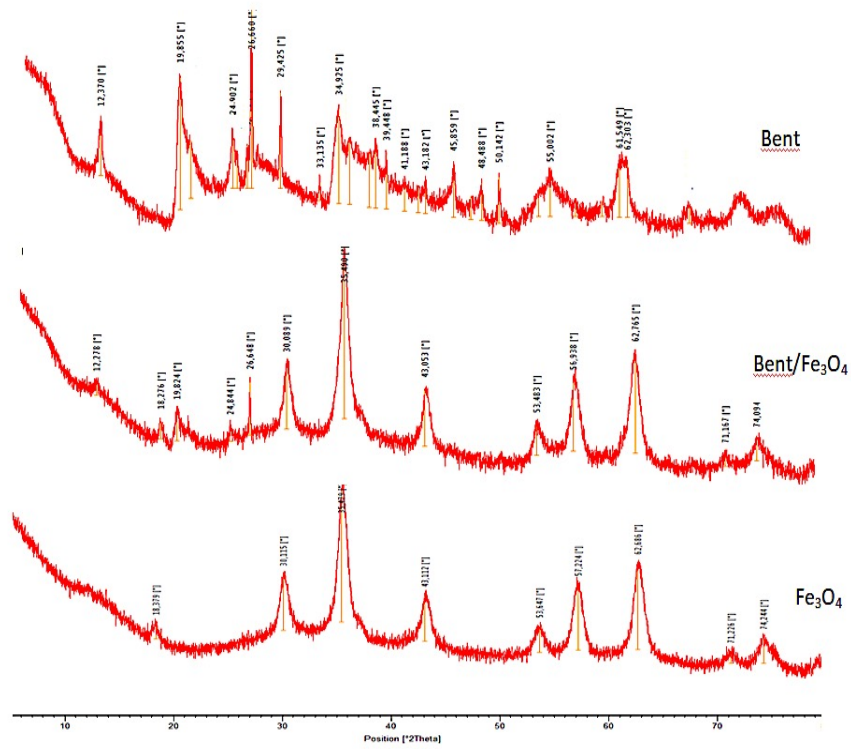**Figure 3.1.** XRD patterns of bentonite (Bent), magnetite-covered bentonite (Bent/Fe$_3$O$_4$), and magnetite particles.
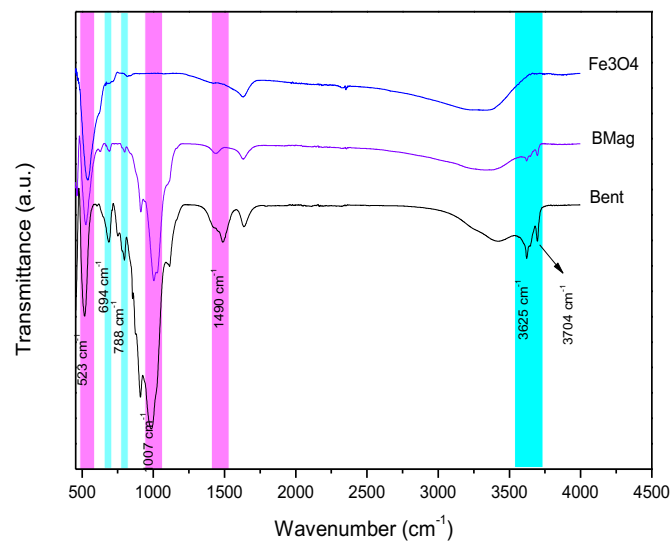

Figure 3.2. FTIR spectra of Bent, BMag and Fe$_3$O$_4$ particles.

The morphology of the composite particles was analyzed in SEM pictures (Figure 3.3). The bentonite particles (Figure 3.3a) appeared as twisted and stacked platelets with a great polydispersity in size. Figure 3.3b shows the BMag particles and, as observed, the primitive clay clusters exhibited a partial coverage by small (around 100-200 nm) bright spots. These tiny spots correspond to the magnetite nanoparticles grown onto the clay surfaces, probably because the clay mesopores (remember that bentonite specific surface area was 70 m^2/g) acted as attachment points that promoted the precipitation of magnetite during the synthesis process.
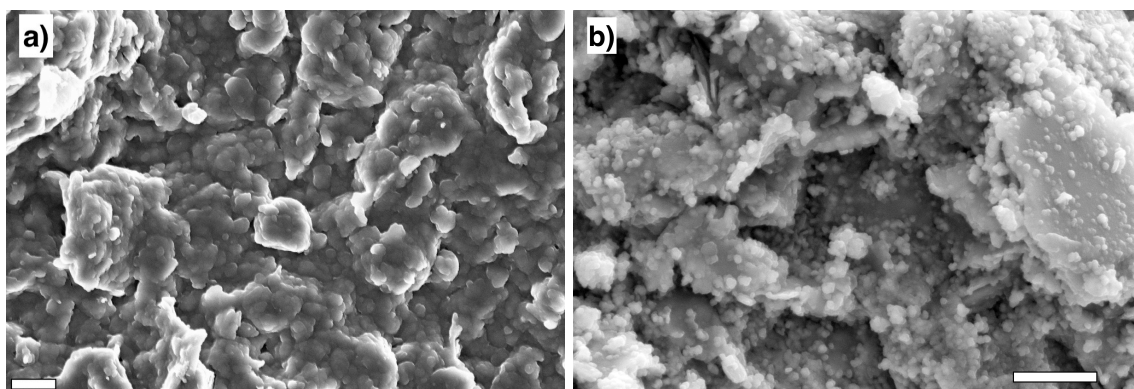
Figure 3.3. Pictures obtained by SEM of Bent (a), and BMag (b) particles. Bar scales: a) 200 nm (line in the lower left corner), b) 1 µm (line in the lower right corner).

The zeta potential of the different particles (Fe$_3$O$_4$, Bent, BMag composites, and the functionalized particles BMagF1 and BMagF2), as a function of the pH of the aqueous medium, are plotted in Figure 3.4. The zeta potential of the magnetite particles presented an isoelectric point at pH(iep) ≈ 6.5, which is in good agreement with those values previously reported in literature (Galindo-González et al., 2005) (Viota et al., 2010) for magnetite nanoparticles obtained by co-precipitation.

The zeta potential curve of bentonite particles follows the typical trend of smectite clays (bentonite, montmorillonite) and silica particles (Abrougui et al., 2019) (Galindo-González et al., 2005) (Ramos-Tejada et al., 2003), that is, the particles bear a negative surface charge (and negative zeta potential) in the entire pH range under study. In the case of the non-functionalized composite particles (sample BMag), the

tendency observed is coherent with a surface electrochemistry that combines those of Bent and Fe_3O_4 samples. Note that the surface reactions that determine the zeta potential of these materials (magnetite, bentonite, clay-magnetite) have also been summarized in our previous work (Abrougui et al., 2019).
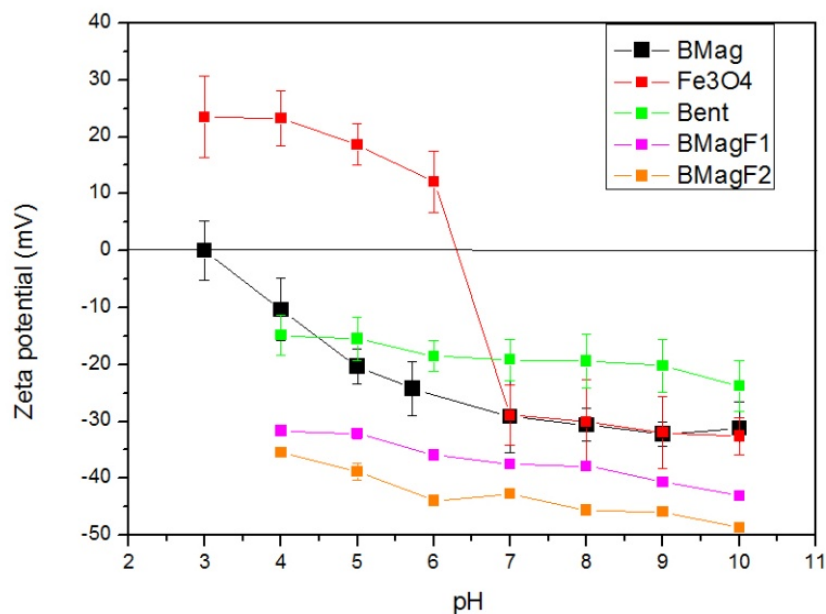
Figure 3.4. Zeta potential of the indicated particles in aqueous suspensions (see Table 1) as a function of the pH of the aqueous medium. Particle concentration 1% w/v. Ionic strength of the solutions 1 mM NaCl.

Finally, the adsorption of the dissociated alginate molecules provoked a clear increase (in absolute value) of the zeta potential of the BMag substrate, more pronounced as the concentration of alginate in solution was increased, as shown in Figure 3.4 in the curves for BMagF1 and BMagF2 suspensions. This effect is a consequence of the surface reactions, via formation of coordination compounds, among the carboxylate groups of the alginate ligands and the Fe (II), Fe (III), and Si(IV) cations in the particles surface. Really, these metal (M = Fe or Si) ions are present in the solid-solution interface as $M\text{-}O^-$ (basic pH), M-O-H (neutral pH), or $M\text{-}O\text{-}H_2^+$ (acid pH), and the alginate adsorption is even more favored at acid pH by electrostatic attraction between the alginate molecules and the $M\text{-}O\text{-}H_2^+$ group. The formation of

these surface alginate complexes on magnetite or bentonite particles have been extensively studied (Xu et al., 2006) (Yang et al., 2010), as well as a similar process in the case of other polyelectrolytes that also bear carboxylate groups (e.g. humic acids) on clay or hematite particles (Xu et al., 2006) (Yang et al., 2010).

The negative zeta potential of the functionalized particles has an additional advantage on the colloidal stability of the suspensions. As demonstrated in a previous work (Galindo-González et al., 2005), the bentonite-magnetite platelets in aqueous suspensions suffer a high degree of aggregation because the van der Waals attraction between the particles faces that overcomes the electrostatic repulsion between them. In consequence, the particles form stacked clusters and settle by gravitational forces.

However, if the particles are functionalized by alginate adsorption, the electro-steric repulsion avoids (at least partially) their aggregation and the subsequent fast sedimentation to a large extent. Figure 3.5 shows the sedimentation of the bare and functionalized particles along one week, demonstrating that the settling of the particles was considerably slowed by alginate adsorption in BMagF1, and BMagF2 samples. As mentioned in section 3.2.4, to minimize the effect of the sedimentation, all the samples were strongly redispersed immediately before carrying the zeta potential and rheological measurements, which in any case took only a few minutes.

The magnetic response of the BMag particles (dry powder) is shown in Figure 3.6. As observed, the composite BMag particles developed strong enough magnetization and negligible remanence (Figure 3.6a). The saturation magnetization can be obtained by fitting the data of the first magnetization curve (Figure 3.6b) to the the Frölich-Kennely equation (Jiles, 1998) :

$$M = \frac{\chi M_S H}{M_S + \chi H} \tag{1}$$

Where χ is the magnetic susceptibility and M_S the saturation magnetization. Their estimated values are χ = 3.90 $\pm$ 0.05 and M_S = 110.0 $\pm$ 0.3 kA/m; coefficient of determination r^2 = 0.995.
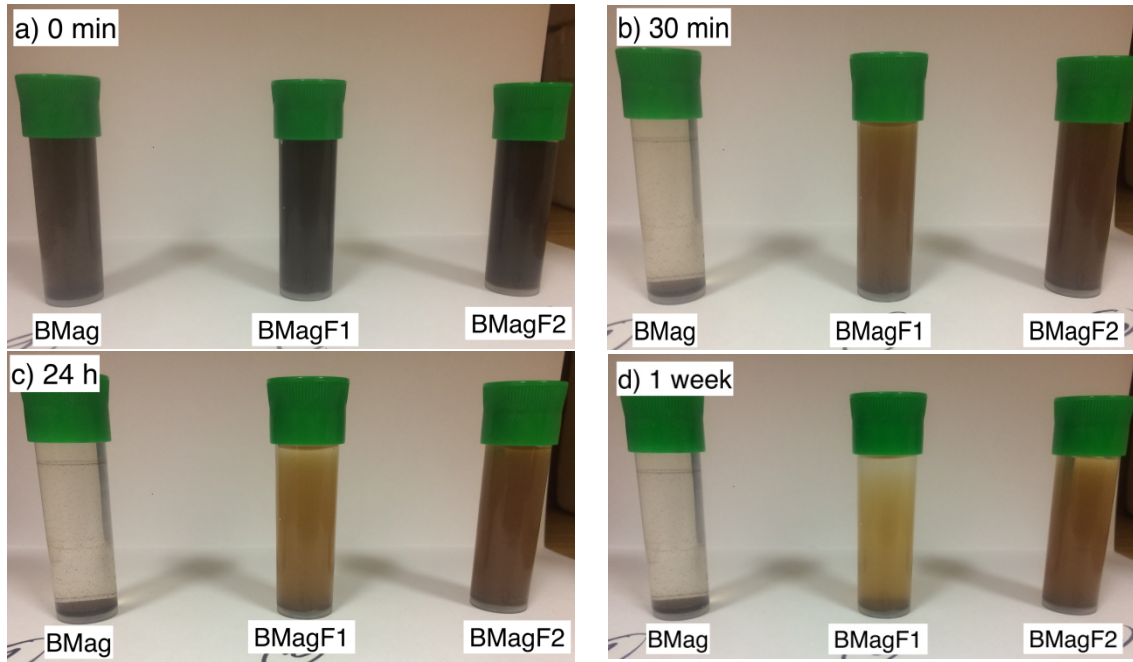
Figure 3.5. Sedimentation of the suspensions of bare (BMag) and functionalized (BMagF1, BMagF2) composite particles. The indicated times correspond to those elapsed from the end of the preparation process (which involved strong redispersion) of the samples. Particle concentration 1% w/v. Ionic strength of the solutions 1 mM NaCl.

Considering this estimated saturation magnetization of the composite particles (M_S) and that of pure magnetite ($M_{S,m}$ = 446 kA/m (Kemp et al., 2016), and the mixing law (Rosensweig, 1985):

$$M_S = \phi M_{S,m} \qquad (2),$$

the estimated volume fraction (ϕ) of magnetic material in the BMag composite particles was ϕ = 24.7%. Taking for the density of bentonite and magnetite 2.1 g/cm^3 and 5.5 g/cm^3, respectively, the average density of the BMag particles was 2.5 g/cm^3. In addition, the data in Figure 3.6 demonstrated that the powder behaved as a magnetically soft material because the magnetic hysteresis was practically negligible given that the remnant magnetization and the coercive field (M_R = 0.45 kA/m and H_C = -0.08 kA/m, respectively) are within the typical measurement error of the VSM magnetometer.
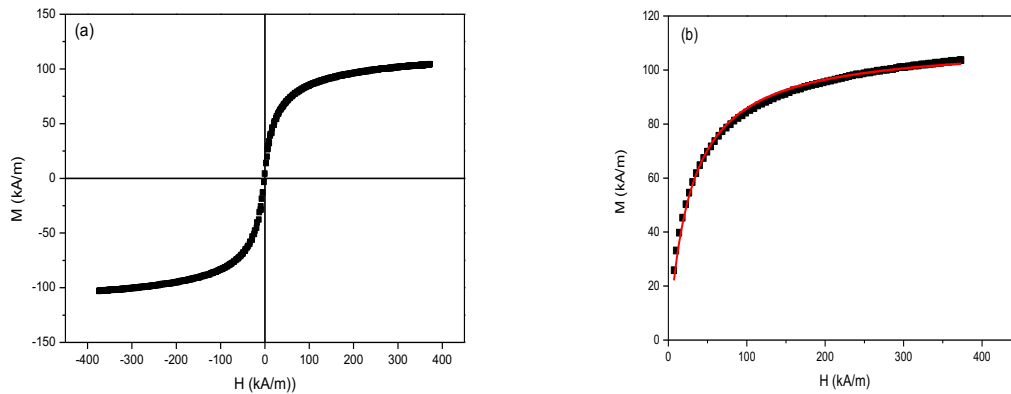
Figure 3.6. a) Magnetization loop of magnetite-covered bentonite particles (sample BMag). b) First magnetization curve of BMag powder; the red line is the best fitting to Frölich-Kennely equation, eq. (1).

3.3.2. Rheological characterization

The viscoelastic moduli for both the suspension of non-functionalized particles (BMag) and the different ferrogels, were obtained by applying a sinusoidal shear stress (oscillatory regime). All the samples studied contained a particle concentration of 10% w/v, equivalent to a particle volume fraction ϕ = 4.05% v/v. During the experiments a stationary external field was applied to the samples with magnetic intensities H = 0, or H = 156 kA/m, or H = 282 kA/m. Figure 3.7 shows the results corresponding to the suspension of BMag particles. In this figure we clearly observe, whatever the applied field, two different regions: an initial psedoplateau, in which G' was practically independent of the strain amplitude (γ_0), which corresponds to the linear viscoelastic region (LVR), followed by a second region (N-LVR) in which G' suffered an abrupt decrease. In the first region, G' was larger than G", as typically expected for a viscoelastic solid. In the second region (N-LVR), as γ_0 increases, there was a progressive transition from a viscoelastic solid to a viscoelastic liquid (G" > G').
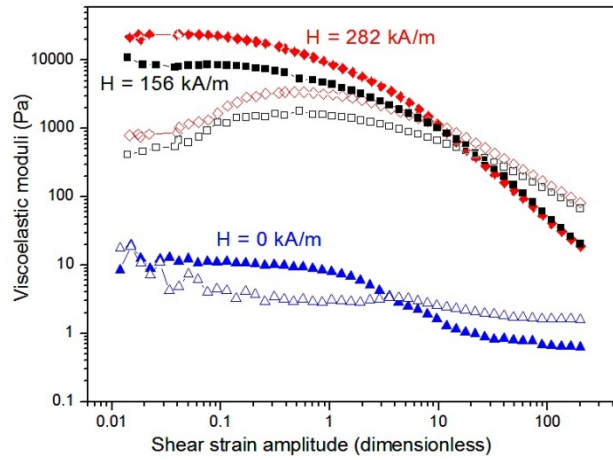
Figure 3.7. Viscoelastic moduli as a function of the strain amplitude, for the aqueous suspension of BMag particles in the absence/presence of the indicated magnetic fields (H). Particle concentration 10% w/v. Solid symbols: elastic modulus G'; open symbols: viscous modulus G".

The magnetic field-induced enhancement of the G' values within the LVR (the so-called magnetorheological effect, MR effect) can be quantified by the equation:

$$MRE(\%) = \frac{G\prime(H \neq 0) - G\prime(H=0)}{G\prime(H=0)} \times 100 \qquad (3)$$

Table 3.2 includes the values of MRE (%) for the suspension, for the two values of the applied field: 76100% (at H = 156 kA/m) and 197200% (at H = 282 kA/m), which are enormous in comparison with those usually reached in ferrogels, as we will see below. Nevertheless, the quantification of the MR effect by equation (3) does not seem appropriate for an almost liquid-like suspension that in the absence of field has a very low elastic modulus (G' ~ 10 Pa). For these suspensions, it seems that a more convenient quantification of the MR effect can be done by considering the plastic viscosity (η) of the suspensions in the absence/presence of applied field, by means of:

$$MRE - \eta(\%) = \frac{\eta(H \neq 0) - \eta(H=0)}{\eta(H=0)} \times 100 \qquad (4)$$

The dynamic yield stress (σ_0) and the plastic viscosities (η) were obtained, respectively, from the intercept and the slope of the shear stress vs. shear rate curves

(Figure 3.8), by linear fitting in the shear rate interval from 1 to 50 s^{-1}. The values obtained were as it follows. i) For H = 0 kA/m: σ_0 = 1.20 ± 0.19 Pa, η = 90 ± 9 mPa·s . ii) For H = 156 kA/m: σ_0 = 2.85 ± 0.17 Pa, η = 94 ± 7 mPa·s. iii) and for H = 282 kA/m: σ_0 = 4.0 ± 0.4 Pa, η = 168 ± 16 mPa·s. The values of these plastic viscosities and the corresponding MR effect calculated by equation (4) are included in Table 3.2. Now, the MRE-η value reached for the maximum field is 87%, which seems a more reasonable estimation of the MR effect.
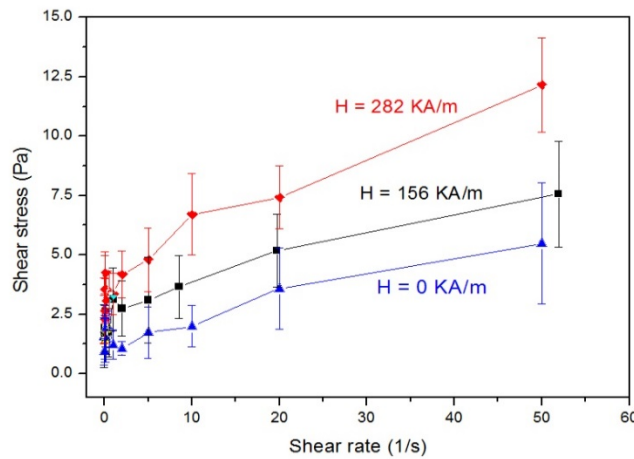
Figure 3.8. Rheogram of the suspension of BMag particles obtained under the indicated applied fields. Particle concentration 10% w/v. Solid lines only are guides for the eye.

For the ferrogels prepared in this work, first we will analyze the viscoelastic behavior in absence of magnetic field. In Figure 3.9 the values of the viscoelastic moduli are plotted as a function of γ_0. Figure 3.9a includes the results for the samples BMagF1+X%Alg that contains 10% w/v of functionalized particles (BMagF1) embedded in hydrogels prepared with increasing concentrations of alginate (from 0.25 to 2% w/v of alginate; see Table 3.1) in the pregel solution. From this Figure 3.9a, it seems evident the pronounced effect of the alginate concentration on the mechanical properties of the resulting hydrogels. The increase of the alginate concentration from 0.25 to 2% w/v provoked an increase in the values of G' corresponding to the LVR (see solid symbols in Figure 3.9a) of around two orders of magnitude. For the BMag

particles functionalized with a larger amount of adsorbed alginate, the viscoelastic moduli of all the ferrogels (samples BMagF2+X%Alg, Figure 3.9b) were even higher: see the exact values of G' for these samples in Table 3.2.
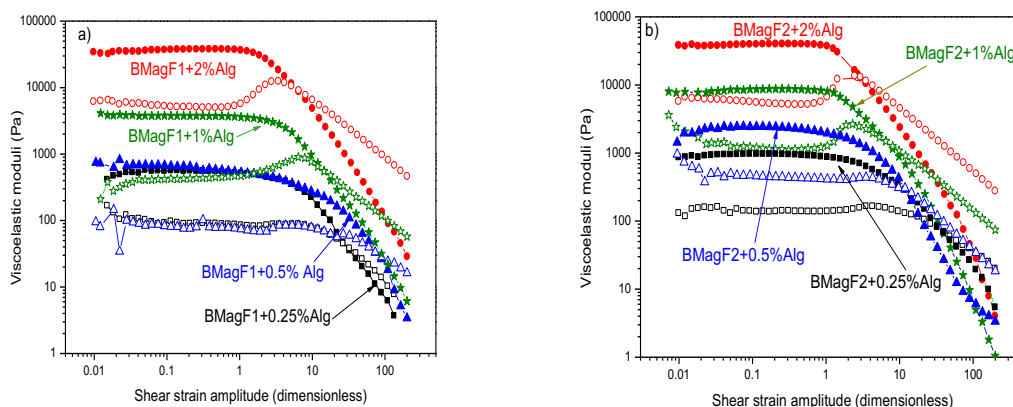
Figure 3.9. Viscoelastic moduli, in the absence of magnetic field, as a function of the strain amplitude for the different hydrogels. a) Hydrogels BMagF1+X%Alg (see composition in Table 1). b) Hydrogels BMagF2+X%Alg (Table 1). Solid symbols G'; open symbols G". Note that the same axis scales are used in both graphs.

Therefore, up to this point we have two different mechanisms to control the mechanical moduli of the ferrogels: the amount of alginate adsorbed on the particles and the concentration of alginate in the pregel solution. This behavior can be explained considering, as demonstrated in a previous work (Abrougui et al., 2019), the crosslinking (by calcium ions) among the alginate molecules adsorbed onto the particles and those present in the pregel solution, which favored the networking among the particles and the polymer fibers. As a consequence, the resulting ferrogels consisted of a network of alginate fibers in which the magnetic particles were not randomly dispersed but acted as knots that reinforced the elasticity of the material.

A third mechanism to control the mechanical properties of ferrogels, as for magnetorheological suspensions, is the action of an external magnetic field of large enough intensity. In this work the applied fields were H = 156 kA/m and H = 282 kA/m, both of them below (but not too far) the field required to reach the magnetic

saturation of the particles; see in Figure 3.6 that the field intensity for the maximum magnetization was around H = 400 kA/m.

Table 3.2. Intensity of the magnetorheological effect quantified by means of eqs. (3) and (4) for the suspensions, and eq. (3) for the ferrogels. The plastic viscosities (η) of the suspensions are given in mPa·s. The G' (Pa) values correspond to a strain amplitude of 0.1 (10%).

	H = 0 kA/m	H = 156 kA/m			H = 282 kA/m		
Sample	η	η	$\Delta\eta$	MRE-η(%)	η	$\Delta\eta$	MRE-η(%)
Suspension BMag particles	90	94	4	4	168	78	87
Sample	G'	G'	ΔG'	MRE(%)	G'	ΔG'	MRE(%)
Suspension BMag particles	11	8380	8369	76100	21700	21689	197200
Ferrogel BMagF2+0.25%Alg	915	1687	772	84	2442	1527	167
Ferrogel BMagF2+0.5% Alg	920	2585	1665	181	5708	4788	520
Ferrogel BMagF2+1% Alg	8187	8501	323	4	9929	1751	21
Ferrogel BMagF2+2%Alg	39310	41020	1710	4	43920	4610	12

In Figure 3.10 we plotted the viscoelastic moduli of the samples BMagF2+X%Alg (X = 0.25; 0.5; 1; 2) for the different applied fields. As observed (see also Table 3.2), for the weakest ferrogel (0.25% alginate, Figure 3.10a) there was a significant effect of the field-induced attraction among the particles that gave MRE values (equation 3) of 84% (H = 156 kA/m) and 167% (H = 282 kA/m). On the contrary, the values of MRE(%) were considerably smaller for the hydrogel with the larger amount of alginate (BMagF2+2%Alg, Figure 3.10d, Table 3.2), for which the MRE(%) was 4% and 12% for H = 156 kA/m and H = 282 kA/m, respectively. In this case, the curves obtained for the different applied fields tended to overlap.

Nevertheless, the data in Figure 3.10 and Table 3.2 show that the maximum MR effect was reached for an intermediate value of the alginate concentration (sample BMagF2+0.5%Alg; Figure 3.10b), with MRE values of 181% (H = 156 kA/m) and 520% (H = 282 kA/m). For this sample, the polymer network seemed to be still weak enough to allow a strong field-induced reinforcement of the ferrogel.
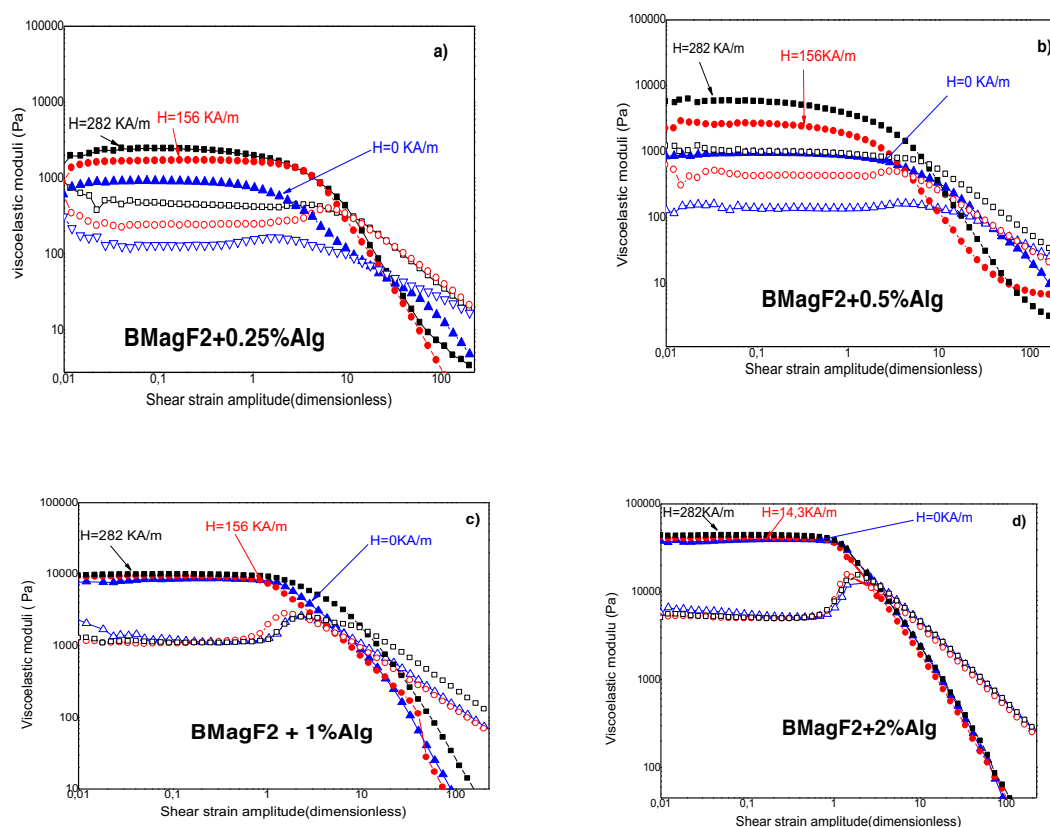
Figure 3.10. Viscoelastic moduli as a function of the strain amplitude for hydrogels BMagF2+X%Alg (see **Table 3.1**). a) Sample BMagF2+0.25%Alg. a) Sample BMagF2+0.5%Alg. c) Sample BMagF2+1%Alg. d) Sample BMagF2+2%Alg. The values of the applied field are indicated. Solid symbols: elastic modulus, G'; open symbols: viscous modulus, G". Note that the same axis scales are used in the four graphs.

Summarizing, the application of an external magnetic field allowed a strong MR effect only if the hydrogel network was not too dense. On the contrary, if the particles were entangled in a hydrogel with a very high concentration of polymer, their field-induced particles migration and chaining was strongly hindered and, consequently, the

stiffness of the ferrogel mainly depended on the resilience of the polymer-particle network, being negligible the role played by the magnetic interactions.

Finally, it is convenient to analyze the influence of the shape of the magnetic particles on the magnetic control of the rheological properties of the ferrogels. For this aim, we need to separate the shape effect from other quantities, such as the particle concentration, the intensity of the field, and the magnetization of the particles. For this purpose, we can consider that, according to the magnetorheological model proposed by (Ginder et al.,1996) (see also (Bossis et al., 2002)), the shear modulus depends linearly on the field applied (H), the particle volume fraction (ϕ), and the particle saturation magnetization (M_S). Although this model is based on a number of restrictive assumptions (particle volume fraction $\phi < 20\% - 30\%$; linear field-induced chaining of spherical particles; intermediate field values, well below the field for saturation magnetization; very low strain), it is useful as a starting point to define a normalized MR effect parameter as (Abrougui et al., 2019):

$$\overline{MRE}(\%) = MRE(\%) \frac{M_{S,0}}{M_S} \frac{H_{max,0}}{H_{max}} \frac{\phi_0}{\phi} \qquad (5)$$

Here the quantities H, M_S and ϕ correspond to those of the ferrogels studied in refs. (Abrougui et al., 2019) (Gila-Vilchez et al., 2018) (Zubarev et al.,2018) and the quantities with subscript "0" correspond to the ferrogel BMagF2+0.5%Alg prepared in this work. All these data are included in Table 3.3.

Chapter 3. Rheology of magnetic colloids containing clusters of particle platelets and polymer nanofibers

Table 3.3. Comparison of the magnetorheological effects, calculated by equations (3) and (5), achieved by ferrogels containing particles with different shapes and compositions.

Ferrogel (reference)	Composition (Particle core-shell /Polymer in hydrogel)	M_S (kA/m)	H (kA/m)	ϕ (% v/v)	MRE (%)	$\overline{MRE}$ (%)
BMagF2+0.5% Alg	Platelets bentonite-Fe_3O_4 /Alginate (0.5% w/v)	110 [a]	282 [a]	4.05 [a]	520	520
Ferrogel BMagF2+1% Alg	Platelets bentonite-Fe_3O_4 /Alginate (1% w/v) [b]	110 [a]	282 [a]	4.05 [a]	21	21
Ferrogel-1 Ref (Abrougui et al., 2019)	Fiber-like sepiolite Fe_3O_4 /Alginate (1% w/v) [b]	169.9	282	0.93	64	180
Ferrogel Ref (Gila-Vilchez et al., 2018) [c]	Spherical Fe-silica /Alginate (1% w/v)	1587	282	4.6	700	43
Ferrogel Refs. (Zubarev et al., 2018) [c]	Spherical Fe_3O_4-polymer / Fibrin-agarose	161	48.6	3.5	8	37

[a] $M_{S,0}$, $H_{max,0}$, ϕ_0 in equation (5); [b] alginate concentration in pregel solution 1% w/v –note that this is the system studied in chapter 2 of this thesis ; [c] see also (Abrougui et al., 2019).

The analysis of the data in Tables 3.2 and 3.3 demonstrated that:

i) The ferrogels prepared with plate-like magnetic particles (bentonite-magnetite) can provide a very high MR effect when the alginate concentration was not too high. The maximum field effect (MRE = 520%) was achieved at 0.5% w/v alginate concentration in the pregel solution.

ii) The alginate concentration in the pregel solution determined to a large extent (and allowed or not a wide control of) the MRE values achieved in the ferrogels containing functionalized magnetic platelets.

iii) If we compare ferrogels containing particles with different shapes (bentonite-magnetite platelets, sepiolite-magnetite fibers, silica-iron spheres) and equal alginate concentration (1% w/v) in the pregel solution, the maximum field effect corresponds to those with fiber-like composite particles. The normalized MRE values are: 21% (platelets), 180% (fibers), and 43% (spheres).

3.4.   Conclusions

Hydrogels containing biocompatible polymer fibers and magnetic micro- or nanoparticles are very promising soft-wet materials for biomedical applications because their internal microstructure can work as patterns (or extracellular matrix or scaffolds, in the terminology used in tissue engineering) for generating soft biological tissues. The configuration of such internal structure depends on a number of variables that allow controlling their macroscopic properties, such as the mechanical moduli and the hydration degree. These variables are mainly: i) the length and crosslinking degree of the polymer fibers; ii) the crosslinking degree among the polymer fibers and the molecules adsorbed onto the solid particles; iii) the kind of bond (covalent, electrostatic) between the crosslinker and the polymer molecules; iv) the volume fraction of solid particles embedded in the hydrogel; v) the magnetic properties of the particles; vi) the intensity of the applied magnetic field.

In this work we used calcium ions as crosslinker agent and the interaction among the alginate molecules was electrostatic. This physical crosslinking favored the formation of soft and easy to handle hydrogels, with an elasticity that could be controlled within a wide range by varying the alginate concentration in the pregel solution. Even more, when the particles were functionalized by adsorption of alginate molecules onto the particle surface, the solid particles were placed as the knots of the internal network, which avoided the settling of the particles inside the gel. Simultaneously, this particle-polymer networking reinforced the mechanical response of the gels under the action of mechanical stresses.

The magnetic particles embedded in the hydrogels prepared in this work were composites of bentonite platelets on which magnetite nanoparticles were synthetized by a coprecipitation reaction, and the resulting composites were finally functionalized by adsorption of alginate molecules. The final composite particles had low density and, consequently, negligible settling rate inside the pregel solution. This fact allowed obtaining homogeneous ferrogels with a high enough magnetorheological effect. We found that the intensity of the MR effect strongly depended on the concentration of

sodium alginate employed for the preparation of the pregel solution, being the optimal concentration 0.5% w/v.

The comparison of the ferrogels based on magnetic particles with different shapes and the same alginate concentration –normalizing other quantities as particle concentration, applied field, and magnetization– demonstrated that the more intense MR effect was achieved in systems containing fiber-like particles. The MR effect attained for systems based on spherical and plate-like particles was of same order of magnitude, possibly because some stacked clay clusters remained in bentonite-based ferrogels, in spite of the electro-steric stabilization imparted by the adsorbed alginate molecules. However, the use of magnetic composites based on clay minerals has the advantage, in comparison with spherical particles of pure magnetite or iron, of the stability (facing settling) of the particles inside the pregel suspension, which is essential to obtain ferrogels with high homogeneity. And this property (homogeneity) is in most cases a crucial condition to mimic natural tissues, when hydrogels are used as scaffolds for tissue engineering.

Chapter 4

Cytotoxicity of suspensions and hydrogels containing sepiolite-magnetite particles

Summary

This chapter is devoted to the analysis of the cytotoxicity magnetic colloids containing nanocomposites of sepiolite particles covered by magnetite ones. For this aim, three different systems were analyzed. The first system consisted of aqueous suspensions of the bare nanocomposites particles. Alternatively, the composites were coated by either alginate or polyethylene glycol and embedded within alginate hydrogels. Human fibroblasts were cultured in contact with any of these three different samples for 48 hours and afterwards their viability and proliferation were evaluated by different techniques. First, the morphology of the fibroblasts was analyzed by phase contrast microscopy as well as by fluorescence microscopy. A live/dead commercial kit was used to analyze the percentage of live and dead cells. In addition, the proliferation of cells was analyzed by WST-1 assay. Finally, the irreversible damage of the nuclear membrane was studied by mean of quantification of the amount of DNA released to the culture medium. Results of experiments demonstrated no significant differences for fibroblasts cultured in contact with bare nanocomposites or hydrogels containing particles coated by alginate, with respect to the positive control group. On the contrary, a reduction in viability and proliferation was observed for fibroblasts cultured in contact with hydrogels containing nanocomposite particles coated by polyethylene glycol.

4.1. Introduction

As a typical soft and wet material, hydrogels have attracted a great deal of interest over the past two decades because of their great similarity to native tissue matrices (Chatterjee et al., 2005). Their main characteristic is the versatility of their physico-chemical properties. It is sufficient to modify the chemical composition or the preparation protocol of the gel to obtain gels with very different characteristics.

Provided by the required biocompatibility, these materials have potential applications in many different scientific and technological fields and, in particular, in the field of biomedicine (Nicodemus & Bryant, 2008). In fact, in tissue engineering, hydrogels are used to mimic the extracellular matrix of different native tissues such as the cornea, oral mucosa, cartilage, peripheral nerve or bladder (Atala et al., 2006) (Campos et al., 2018). Similarly, porous hydrogels have been used for the controlled or local release of drugs or, by taking advantage of their microchannel network, to generate micro-structures in which cells can grow under conditions of controlled metabolite flow (Langer, 1989) (Choi et al., 2007).

In addition, hydrogels may contain materials that modify their properties, such as synthetic nanoparticles or microparticles. We will refer to these materials as nanocomposite hydrogels, or even bio-nanocomposite hydrogels if all their components are biocompatible materials. One important category among nanocomposite hydrogels are magnetic hydrogels (or ferrogels), which consist of dispersion of magnetic particles in a polymer matrix (Thévenot et al., 2013). Magnetic hydrogels are able to respond to an external magnetic field, modifying their properties (microstructure, mechanical behavior). Furthermore, the presence of magnetic material allows detection and control without direct contact with the ferrogel (Lopez-Lopez et al., 2015) (Lopez-Lopez et al., 2017). These magnetic hydrogels may be preferred to nonmagnetic hydrogels for applications because of the controllability of their macroscopic properties as well as their microstructure by means of noncontact magnetic forces. Recent works highlight the advantages that magnetic hydrogels can offer over non-magnetic hydrogels. For example, the presence of magnetic particles makes possible to visualize and monitor hydrogels *in vivo* by magnetic resonance

(Margel, 2012). In addition, *ex vivo* experiments suggest that the presence of magnetic material in the hydrogel stimulates cell adhesion and proliferation (Ban, 2014) (Bock et al., 2010).

For any biomedical application, hydrogels should satisfy biocompatibility requirements. In the case of magnetic hydrogels, the potential cytotoxicity of magnetic nanoparticles is one of the main concerns about using them in biomedicine. In the last few years, understanding the pathways by which nanoparticles, as a extraneous object to the human body, react or interact with living cells has become a key research challenge.

In this chapter we analyze the cytotoxicity of sepiolite particles covered by magnetite nanoparticles. For this aim, we coated these composites with poly(ethylene glycol) (PEG), which is considered as an adequate coating for particles intended for biomedical applications, because of its limited interaction with biological molecules, including proteins (Peppas et al., 2006). The resulting composites were then incorporated within alginate hydrogels and their cytotoxicity was analyzed using a series of standard methods. In parallel, a similar system with alginate molecules covering the particles instead PEG, was tested following the same experimental methods. Additionally, the cyctoxicity of suspensions of bare (non-functionalized) sepiolite-magnetite nanocomposites was investigated.

4.2. Materials and methods

4.2.1. Materials

The sepiolite covered by magnetite nanoparticles (SM) were used for the preparation of the nanocomposite hydrogels. The reagents used for the synthesis of these nanoparticles are detailed in Chapter 2 (Section: Materials and Methods). The chemicals employed in the preparation of the hydrogels based on alginate polymer are also detailed in Chapter 2 (Section: Materials and Methods). For covering the particles, in addition to the coating polymer, polyethylene glycol (PEG) (25 wt. %), the chemicals

employed were: mineral oil, n-hexane (99%), sorbitan sesquioleate (SSO), and glutaric dialdehyde, (25 wt.%). All these chemicals were supplied by Sigma-Aldrich (USA), and used without further purification.

4.2.2. Synthesis of the magnetite-covered sepiolite particles and their functionalization by PEG or alginate molecules.

The steps in the synthesis of the sepiolite-magnetite particles (SM) for the preparation of the PEG-coated SM hydrogels were as follows:

i) First, 1.5 g of sepiolite particles were dispersed in a solution containing 4.410 g of $FeCl_3 \cdot 6H_2O$ in 200 mL of deionized water.

ii) The resulting suspension was kept during 30 min under sonication in an ultrasonic bath. Then, it was deoxygenated by bubbling nitrogen during 15 min. Finally, the flask was closed, and the suspension magnetically stirred for 12 h.

iii) Then, 1.614 g of $FeCl_2 \cdot 4H_2O$ were added to the suspension obtained in step (ii). This new suspension was heated to 90°C and, after that; 6 mL of NH_4OH were rapidly added under stirring. A black precipitate appeared immediately. The resulting suspension was stirred under nitrogen atmosphere for 1 h at 90°C.

iv) The mixture obtained in step (iii) was cooled down to room temperature and, finally, washed by repeated cycles of decantation (using a powerful magnet) and redispersion in fresh deionized water until the supernatant conductivity was less than 20 μS/cm.

In order to coat the sepiolite-magnetite particles by adsorption of PEG molecules we followed an adaptation of the method proposed in (Chatterjee et al., 2005), which is based on the formation of a water-in-oil microemulsion. A detailed description of the method can be found in (Rodriguez-Arco et al., 2016). It can be summarized as follows.

i) The oil phase consisted of a mixture containing 75 mL of mineral oil, 225 mL of hexane and 400 μL of sorbitan sesquioleate (surfactant), all of them supplied by Sigma-Aldrich (USA).

ii) The aqueous phase consisted of a mixture containing 1 g of the magnetic composites (SM) and 0.5 g of PEG in 7.5 mL of distilled water. This mixture was homogenized by an ultrasonic bath.

iii) Both oil and water phases were mixed by ultrasonication for 5 min.

iv) Finally, we added 75 mL of glutaraldehyde (Sigma-Aldrich) and stirred the resulting mixture for 2 hours. The final product was cleaned by consecutive cycles of decantation (using a powerful magnet) and redispersion in hexane (3 times) and ethanol (3 times).

In the next sections we also refer to SM+ALG particles, as the sepiolite–magnetite particles coated by adsorption of sodium alginate molecules. For this purpose, first, 1.0 g of SM particles was dispersed in a solution that contained 0.25 g of sodium alginate in 50 mL of water. Second, this suspension was mechanically stirred at room temperature during 1 h and, finally, washed by repeated cycles of decantation (using a powerful magnet) and redispersion in fresh distilled water until the supernatant conductivity was less than 20 µS/cm.

4.2.3. Preparation of the magnetic hydrogels

The magnetic hydrogels, consisting of SM particles (either coated by PEG or by alginate) dispersed in alginate hydrogels, were prepared according to the following steps:

i) A suspension with a concentration of 10% w/v of the functionalized –by PEG or alginate adsorption– SM particles in deionized water was prepared by mechanical stirring.

ii) A solution of sodium alginate containing 0.25 g of sodium alginate salt in 50 mL of water (0.5% w/v) was prepared.

iii) Aliquots of 2.5 mL of the suspension prepared in step (i) were mixed with 2.5 mL of the 0.5% w/v alginate solution prepared in step (ii). This pre-gel mixture was carefully shaken by hand until the resulting suspension was homogeneous.

iv) Then, 22.5 mg of $CaCO_3$ were added to the pre-gel suspension prepared in the previous step and stirred by a vortex mixer during a few seconds.

v) An amount of 26.7 mg of GDL was added to the resulting mixture prepared in step (iv), shaking by hand, and afterwards placed in a Petri dish and left at rest during 4 h.

vi) Finally, 5 mL of a 45 mM CaCl$_2$ solution was added and the mixture was left overnight at room temperature in order to obtain the final ferrogel.

4.2.4. Cytotoxicity analysis of magnetic particles and magnetic hydrogels

We evaluated the cytotoxicity of: i) suspension of sepiolite-magnetite particles (SM); ii) ferrogels prepared with SM particles coated with alginate (SM+ALG), and iii) ferrogels prepared with SM particles coated with polyethylene glycol (SM+PEG).

For cytotoxity tests, we carried out 2-D cultures of human fibroblasts in contact with magnetic dispersions (suspensions or ferrogels) that contained 1 % v/v particle concentration. These magnetic dispersions, in a volume proportion of 5%, were mixed with each one of the 2D culture medium describe below.

The human fibroblast cells were previously isolated from healthy donors, expanded them until passage 5 and finally seeded in the culture medium (DMEM) in contact with the magnetic samples, at a cellular density of 1.3×10^5 cells per mL. For this we used well described protocols reported in (Bonhome-Espinosa et al., 2017). Briefly, samples were kept under culture conditions (37ºC, 5% CO$_2$) with DMEM, supplemented with antibiotics and antimycotics cocktail solution and 10% fetal bovine serum supplied by Sigma Aldrich, Germany. Alternatively, as a negative control, the cells were incubated with a 2% solution of Triton X-100 (a nonionic surfactant). In addition, as a positive technical control, a 2D cell culture without magnetic dispersions was carried out.

After 48 h of cell culture in the different culture media, we evaluated the ex vivo biocompatibility by using the histological and DNA quantification methods that we briefly described below. These methods were more precisely reported in (Campos et al., 2016).

4.2.5. Analyses of cells morphology, viability and proliferation

We analyzed the morphology of the cells by means of phase contrast microscopy observation.

The analysis of cell viability and proliferation was carried out by different techniques as described below.

i) The cell viability was evaluated by measuring intracellular esterase activity, and by examining the integrity of the plasma and nuclear membranes with a fluorescence-based method using the Live/Dead commercial kit (Life Teechnologles, Carlsbad, CA, USA). This method uses calcein-AM, which is metabolically modified by living cells to a green pigment, and ethidium homodimer-1, which stains the nuclei of dead cells in red colour. We obtained aliquots of the cell cultures, incubated them with the Live/Dead solution for 15 min as indicated by the manufacturer, and washed them with PBS. Then, the samples were observed by fluorescence microscopy and the images processed with image software to quantify the number of live (green) and dead (red) cells.

ii) We also quantified cell proliferation and viability by using the water-soluble tetrazolim salt-1 (WST-1) colorimetric assay (Cell Proliferation Reagent WST-1, Roche Diagnostics). WST-1 is a tetrazolium dye containing an electron coupling reagent that is cleared by the mitochondrial dehydrogenase enzyme to a formazan dye. The reaction directly correlates with the number of metabolically active proliferating cells and can serve as a marker of cell viability and cell proliferation. For this assay, cells were cultured with the working solution for 4 h at 37° C, and the absorbance of the colorimetric reaction was measured with an Assay UVM 340 spectrophotometer in triplicate.

iii) Finally, we evaluated the cell death by analysing the nuclear membrane integrity. For this purpose, the DNA released to the culture medium was quantified by extracting the supernatant of each culture condition and stored it

in Ependorf tubes. Then, the DNA concentration was measured with a UV-VIS NanoDrop 2000 spectrophotometer.

4.2.6. Statistics

The mean values ± standard deviations of 12 independent experiments were reported for each experimental group and each analysis. The Kruskal–Wallis test was used to identify statistical differences among study groups. In addition, the Mann–Whitney test was used to identify significant differences between two groups. Values of p less than 0.05 were considered statistically significant in two-tailed tests.

Ethics statement: This study was approved by the Ethics Committee of the Province of Granada, Spain. Each tissue donor signed an informed consent form for the study.

4.3. Results and discussion

Morphological analysis of cells cultured as a positive technical control (CTR+) showed normally shaped fusiform and star-shaped cells (Figure 4.1). Similar results were obtained for cells cultured in contact with the suspension containing bare SM particles and with hydrogels with SM+ALG particles, although some round-shape cells were observed in the last case. Finally, cells cultured in contact with hydrogels containing SM+PEG particles showed a round shape. It should be noted that round shape, which reveals a radical morphological change, is an indication of the lack of adaptation of the cells to the medium.

Representative fluorescent microscopy images from viability tests (Live/Dead) for suspension SM, (SM+ALG) and (SM+PEG) hydrogels are shown in Figure 4.2. In this kind of study, live cells are stained in green color, whereas dead cells are stained in red. As observed, there was a favorable response of the fibroblasts exposed to both the SM particles, as well as the fibroblasts exposed to the hydrogels containing SM+ALG particles, with results very similar to those of the positive control group (CRT+). In these three cases, very few dead cells were observed. Most cells were living cells, with good morphology and they looked similar in the SM and SM+ALG groups to those of the control group. On the contrary, cells in the SM+PEG group appeared dead,

with a round and red look. Overall, these results are consistent with those in Figure 4.1.
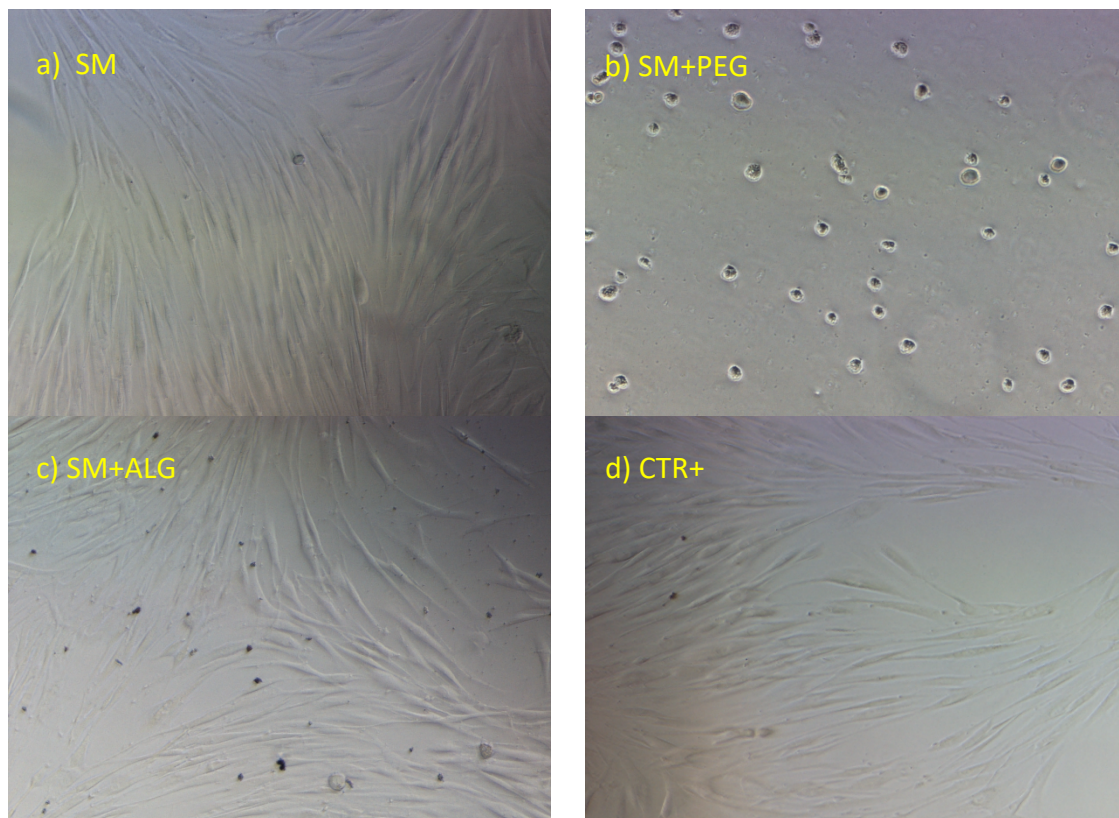
Figure 4.1. Microscopic images of cells, in contact with the indicated cell culture media, as observed under phase contrast microscope. a) magnetic suspension with SM particles; b) ferrogel with SM particles coated by PEG, c) ferrogel with SM particles coated by alginate; d) positive control, CTR+.

From images like these of Figure 4.2 the number of live and dead cells in a specific surface area were counted and the results are shown in Figure 4.3, whereas Figure 4.4 shows the percentage of live cells. As observed (Figure 4.3), for the sepiolite covered by magnetite (SM) nanoparticles, there were no statiscally significant differences ($p > 0.05$) with respect to the positive control group (CRT+). The results of the hydrogel containing SM+ALG show that the cell viability was also favorable and close to that of the positive control group, without statistically significant differences ($p > 0.05$). This indicates minimal or no leaching of the hydrogel substances, as it was expected. On the contrary, cell count for the group SM+PEG shows similar number of

dead and live cells. Finally, in the negative control group (CTR-) there were no live cells as expected for fibroblasts exposed to a toxic substance.
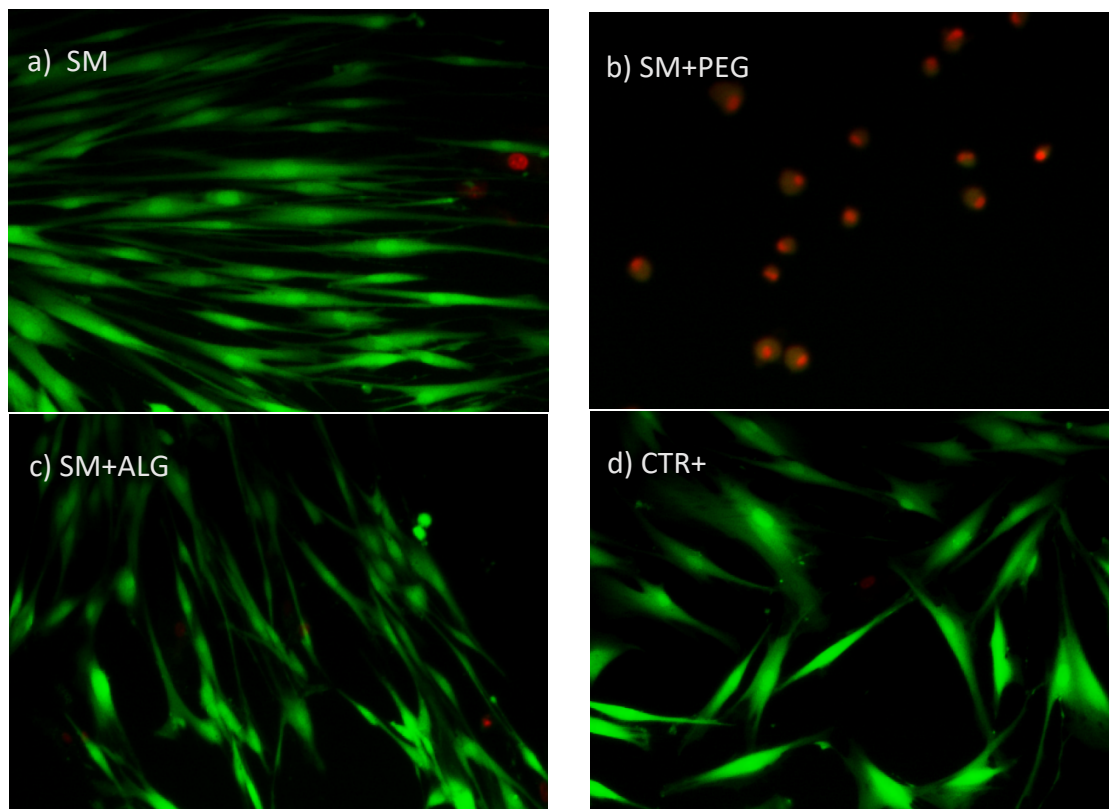
Figure 4.2. Similar to Figure 1, but here with flourescence microscopy images representative of the live/dead experiments. Live cells are stained in green, whereas dead cells are stained in red. Note the elongated, star-like shape of live cells, in contrast to the round-like shape of dead cells.

Biochemical analysis of cell proliferation with the WST-1 test (Figure 4.4) showed significantly higher mean values of proliferation in the SM, and SM+ALG groups, compared to the positive group, although no statistically significant differences were obtained p>0.05. All these three groups presented values significantly different to the negative control group (CTR-). On the contrary, results for the SM+PEG group shows low cell proliferation, similar to the value for the negative control group, with no statistically significant difference with respect to this group (p > 0.05).

	CTR+	CTR-	SM	SM+PEG	SM+ALG
Live	595,333	0,000	490,333	115,333	318,333
Dead	39,000	581,000	17,000	107,333	48,333
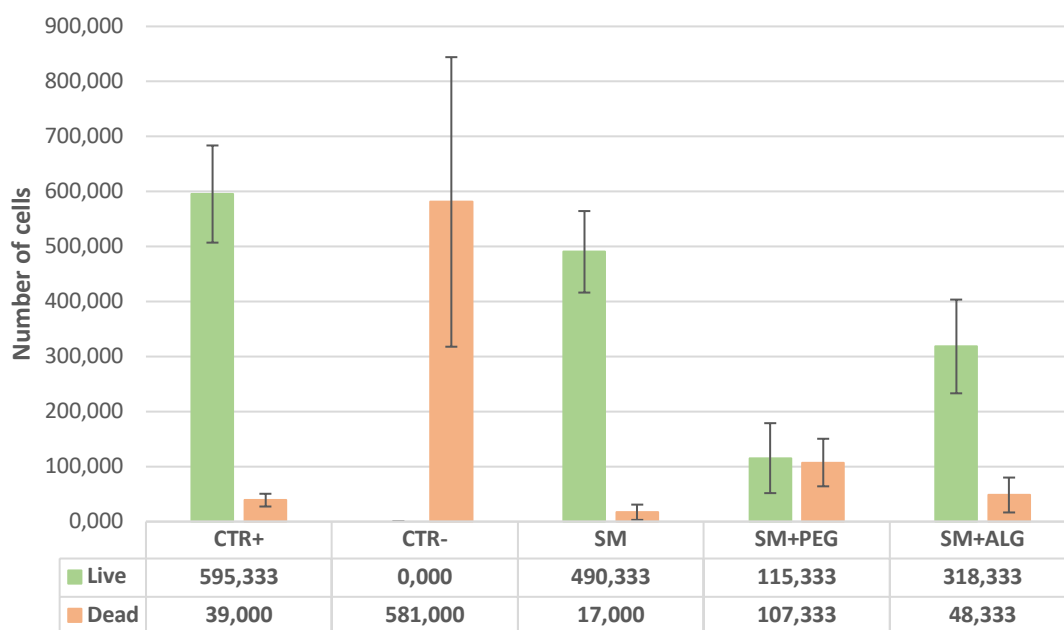
Figure 4.3. Number of live and dead cells in a specific surface area for the different experimental groups.

	CTR+	CTR-	SM	SM+PEG	SM+ALG
Values	93,644	0,000	96,363	50,262	87,004

Figure 4.4. Mean values ± standard deviations for live cells for the different experimental groups. Note that percentage of live cells is zero for the negative control group (CTR-).
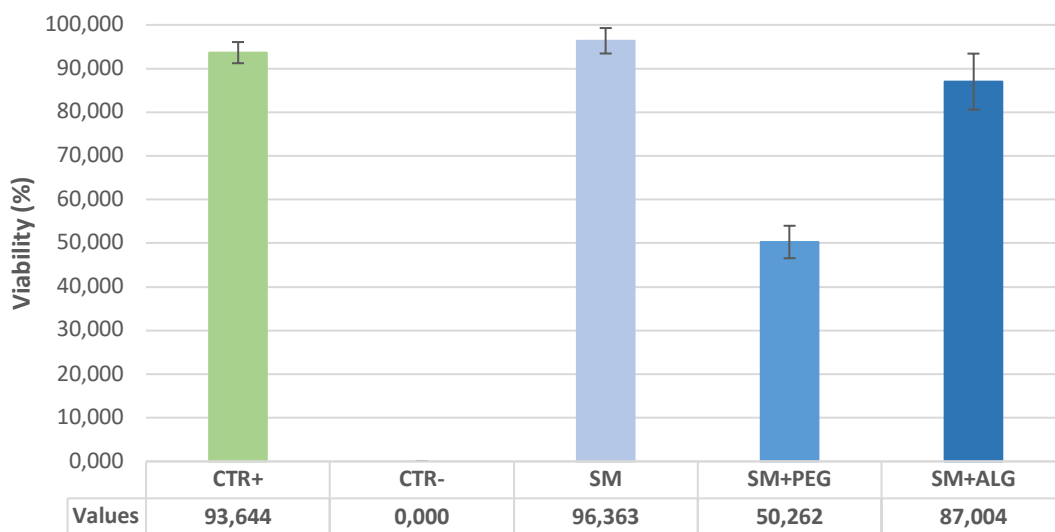
Finally, analysis of damage to the nuclear membrane by the quantification of DNA release to the culture medium (Figure 4.5), demonstrated that all experimental groups presented some extent of irreversible damage to the cell membrane but, considerably lower than that observed in the negative control group (CTR-). With respect to the specific comparison among the different groups, SM group shows the minimum damage to the cell membrane, with a statistically significant difference with respect to the control group. Similarly, the SM+ALG group shows very good values, with less DNA release to the medium that in the positive control group. On the contrary, the SM+PEG samples showed slightly higher values of the DNA release than the CTR+ group, albeit without statistically significant differences.

	CTR +	CTR -	SM	SM+PEG	SM+ALG
Value	149,658	926,850	122,425	155,125	139,750
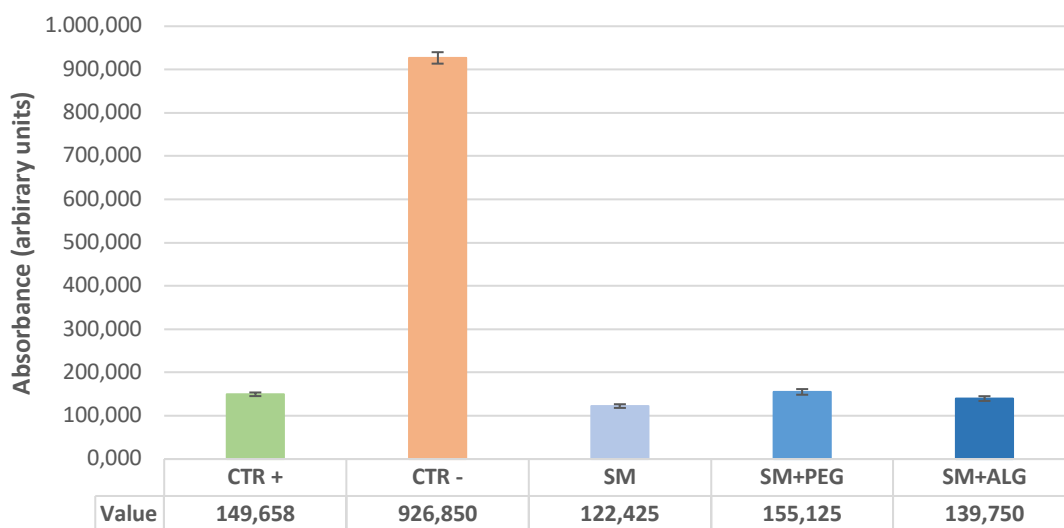
Figure 4.5. Quantification of DNA release. The integrity of the nuclear membrane was studied through the amount of the DNA released to the culture medium.

As a whole, we can conclude that the results of all the cell viability experiments are consistent and indicate that cell viability and proliferation of fibroblasts cultured in contact with SM particles or hydrogels containing (SM+ALG) nanoparticles did not present statistically significant differences with respect to the control positive group.

On the other hand, cell viability and proliferation are worst for fibroblasts cultured in contact with hydrogels containing (SM+PEG) nanoparticles, although significantly better than for the negative control group. Furthermore, for all the

experimental groups, results of DNA release are similar and very close to the positive control group, from which we can conclude that even though cell proliferation may be worst for fibroblasts cultured in contact with hydrogels containing SM+PEG, the nuclear membrane was not appreciably damaged with respect to the positive control group.

In what respect to the comparison of the results of our work with some other previous works like that by (Bock et al., 2010), we interpret that our results imply that magnetic tissue substitutes could likely be good candidates to be safety used in vivo. It is noticeable that in a previous work, for fibroblasts cultured in contact with magnetic composites (consisting of polymer nuclei covered by a layer of magnetite and an outer layer of PEG), no statistically significant differences were observed in terms of cytotoxicity as compared with the control positive group (Rodriguez-Arco et al., 2016). What is more, in that previous work it was found that the PEG coating improved the cell viability and proliferation with respect to the magnetic nanocomposites not containing the PEG coating. A possible hypothesis to explain the discrepancies between the results of the present chapter and those reported by (Rodriguez-Arco et al., 2016) is that the combination of alginate and PEG is not appropriate from the point of view of cell viability.

Finally, in what concerns to the overall cytotoxicity of the bare composites and the composites covered by alginate, we can conclude that for the quantities employed in the present work, there are no adverse effects in the viability and proliferation of fibroblasts. This indicates that for low amounts, the sepiolite nanoparticles covered by magnetite have the potential to be biocompatible and thus should not be recognized by the body as extraneous matter.

4.4. Conclusions

In this chapter we have described the cytotoxicity analysis of magnetic hydrogels consisting of sepiolite nanoparticles coated by magnetite. For this aim we have used three different systems: (i) bare nanocomposite particles (sample SM) dispersed directly in the culture medium; (ii) composite SM particles coated by alginate and

embedded within alginate hydrogel (sample SM+ALG); (iii) composite SM particles coated by polyethylene glycol and imbedded within alginate hydrogel (sample SM+PEG). In all the cases, the amount of nanocomposite particles in the culture media was the same and the fibroblast were cultured in contact with these three systems (prepared in sterile conditions) for 48 h under standard culture conditions (37° C and 5% CO_2), in DMEM culture medium, supplemented with a solution of antibiotics and antifungal agents. After this time cell viability and proliferation were analyzed by different techniques. For comparison we employed a negative control group consisting of fibroblasts incubated with 2% Triton -100, and also a 2D cell culture positive technical control.

Morphological analysis indicated no significant differences between SM and SM+ALG samples with respect to the positive control group, showing in all cases an elongated star-like shape compatible with living fibroblasts. However, fibroblasts cultured in contact with the SM+PEG ferrogel presented a round morphology, indicating rejection of the cell for the sample.

In agreement, results of Live/Dead commercial test indicated that no significant differences existed between fibroblasts cultured in contact with SM or SM+ALG samples, with respect to fibroblasts of the positive control being the percentage of live cells around 90% in these three cases. On the contrary, for fibroblasts cultured in contact with SM+PEG sample, a significant decrease in the percentage of live cells was observed, with dead cells reaching 50% of the total number of cells. However, the percentage of live cells was still high (50%) and significantly different from the 0% observed for the negative control group. Similar results were obtained for the proliferation of cells, analyzed by mean of WST-1 test.

Finally, results of DNA release indicated that the nuclear membrane of the cells was not appreciably damaged by either of the experimental groups (SM, SM+ALG or SM+PEG), being the released DNA in all cases similar to the control group. Thus, we can state that even though the culture medium in contact with SM+PEG sample was not optimum for fibroblast culture, no irreversible damage of the nuclear membrane

took place. The comparison between bare nanocomposites (sample SM) or nanocomposites coated with alginate and embedded in alginate hydrogel (sample SM+ALG) showed that no significant differences of cell viability/proliferation were obtained with respect to positive control group. These positive results of the cytotoxicity analysis are promising for the potential use of magnetic nanocomposites consisting of sepiolite coated by magnetite in biomedical applications. Further studies involving 3-D cultures within magnetic hydrogels containing these nanocomposites will show if they can be safely introduced in scaffolds for the generation of artificial tissues by tissue engineering techniques.

Chapter 5

Conclusions

Magnetic hydrogels are heterogeneous systems consisting of magnetic nano- or microparticles dispersed in a network of hydrophilic polymer chains swollen by water or aqueous liquids. The macroscopic physicochemical properties of these materials depend on a number of variables related to the properties of the solid particles, the polymer composition and conformation, and the water content of the whole system. If, in addition, we take into account that the internal structure of the hydrogel –that is, the arrangement of their components– can be modified by chemical or physical internal/external stimuli, we are facing nanomaterials with extraordinary versatile benefits in very different fields of science and technology. Following a very recent review about these systems (Liu et al., 2020), we can mention four main areas of potential applications: i) drug delivery, ii) tissue engineering, iii) biological research, and iv) hydrogel machines. All these applications lay on the possibility of regulating, even dramatically, the mechanical softness and water (or aqueous solutions of different bioactive molecules) content of the hydrogels. Thus, the mechanical moduli (e. g. Young's modulus E, rigidity modulus G) of the hydrogels can range from values less than those of brains, nervous or spinal cords ($E \sim 10^2$ Pa – 10^4 Pa; $G \sim 10^2$ Pa – 10^3 Pa) to those of cartilage tissues ($E \sim 10^5$ Pa – 10^7 Pa; $G \sim 10^5$ Pa – 10^6 Pa) (Scionti et al., 2014) (Liu et al., 2020).

In the case of magnetic hydrogels, the possible rearrangement of their microstructure by remote (non-contact) action of a magnetic field confers to ferrogels a smart (adaptative) nature, which improves even more the capabilities of these soft-wet materials.

In this work we aimed to contribute to the materials science of magnetic hydrogels by incorporating magnetic particles, with at least four main characteristics. a) Non-spherical shape. b) Low average density. c) Biocompatibility, facing their potential applications in tissue engineering. d) And all these previous properties,

without losing the control of the viscoelastic properties of the resulting ferrogels by the action of external magnetic fields of not too high intensity (up to H in the order of 10^2 kA/m).

To fulfill these features, the magnetic hydrogel designed in this work consisted of composite particles based on clay particles with two different shapes (fibers, platelets) covered by magnetic nanoparticles. These particles were imbedded into a polymer matrix of a natural polymer (alginate, a polysaccharide), which can be easily cross-linked by physical interactions among the alginate molecules and even among the polymer chains and the alginate molecules adsorbed onto the particles surface. The functionalization of the particles can play a double role: the reinforcement of the internal network of the hydrogels and, in addition, conferring the required biocompatibity to the obtained ferrogels.

The determination of the mechanical (rheological) properties of the ferrogels had been a central point of this work. Ferrogels behave as soft viscoelastic materials in which the corresponding viscoelastic moduli, which quantified their response to external forces (more properly normal or shear stress), depend on a number of variables. These variables are: i) the length and crosslinking degree of the polymer chains; ii) the degree of attachment (if it exists) among the polymer chains and the solid particles or, more precisely, the molecules adsorbed onto the particles; iii) the strength of the bond (covalent, electrostatic) between the crosslinker agent and the polymer molecules; iv) the concentration and aggregation degree of the solid particles imbedded in the hydrogel; v) the magnetic properties of the particles; vi) the intensity of the applied magnetic field; vii) and finally, but no less important as demonstrated in this work, the shape of the solid particles.

The main conclusions of this work can be summarized as it follows.

A) From the results in Chapter 2 (sepiolite-magnetite ferrogels) we can conclude:

A.1. The synthesized composite particles are actually composed by a fiber or rod-like core of sepiolite and a shell of magnetite nanoparticles (SM particles). These composite particles were efficiently functionalized by

adsorption of alginate molecules (SMA particles). These statements were checked by using different and complementary experimental methods.

A.2. The magnetic response (e.g. saturation magnetization M_S) of these composite particles (SM and SMA) was large enough in comparison to that of pure magnetite (M_S = 446 kA/m): M_S (SM) = 261 kA/m; M_S (SMA) = 170 kA/m. This implied that the composite particles contained a volume fraction of magnetic material around 40 %.

A.3. In consequence, the magnetorheological effect reached, even for non-concentrated suspensions (particle volume fraction 10 %), was very high, with the additional advantage of their very low setting rate in comparison with this of suspensions of non-composite magnetic microparticles (magnetite, iron). This last point (slow gravitational settling) was particularly pronounced when the particles were functionalized by alginate adsorption.

A.4. The cross-linking among the polymer chains, and among these ones and the alginate-functionalized SM particles, was achieved by controlled addition of calcium ions using pre-gel solutions with different sodium alginate concentrations. The hydrogel network was formed by alginate chains bonded to the solid particles, with these ones placed as net knots. The variation in the crosslinking degree and also in the particle concentration allowed obtaining ferrogels with different softness and magnetic response.

A.5. We have prepared two different ferrogels, with different alginate concentrations in the pregel solutions. This variable, coupled with the particle concentration, determined the stiffness of the resulting ferrogel avoiding both an excessive softness –what would be a problem to handle the gel– and at the opposite extreme an excessively rigidity –what would avoid the magnetic control of the rheological properties. Thus, we obtained two different ferrogels for which the elastic modulus ranged, in the absence of applied field, from $G' \approx 20$ kPa ("Ferrogel-1") up to $G' \approx 30$ kPa ("Ferrogel 2").

A.6. The magnetorheological effect (MRE) achieved in ferrogels containing SMA particles depended on the role played by both the magnetic forces

among particles and the elastic forces developed inside the particle-polymer network.

Thus, when the ferrogels were subjected to a low shear strain the MRE-G' – MRE quantified by the relative field-induced increase in G'– reached a value as high as 64% (conditions: strain 3%, particle concentration less than 1 % v/v, Ferrogel-1, H of the order of M_S). This relatively strong MRE value indicated that, at low strain, the mechanical response of the ferrogels was mainly dominated by the particle-particle magnetic interactions and it can be controlled by the external field. On the contrary, at larger shear strains (10%; other conditions identical as above) the MRE-G' values were considerably reduced: MRE $\leq$ 22%. Thus, the enlarged gap between particles weakens the magnetic interactions, and the mechanical response of the ferrogel was mainly determined by the elastic resilience of the knotted particle-polymer network.

A.7.   The effect of the particles shape on the MRE has been studied by defining a normalized MRE-G' parameter, $\overline{MRE}(\%)$, that mainly accounted for the particle morphology. This parameter allows the comparison among ferrogels with different kinds and concentrations of magnetic particles, and intensity of the applied fields. The comparison, among the $\overline{MRE}(\%)$ values in the fiber-like SMA ferrogels in this work with other ferrogels previously reported containing spherical particles, demonstrated that the imbedding of elongated particles significantly enhanced the MRE effect in ferrogels. For example, the maximum value $\overline{MRE}(\%)$ reached in Ferrogel-1 was 64%, while in a similar alginate ferrogel with spherical silica-iron particles $\overline{MRE}(\%)$ was 15%.

B) From the results in Chapter 3 (bentonite-magnetite ferrogels) we can conclude:

B.1.   First of all, we have to note that, unlike the sepiolite employed in the previous chapter, the bentonite particles employed in this chapter were of mineral origin, collected form a Tunisian deposit, containing significant amounts of calcite and quartz and, in addition, most of the exchange cations in the clay were calcium ions (calcium bentonite).

Thus, the purification process was different of a simple homoionization process, like that employed in the previous chapter. In this case, the so-called hydrocyclone separation method –a wet separation method previously applied in the Tunisian PhD thesis of this candidate– was used to simultaneously remove the mineral impurities and substitute the Ca^{2+} ions by Na^+ ones. The so obtained sodium bentonite particles had the typical platelet-like shape of the smectite clays.

Nevertheless, the well-known strong van der Waals attraction between the clay faces favored the formation of aggregates with rounded stacked platelets. This arrangement of the bentonite particles remained at least partially after the coverage by magnetite and even after the functionalization by alginate adsorption. Therefore, we have to keep in mind that the MRE effect in the bentonite-based ferrogels had to be conditioned, not only by the particles shape, but also by the presence of these bentonite clusters.

B.2. The bentonite particles were effectively covered by magnetite nanoparticles using the same coprecipitation method employed in chapter 2.

B.3. The magnetite-covered bentonite particles (BMag) had a strong enough magnetic character (M_S = 110 kA/m) and an internal volume fraction of magnetic material of approximately 25%.

B.4. The BMag particles were functionalized by alginate adsorption. In this case, two functionalized magnetic composites were obtained by adsorption of alginate molecules from solutions of this polysaccharide with a concentration ratio 1:4 (BMagF1 : BMagF2 samples, respectively).

B.5. The first advantage of the functionalization was a very significant decrease in the settling rates of the aqueous suspension of the functionalized particles in comparison with that of bare ones. In fact, the BMagF2 composites suffered a practically negligible sedimentation during one week at rest. This fact, together with the low average density of the particles, represents a key point to obtain homogeneous

ferrogels, avoiding significant gradients of particle concentration during the gelation process.

B.6. The MRE in suspensions containing 10% w/v of bare BMag particles demonstrated an intense magnetorheological response that reached up to 87 % for field intensity close to 300 kA/m. In this case, the MRE was more reasonably calculated from the values of the plastic viscosity of the suspension, taking into account the very low elastic behavior (G' at H = 0 kA/m was only 11 Pa) of this relatively diluted suspension.

B.7. More interesting, in the context of the present work, were the MRE values reached by the ferrogels. The MRE values were determined in ferrogels containing the largest coverage by alginate molecules (BMagF2) because of their better homogeneity. In this case, four different ferrogels were prepared, differenced only in the concentration of alginate in the pre-gel solution, which ranged from 0.25% w/v up to 2% w/v. Thus, the most diluted ferrogel (BMagF2+0.25%Alg) contained an alginate proportion 1:8 with respect to the most concentrated one (BMagF2+2%Alg).

As expected, the MRE-G' values did not vary linearly with the alginate concentration. The maximum MRE-G' value (520%) was obtained for an intermediate alginate concentration (ferrogel BMagF2+0.5%Alg; H = 282 kA/m; strain 10%) and the minimum (MRE-G' = 12%) for the most concentrated one (ferrogel BMagF2+2%Alg; same experimental conditions), demonstrating that an excessive cross-linking inside the ferrogel network largely hindered the effect of the magnetic field application.

B.8. Finally, the normalized $\overline{MRE}(\%)$ values were obtained to compare the shape effect on the field control of the mechanical behavior of the ferrogels. In this case, the most significant conclusion was obtained by comparing ferrogels with the same alginate concentration in the pre-gel solution (1% w/v) and different morphologies.

The $\overline{MRE}(\%)$ values obtained for the different core-shell particles analyzed were: 21% (bentonite-magnetite platelets), 43% (silica-iron

spheres), and 180% (sepiolite-magnetite fibers). Likely, the presence of bentonite stacked clusters provoked the lowest value for this ferrogel. This fact represents a disadvantage partially compensated by the higher homogeneity of this clay-based system –because of the lower average density of the BMag particles– as compared with that of the silica-iron ones.

C) Chapter 4 was devoted to the analysis of the biocompatibility of the ferrogels based on sepiolite-magnetite composites. The cytotoxicity of these magnetic colloids was studied ex vivo following different techniques usually employed in histological essays and, more particularly, in tissue engineering. These tests are intended to verify the possible damaging effects of biomaterials on living cells. More specifically, they can be also applied to analyze the viability and proliferation of cells cultured in the polymer matrices (magnetic hydrogels in our case) designed as potential tissue scaffolds.

C.1. The toxicity of different magnetic dispersions was tested by using four different 2D ex vivo techniques. The first one was based on the visualization of the morphology of the cells cultured in the presence of the magnetic dispersions. The second and third techniques –Live/Dead test, based on the intracellular estearase activity; WST-1 test, based on the reaction of mitochondrial dehydrogenase enzyme with a dye– were useful to count the number of live cells after 48 h of cell culture. The fourth technique quantified the cytotoxicity by measuring the DNA released to the culture medium when the cell membrane integrity is compromised.

C.2. These fourth techniques were employed to evaluate the cytotoxicity on fibroblasts in different culture media containing: i) a non-toxic standard solution (positive control); ii) the same non-toxic solution including a proportion of the magnetic dispersions studied; and iii) as negative control group, the cells were incubated in a solution of a surfactant.

C.3. The ferrogels evaluated contained sepiolite-magnetite (SM) particles in an alginate hydrogel. The particles were functionalized by adsorption of alginate molecules. Alternatively, and for comparison, the particles were functionalized by adsorption of a polymer (polyethylene glycol, PEG) that in

previous works had been reported as appropriate for conferring biocompatibility to magnetic nanoparticles. Finally, a magnetic suspension containing bare SM particles was tested. In all these magnetic dispersions the particle volume fraction was 1%, which is large enough to check the toxic effect on the cultured fibroblasts.

C.4.   The morphological analysis demonstrated that the cells in contact with bare SM particles or alginate-functionalized SM particles did not lose their characteristic elongated shape, compatible with living fibroblast, while the cells in contact with SM-PEG particles had a rounded shape as a consequence of the possible toxic effect of the particles.

C.5.   The Live/Dead test demonstrated the cell viability (around 90 % of living cells) in the colloids containing bare SM or SM-alginate particles. On the contrary, in the cell culture in the presence of SM-PEG a percentage as high as 50% of the fibroblast was dead cells.

C.6.   The results obtained by means of the WST-1 test gave similar results to those with the Dead/Live test, demonstrating the consistence between the two tests that evaluated the number of dead cells in the culture media.

C.7.   Finally, the test that checked the integrity of the nuclear membrane (and the DNA released) showed that, for all the magnetic dispersions tested, the results obtained were similar to that in the positive control media (and opposite to the negative one). Thus, it seems that the SM particles (bare or recovered by alginate or PEG) did not provoke a significant damage to the nuclear membrane.

C.8.   All these *ex vivo* essays demonstrated that the alginate ferrogels, with alginate-covered SM particles imbedded, could be a good (because of their biocompatibility) scaffold candidate for generating artificial tissues for tissue engineering purposes.

Chapter 6

References

Abrougui, M. M., Bahri, D., & Srasra, E. (2019). Structural Characterizations and Viscosity Behavior of Purified Clay Obtained by Hydrocyclone Process. *Chemistry Africa*, (0123456789). https://doi.org/10.1007/s42250-019-00076-9

Abrougui, M. M., Bonhome-Espinosa, A. B., Bahri, D., López-López, M. T., Durán, J. D. G., & Srasra, E. (2018). Rheological Properties of Clay Suspensions Treated by Hydrocyclone Process. *Journal of Nanofluids*, *7*(2), 258–268. https://doi.org/10.1166/jon.2018.1460

Abrougui, M. M., Lopez-Lopez, M. T., & Duran, J. D. G. (2019). Mechanical properties of magnetic gels containing rod-like composite particles. *Philosophical Transactions of the Royal Society A: Mathematical, Physical and Engineering Sciences*, *377*(2143). https://doi.org/10.1098/rsta.2018.0218

Adams, D. J. (2011). Dipeptide and Tripeptide Conjugates as Low-Molecular-Weight Hydrogelators. *Macromolecular Bioscience*, *11*(2), 160–173. https://doi.org/10.1002/mabi.201000316

Agirre-Olabide, I., Berasategui, J., & Elejabarrieta, M. J. (2014). Characterization of the linear viscoelastic region of magnetorheological elastomer. *Journal of Intelligent Material Systems and Structures, 25*(16), 2074-2081. https://doi.org/10.1177/1045389X13517310

Ahribesh, A. A., Lazarević, S., Janković-Častvan, I., Jokić, B., Spasojević, V., Radetić, T., Petrović, R. (2017). Influence of the synthesis parameters on the properties of the sepiolite-based magnetic adsorbents. *Powder Technology*, *305*, 260–269. https://doi.org/10.1016/j.powtec.2016.09.086

Akhtar, M. F., Hanif, M., & Ranjha, N. M. (2016). Methods of synthesis of hydrogels. A review. *Saudi Pharmaceutical Journal*, *24*(5), 554–559. https://doi.org/10.1016/j.jsps.2015.03.022

Alaminos, M., Sánchez-Quevedo, M. D. C., Muñoz-Ávila, J. I., Serrano, D., Medialdea, S., Carreras, I., & Campos, A. (2006). Construction of a complete rabbit cornea substitute using a fibrin-agarose scaffold. *Investigative Ophthalmology and Visual Science*, *47*(8), 3311–3317. https://doi.org/10.1167/iovs.05-1647

Aliyan, H., Fazaeli, R., & Jalilian, R. (2013). Fe 3 O 4 @mesoporous SBA-15: A magnetically recoverable catalyst for photodegradation of malachite green. *Applied Surface Science*, *276*, 147–153. https://doi.org/10.1016/j.apsusc.2013.03.049

Alkan, M., Demirbaş, Ö., & Doğan, M. (2005). Electrokinetic properties of sepiolite suspensions in different electrolyte media. *Journal of Colloid and Interface Science*, *281*(1), 240–248. https://doi.org/10.1016/j.jcis.2004.08.036

Arizaga, A., Ibarz, G., & Piñol, R. (2010). Stimuli-responsive poly(4-vinyl pyridine) hydrogel nanoparticles: Synthesis by nanoprecipitation and swelling behavior. *Journal of Colloid and Interface Science*, *348*(2), 668–672. https://doi.org/10.1016/j.jcis.2010.05.051

Chapter 6. References

Atala, A., Bauer, S. B., Soker, S., Yoo, J. J., & Retik, A. B. (2006). Tissue-engineered autologous bladders for patients needing cystoplasty. *Lancet*, *367*(9518), 1241–1246. https://doi.org/10.1016/S0140-6736(06)68438-9

Ban, M. (2014). Poly (caprolactone) based magnetic scaffolds for bone tissue engineering. *Journal of Applied physics,* 2009–2012. https://doi.org/10.1063/1.3561149

Bell, R. C., Karli, J. O., Vavreck, A. N., Zimmerman, D. T., Ngatu, G. T., & Wereley, N. M. (2008). Magnetorheology of submicron diameter iron microwires dispersed in silicone oil. *Smart Materials and Structures*, *17*(1). https://doi.org/10.1088/0964-1726/17/01/015028

Beniash, E., Hartgerink, J. D., Storrie, H., Stendahl, J. C., & Stupp, S. I. (2005). Self-assembling peptide amphiphile nanofiber matrices for cell entrapment. *Acta Biomaterialia*, *1*(4), 387–397. https://doi.org/10.1016/J.ACTBIO.2005.04.002

Bock, N., Riminucci, A., Dionigi, C., Russo, A., Tampieri, A., Landi, E., Dediu, V. (2010). Acta Biomaterialia A novel route in bone tissue engineering : Magnetic biomimetic scaffolds. *Acta Biomaterialia*, *6*(3), 786–796. https://doi.org/10.1016/j.actbio.2009.09.017

Bonhome-Espinosa, A. B., Campos, F., Rodriguez, I. A., Carriel, V., Marins, J. A., Zubarev, A., Lopez-Lopez, M. T. (2017). Effect of particle concentration on the microstructural and macromechanical properties of biocompatible magnetic hydrogels. *Soft Matter*, *13,* 2928-2941. https://doi.org/10.1039/C7SM00388A

Borin, D., Odenbach, S., Iskakova, L., & Zubarev, A. (2018). Non-ergodic tube structures in magnetic gels and suspensions. *Soft Matter 14*, 8537–8544. https://doi.org/10.1039/c8sm01456f

Bossis, G., Volkova, O., Lacis, S., & Meunier, A. (2002). Magnetorheology : Fluids , Structures and Rheology, 202–230.

Caló, E., & Khutoryanskiy, V. V. (2015). Biomedical applications of hydrogels: A review of patents and commercial products. *European Polymer Journal*, *65*, 252–267. https://doi.org/10.1016/j.eurpolymj.2014.11.024

Campos, F., Bonhome-Espinosa, A. B., García-Martínez, L., Durán, J. D. G., López-López, M. T., Alaminos, M., Carriel, V. (2016). *Ex vivo* characterization of a novel tissue-like cross-linked fibrin-agarose hydrogel for tissue engineering applications. *Biomedical Materials*, *11*(5), 055004. https://doi.org/10.1088/1748-6041/11/5/055004

Campos, F., Bonhome-Espinosa, A. B., Vizcaino, G., Rodriguez, I. A., Duran-Herrera, D., López-López, M. T., Carriel, V. (2018). Generation of genipin cross-linked fibrin-agarose hydrogel tissue-like models for tissue engineering applications. *Biomedical Materials (Bristol)*, *13*(2), 0–32. https://doi.org/10.1088/1748-605X/aa9ad2

Carl, B., & Brook, S. (1985). United States patent. *Geothermics*, *14*(4), 595–599. https://doi.org/10.1016/0375-6505(85)90011-2

Chan, R. W., & Titze, I. R. (1999). Viscoelastic shear properties of human vocal fold mucosa: Measurement methodology and empirical results. *The Journal of the Acoustical Society of America*, *106*(4), 2008–2021. https://doi.org/10.1121/1.427947

Chang, C. W., Van Spreeuwel, A., Zhang, C., & Varghese, S. (2010). PEG/clay nanocomposite

hydrogel: A mechanically robust tissue engineering scaffold. *Soft Matter*, *6*(20), 5157–5164. https://doi.org/10.1039/c0sm00067a

Chatterjee, J., Bettge, M., Haik, Y., & Jen Chen, C. (2005). Synthesis and characterization of polymer encapsulated Cu-Ni magnetic nanoparticles for hyperthermia applications. *Journal of Magnetism and Magnetic Materials*, *293*(1), 303–309. https://doi.org/10.1016/j.jmmm.2005.02.024

Choi, N. W., Cabodi, M., Held, B., Gleghorn, J. P., Bonassar, L. J., & Stroock, A. D. (2007). Microfluidic scaffolds for tissue engineering. *Nature Materials*, *6*(11), 908–915. https://doi.org/10.1038/nmat2022

Chu, L. Y., Li, Y., Zhu, J. H., Wang, H. D., & Liang, Y. J. (2004). Control of pore size and permeability of a glucose-responsive gating membrane for insulin delivery. *Journal of Controlled Release*, *97*(1), 43–53. https://doi.org/10.1016/j.jconrel.2004.02.026

Conejero-Muriel, M., Gavira, J. A., Pineda-Molina, E., Belsom, A., Bradley, M., Moral, M., Duran, J. D. G., Álvarez De Cienfuegos, L. (2015). Influence of the chirality of short peptide supramolecular hydrogels in protein crystallogenesis. *Chemical Communications*, *51*(18), 3862–3865. https://doi.org/10.1039/c4cc09024a

Contreras-Montoya, R., Bonhome-Espinosa, A. B., Orte, A., Miguel, D., Delgado-López, J. M., Duran, J. D. G., Álvarez De Cienfuegos, L. Á. (2018). Iron nanoparticles-based supramolecular hydrogels to originate anisotropic hybrid materials with enhanced mechanical strength. *Materials Chemistry Frontiers*, *2*(4), 686–699. https://doi.org/10.1039/c7qm00573c

Culver, H. R., Clegg, J. R., & Peppas, N. A. (2017). Analyte-Responsive Hydrogels: Intelligent Materials for Biosensing and Drug Delivery. *Accounts of Chemical Research*, *50*(2), 170–178. https://doi.org/10.1021/acs.accounts.6b00533

Duran JD, Ramos-Tejada, M. M., Arroyo, F. J., & Gonzalez-Caballero F. (2000). Rheological and Electrokinetic Properties of Sodium Montmorillonite Suspensions. *Journal of colloid and interface Science*, *229,* 107–117. https://doi.org/10.1006/jcis.2000.6956

Gaharwar, A. K., Peppas, N. A., & Khademhosseini, A. (2014). Nanocomposite hydrogels for biomedical applications. *Biotechnology and Bioengineering*, *111*(3), 441–453. https://doi.org/10.1002/bit.25160

Galindo-González, C., De Vicente, J., Ramos-Tejada, M. M., López-López, M. T., González-Caballero, F., & Durán, J. D. G. (2005). Preparation and sedimentation behavior in magnetic fields of magnetite-covered clay particles. *Langmuir*, *21*(10), 4410–4419. https://doi.org/10.1021/la047393q

Gans, B. J. De, Blom, C., Philipse, A. P., & Mellema, J. (1999). Linear viscoelasticity of an inverse ferrofluid. *Physical review E* , *60*(4), 4518–4527. https://doi.org/10.1103/physRevE.60.4518

Giammanco, G. E., Sosnofsky, C. T., & Ostrowski, A. D. (2015). Light-responsive Iron(III)-polysaccharide coordination hydrogels for controlled delivery. *ACS Applied Materials and Interfaces*, *7*(5), 3068–3076. https://doi.org/10.1021/am506772x

Gila-Vilchez, C., Bonhome-Espinosa, A. B., Kuzhir, P., Zubarev, A., Duran, J. D. G., & Lopez-

Chapter 6. References

Lopez, M. T. (2018). Rheology of magnetic alginate hydrogels. *Journal of Rheology*, *62*(5), 1083–1096. https://doi.org/10.1122/1.5028137

Gila-Vilchez, C., Manas-Torres, M. C., Contreras-Montoya, R., Alaminos, M., Duran, J. D. G., De Cienfuegos, L. A., & Lopez-Lopez, M. T. (2019). Anisotropic magnetic hydrogels: Design, structure and mechanical properties. *Philosophical Transactions of the Royal Society A: Mathematical, Physical and Engineering Sciences*, *377*(2143). https://doi.org/10.1098/rsta.2018.0217

Gómez-Ramírez, A., Kuzhir, P., López-López, M. T., Bossis, G., Meunier, A., & Durán, J. D. G. (2010). Steady shear flow of magnetic fiber suspensions: Theory and comparison with experiments. *Journal of Rheology*, *55*(1), 43–67. https://doi.org/10.1122/1.3523477

Gómez-Ramírez, A., López-López, M. T., Durán, J. D. G., & González-Caballero, F. (2009). Influence of particle shape on the magnetic and magnetorheological properties of nanoparticle suspensions. *Soft Matter*, *5*(20), 3888–3895. https://doi.org/10.1039/b906505a

Haraguchi, K., & Takehisa, T. (2002). Nanocomposite Hydrogels: A Unique Organic–Inorganic Network Structure with Extraordinary Mechanical, Optical, and Swelling/De-swelling Properties. *Advanced Materials*, *14*(16), 1120. https://doi.org/10.1002/1521-4095(20020816)14:16<1120::aid-adma1120>3.0.co;2-9

Hoare, T. R., & Kohane, D. S. (2008). Hydrogels in drug delivery: Progress and challenges. *Polymer*, *49*(8), 1993–2007. https://doi.org/10.1016/j.polymer.2008.01.027

Hoffman, A. S. (2012). Hydrogels for biomedical applications. *Advanced Drug Delivery Reviews*, *64*(SUPPL.), 18–23. https://doi.org/10.1016/j.addr.2012.09.010

Hu, Z., & Chen, G. (2014). Novel nanocomposite hydrogels consisting of layered double hydroxide with ultrahigh tensibility and hierarchical porous structure at low inorganic content. *Advanced Materials*, *26*(34), 5950–5956. https://doi.org/10.1002/adma.201400179

Hua, S., Ma, H., Li, X., Yang, H., & Wang, A. (2010). pH-sensitive sodium alginate/poly(vinyl alcohol) hydrogel beads prepared by combined Ca2+crosslinking and freeze-thawing cycles for controlled release of diclofenac sodium. *International Journal of Biological Macromolecules*, *46*(5), 517–523. https://doi.org/10.1016/j.ijbiomac.2010.03.004

Illés, E., & Tombácz, E. (2006). The effect of humic acid adsorption on pH-dependent surface charging and aggregation of magnetite nanoparticles. *Journal of Colloid and Interface Science*, *295*, 115–123. https://doi.org/10.1016/j.jcis.2005.08.003

Ismail, Y. A., Martínez, J. G., Al Harrasi, A. S., Kim, S. J., & Otero, T. F. (2011). Sensing characteristics of a conducting polymer/hydrogel hybrid microfiber artificial muscle. *Sensors and Actuators, B: Chemical*, *160*(1), 1180–1190. https://doi.org/10.1016/j.snb.2011.09.044

Jiles, D.C. (1998). Introduction to Magnetism and Magnetic Materials. *Chapman &Hall, London; 1998. p.115, p.94.*

J.M. Ginder, L.C. Davis and L.D. Elie (1996). Rheology of magnetorheological fluids : Models and measurements. *International Journal of Modern Physics B*, 10 , 3293-

Chapter 6. References

3303.https://doi.org/10.1142/S0217979296001744

Kara, M., Yuzer, H., Sabah, E., & Celik, M. S. (2003). Adsorption of cobalt from aqueous solutions onto sepiolite. *Water Research*, *37*(1), 224–232. https://doi.org/10.1016/S0043-1354(02)00265-8

Kemp, S. J., Ferguson, R. M., Khandhar, A. P., & Krishnan, K. M. (2016). Monodisperse magnetite nanoparticles with nearly ideal saturation magnetization. *RSC Advances*, *6*(81), 77452–77464. https://doi.org/10.1039/c6ra12072e

Khabbouchi, M., Hosni, K., Mezni, M., Zanelli, C., & Doggy, M. (2017). Applied Clay Science Interaction of metakaolin-phosphoric acid and their structural evolution at high temperature. *Applied Clay Science*, (January), 0–1. https://doi.org/10.1016/j.clay.2017.07.006

Kokabi, M., Sirousazar, M., & Hassan, Z. M. (2007). PVA-clay nanocomposite hydrogels for wound dressing. *European Polymer Journal*, *43*(3), 773–781. https://doi.org/10.1016/j.eurpolymj.2006.11.030

Kuo, C. K., & Ma, P. X. (2001). Ionically crosslinked alginate hydrogels as scaffolds for tissue engineering: Part 1. Structure, gelation rate and mechanical properties. *Biomaterials*, *22*(6), 511–521. https://doi.org/10.1016/S0142-9612(00)00201-5

Kuzhir, P., Lopez-Lopez, M., & Bossis, G. (2010). Magnetorheology of fiber suspensions . II . *Journal of Rheology, 53*, 127–151. https://doi.org/10.1122/1.3005405

R.Langer , L.Brown , E.Edelman (1985). 30 Controlled release and magnetically modulated release systems for macromolecules. *Methods in Enzymology, 112, 399-422.* https://doi.org/10.1016/S0076-6879(85)12032-X

Li, J., & Mooney, D. J. (2016). Designing hydrogels for controlled drug delivery. *Nature Reviews Materials*, *1*(12), 1–18. https://doi.org/10.1038/natrevmats.2016.71

Li, Y., Huang, G., Zhang, X., Li, B., Chen, Y., Lu, T., … Xu, F. (2013). Magnetic hydrogels and their potential biomedical applications. *Advanced Functional Materials*, *23*(6), 660–672. https://doi.org/10.1002/adfm.201201708

Liu, X., Liu, J., Lin, S., & Zhao, X. (2020). Hydrogel machines. *Materials Today*, 36, 102_124. https://doi.org/10.1016/j.mattod.2019.12.026

Liu, Y., Liu, P., Su, Z., Li, F., & Wen, F. (2008). Attapulgite-Fe3O4 magnetic nanoparticles via co-precipitation technique. *Applied Surface Science*, *255*(5 PART 1), 2020–2025. https://doi.org/10.1016/j.apsusc.2008.06.193

Lo, M. T. (2007). New magnetorheological fluids based on magnetic fibers. *Journal of Materials Chemistry*. 17, 3839–3844. https://doi.org/10.1039/b705871c

Lo, M. T., Go, A., Rodr, L., Dura, J. D. G., Iskakova, L., & Zubarev, A. (2012). Colloids on the Frontier of Ferrofluids . Rheological Properties. *Langmuir* , 28, 6232–6245 http://doi.org/10.1021/la204112w

Lopez-Lopez, M. T., Durán, J. D. G., Iskakova, L. Y., & Zubarev, A. Y. (2016). Mechanics of Magnetopolymer Composites: A Review. *Journal of Nanofluids*, *5*(4), 479–495.

Chapter 6. References

https://doi.org/10.1166/jon.2016.1233

Lopez-Lopez, M. T., Rodriguez, I. A., Rodriguez-Arco, L., Carriel, V., Bonhome-Espinosa, A. B., Campos, F., Duran, J. D. G. (2017). Synthesis, characterization and in vivo evaluation of biocompatible ferrogels. *Journal of Magnetism and Magnetic Materials*, *431*, 110–114. https://doi.org/10.1016/j.jmmm.2016.08.053

Lopez-Lopez, M. T., Scionti, G., Oliveira, A. C., Duran, J. D. G., Campos, A., Alaminos, M., & Rodriguez, I. A. (2015). Generation and characterization of novel magnetic field-responsive biomaterials. *PLoS ONE*, *10*(7), 1–17. https://doi.org/10.1371/journal.pone.0133878

Lopez-Lopez, M. T., de Vicente, J., Bossis, G., Gonzalez-Caballero, F., Duran, J. D. G. (2005). Preparation of stable magnetorheological fluids based on extremely bimodal iron – magnetite suspensions. *Journal of Materials Research, 20*, 874-881. https://doi.org/10.1557/JMR.2005.0108

Magnussen, R. A., Guilak, F., & Vail, T. P. (2005). Cartilage degeneration in post-collapse cases of osteonecrosis of the human femoral head: Altered mechanical properties in tension, compression, and shear. *Journal of Orthopaedic Research*, *23*(3), 576–583. https://doi.org/10.1016/j.orthres.2004.12.006

Mahdavinia, G. R., & Asgari, A. (2013). Synthesis of kappa-carrageenan-g-poly(acrylamide)/sepiolite nanocomposite hydrogels and adsorption of cationic dye. *Polymer Bulletin*, *70*(8), 2451–2470. https://doi.org/10.1007/s00289-013-0966-4

Malda, J., Visser, J., Melchels, F. P., Jüngst, T., Hennink, W. E., Dhert, W. J. A., Hutmacher, D. W. (2013). 25th anniversary article: Engineering hydrogels for biofabrication. *Advanced Materials*, *25*(36), 5011–5028. https://doi.org/10.1002/adma.201302042

Mao, H., Zhu, K., Liu, X., Yao, C., & Kobayashi, M. (2016). Facile synthetic route to Fe3O4/silica nanocomposites pillared clay through cationic surfactant-aliphatic acid mixed system and application for magnetically controlled drug release. *Microporous and Mesoporous Materials*, *225*, 216–223. https://doi.org/10.1016/j.micromeso.2015.11.045

Margel, S. (2012). Novel magnetic fibrin hydrogel scaffolds containing thrombin and growth factors conjugated iron oxide nanoparticles for tissue engineering.*International Journal of Nanomedicine, 7(1)*, 1259-74 .https://doi.org/10.2147/IJN.S26533

Mayer, B. C. R., Cabuil, V., & Lalot, T. (2000). Magnetic Nanoparticles Trapped in pH 7 Hydrogels as a Tool to Characterize the Properties of the Polymeric Network .*Advanced Materials*, 417–420.

Mousa, M., Evans, N. D., Oreffo, R. O. C., & Dawson, J. I. (2018). Clay nanoparticles for regenerative medicine and biomaterial design: A review of clay bioactivity. *Biomaterials*, *159*(2018), 204–214. https://doi.org/10.1016/j.biomaterials.2017.12.024

Muniz, E. C., & Geuskens, G. (2001). Polyacrylamide hydrogels and semi-interpenetrating networks (IPNs) with poly(N-isopropylacrylamide): Mechanical properties by measure of compressive elastic modulus. *Journal of Materials Science: Materials in Medicine*, *12*(10–12), 879–881. https://doi.org/10.1023/A:1012863705484

Murray, H. H. (2000). Traditional and new applications for kaolin, smectite, and palygorskite: A

general overview. *Applied Clay Science*, *17*(5–6), 207–221. https://doi.org/10.1016/S0169-1317(00)00016-8

Nicodemus, G. D., & Bryant, S. J. (2008). Cell encapsulation in biodegradable hydrogels for tissue engineering applications. *Tissue Engineering - Part B: Reviews*, *14*(2), 149–165. https://doi.org/10.1089/ten.teb.2007.0332

Norouzi, M., Nazari, B., & Miller, D. W. (2016). Injectable hydrogel-based drug delivery systems for local cancer therapy. *Drug Discovery Today*, *21*(11), 1835–1849. https://doi.org/10.1016/j.drudis.2016.07.006

Odenbach, S. (2013). Ferrofluids and their applications. *MRS Bulletin*, *38*(11), 921–924. https://doi.org/10.1557/mrs.2013.232

Park, K. M., Lee, S. Y., Joung, Y. K., Na, J. S., Lee, M. C., & Park, K. D. (2009a). Thermosensitive chitosan-Pluronic hydrogel as an injectable cell delivery carrier for cartilage regeneration. *Acta Biomaterialia*, *5*(6), 1956–1965. https://doi.org/10.1016/j.actbio.2009.01.040

Park, K. M., Lee, S. Y., Joung, Y. K., Na, J. S., Lee, M. C., & Park, K. D. (2009b). Thermosensitive chitosan-Pluronic hydrogel as an injectable cell delivery carrier for cartilage regeneration. *Acta Biomaterialia*, *5*(6), 1956–1965. https://doi.org/10.1016/j.actbio.2009.01.040

Peppas, B. N. A., Hilt, J. Z., Khademhosseini, A., & Langer, R. (2006). Hydrogels in Biology and Medicine : From Molecular Principles to Bionanotechnology. *Advanced Materials*, 18, 1345–1360. https://doi.org/10.1002/adma.200501612

Ramos-Tejada, M. M., de Vicente J., Ontiveros A., Duran J.D.G. (2001). Effect of humic acid adsorption on the rheological properties of sodium montmorillonite suspensions. *Journal of Rheology*, 45, *1159*. https://doi.org/10.1122/1.1392297

Ramos-Tejada, M. M., Ontiveros, A., Viota, J. L., & Durán, J. D. G. (2003). Interfacial and rheological properties of humic acid/hematite suspensions. *Journal of Colloid and Interface Science*, *268*(1), 85–95. https://doi.org/10.1016/S0021-9797(03)00665-9

Rezwan, K., Chen, Q. Z., Blaker, J. J., & Boccaccini, A. R. (2006). Biodegradable and bioactive porous polymer/inorganic composite scaffolds for bone tissue engineering. *Biomaterials*, *27*(18), 3413–3431. https://doi.org/10.1016/j.biomaterials.2006.01.039

Rodriguez-Arco, L., Rodriguez, I. A., Carriel, V., Bonhome-Espinosa, A. B., Campos, F., Kuzhir, P., Duran, J. D. G., Lopez-Lopez, M. T. (2016). Biocompatible magnetic core-shell nanocomposites for engineered magnetic tissues. *Nanoscale*, *8*, 8138–8150. https://doi.org/10.1039/C6NR00224B

Rosenweig, RE. (1985) Ferrohydrodynamics, p. 58. *New York, NY: Cambridge University Press*

Sannino, A., Demitri, C., & Madaghiele, M. (2009). Biodegradable cellulose-based hydrogels: Design and applications. *Materials*, *2*(2), 353–373. https://doi.org/10.3390/ma2020353

Scionti, G., Moral, M., Toledano, M., Osorio, R., Durán, J. D. G., Alaminos, M., … Lõpez-Lõpez, M. T. (2014). Effect of the hydration on the biomechanical properties in a fibrin-agarose tissue-like model. *Journal of Biomedical Materials Research - Part A*, *102*(8), 2573–2582. https://doi.org/10.1002/jbm.a.34929

Chapter 6. References

Stammen, J. A., Williams, S., Ku, D. N., & Guldberg, R. E. (2001). Mechanical properties of a novel PVA hydrogel in shear and unconfined compression. *Biomaterials*, *22*(8), 799–806. https://doi.org/10.1016/S0142-9612(00)00242-8

Thévenot, J., Oliveira, H., Sandre, O., & Lecommandoux, S. (2013). Magnetic responsive polymer composite materials. *Chemical Society Reviews*, *42*(17), 7099–7116. https://doi.org/10.1039/c3cs60058k

Ullah, F., Othman, M. B. H., Javed, F., Ahmad, Z., & Akil, H. M. (2015). Classification, processing and application of hydrogels: A review. *Materials Science and Engineering C*, *57*, 414–433. https://doi.org/10.1016/j.msec.2015.07.053

Valentini, F., Diamanti, A., Carbone, M., Bauer, E. M., & Palleschi, G. (2012). New cleaning strategies based on carbon nanomaterials applied to the deteriorated marble surfaces: A comparative study with enzyme based treatments. *Applied Surface Science*, *258*(16), 5965–5980. https://doi.org/10.1016/j.apsusc.2012.01.076

Van Vlierberghe, S., Dubruel, P., & Schacht, E. (2011). Biopolymer-based hydrogels as scaffolds for tissue engineering applications: A review. *Biomacromolecules*, *12*(5), 1387–1408. https://doi.org/10.1021/bm200083n

Varaprasad, K., Raghavendra, G. M., Jayaramudu, T., Yallapu, M. M., & Sadiku, R. (2017). A mini review on hydrogels classification and recent developments in miscellaneous applications. *Materials Science and Engineering C*, *79*, 958–971. https://doi.org/10.1016/j.msec.2017.05.096

Varga, Z. (2006). Magnetic field sensitive functional elastomers with tuneable elastic modulus. *Polymer*, *47*, 227–233. *https://doi.org/10.1016/j.polymer.2005.10.139*

Viota, J. L., Arroyo, F. J., Delgado, A. V., & Horno, J. (2010). Electrokinetic characterization of magnetite nanoparticles functionalized with amino acids. *Journal of Colloid and Interface Science*, *344*(1), 144–149. https://doi.org/10.1016/j.jcis.2009.11.061

Wagner, N. J., & Brady, J. F. (2009). Shear thickening in colloidal dispersions. *Physics Today*, *62*(10), 27–32. https://doi.org/10.1063/1.3248476

Wiedenmann, A. (2002). Magnetic and Crystalline Nanostructures in Ferrofluids as Probed by Small Angle Neutron Scattering. *Springer-VerlagBerlin Heidelberg*, 33–58. https://doi.org/10.1007/3-540-45646-5_3

Xu, J., & Wang, A. (2012). Electrokinetic and Colloidal Properties of Homogenized and Unhomogenized Palygorskite in the Presence of Electrolytes. *J. Chem. Eng*, 57, 5, 1586–1593. https://doi.org/10.1021/je300213u

Xu, X. Q., Shen, H., Xu, J. R., Xie, M. Q., & Li, X. J. (2006). The colloidal stability and core-shell structure of magnetite nanoparticles coated with alginate. *Applied Surface Science*, *253*(4), 2158–2164. https://doi.org/10.1016/j.apsusc.2006.04.015

Yang, Z., Peng, H., Wang, W., & Liu, T. (2010). Crystallization behavior of poly(ε-caprolactone)/layered double hydroxide nanocomposites. *Journal of Applied Polymer Science*, *116*(5), 2658–2667. https://doi.org/10.1002/app

Zhang, J. T., Bhat, R., & Jandt, K. D. (2009). Temperature-sensitive PVA/PNIPAAm semi-IPN

hydrogels with enhanced responsive properties. *Acta Biomaterialia*, *5*(1), 488–497. https://doi.org/10.1016/j.actbio.2008.06.012

Zhang, Z., Wang, W., & Wang, A. (2015). High-pressure homogenization associated hydrothermal process of palygorskite for enhanced adsorption of Methylene blue. *Applied Surface Science*, *329*, 306–314. https://doi.org/10.1016/j.apsusc.2014.12.187

Zubarev, A., Bonhome-Espinosa, A. B., Alaminos, M., Durán, J. D. G., & Lopez-lopez, J. D. G. D. M. T. (2019). Rheological properties of magnetic biogels. *Archive of Applied Mechanics, 89*, 91-103. https://doi.org/10.1007/s00419-018-1450-2